Synthesis and Characterization of New Associating Polymers and Hydrogels for Biological Applications

Thesis Submitted to AcSIR for the Award of
the Degree of

DOCTOR OF PHILOSOPHY
In Chemical Sciences

By
Neha Tiwari
Registration Number: 10CC11A26015

Under the Guidance of

Dr. Manohar V. Badiger (Research Guide)

CSIR- National Chemical Laboratory,
Pune-411008, India.
Dec. 2017

Declaration

I declare that the thesis entitled "**Synthesis and Characterizations of New Associating Polymers and Hydrogels for Biological Applications**" submitted for the degree of **Doctor of Philosophy** in Chemical Sciences to the Academy of Scientific & Innovative Research (AcSIR), has been carried out by me at the Polymer Science and Engineering Division of National Chemical Laboratory, Pune under the guidance of **Dr. Manohar V. Badiger**. Material obtained from other sources has been duly acknowledged in this thesis. The work is original and has not been submitted in part or full by me for any other degree or diploma to any other University.

Neha Tiwari

Date: Dec. 21st 2017
CSIR- National Chemical Laboratory
Pune-411008

Neha Tiwari
(Research Student)

सीएसआईआर - राष्ट्रीय रासायनिक प्रयोगशाला
(वैज्ञानिक तथा औद्योगिक अनुसंधान परिषद)
डॉ. होमी भाभा मार्ग, पुणे - 411 008, भारत
CSIR - NATIONAL CHEMICAL LABORATORY
(Council of Scientific & Industrial Research)
Dr. Homi Bhabha Road, Pune - 411 008, India

Certificate

This is to certify that the work reported in this Ph.D. thesis entitled "**Synthesis and Characterization of New Associating Polymers and Hydrogels for Biological Applications**" submitted by **Ms. Neha Tiwari** to Academy of Scientific and Innovative Research (AcSIR) in the fulfilment of requirements for the award of the Degree of **Doctor of Philosophy in Chemical Sciences**, embodies original research work under my supervision. I further certify that this work has not been submitted to any other University or Institution in part or full for the award of any degree or diploma. Any text, illustration, table etc., used in the thesis from other sources, have been duly cited and acknowledged.

Neha Tiwari

Research Student
Ms. Neha Tiwari

Research Guide
Dr. Manohar V. Badiger

Communication Channels
NCL Level DID : 2590
NCL Board No. : +91-20-25902000
EPABX : +91-20-25893300
: +91-20-25893400
FAX
Director's Office : +91-20-25902601
COA's Office : +91-20-25902660
SPO's Office : +91-20-25902664
WEBSITE
www.ncl-india.org

Acknowledgements

Obtaining a PhD degree is the biggest dream of my life and it was not possible without the constant efforts, advice, support and encouragement of many people directly or indirectly. Here, I would like to thank my family and friends who made it possible to make my dream come true.

First and foremost, I would like to sincerely thank my research supervisor, Dr. Manohar V. Badiger who has supported, advised and encouraged me to carry out my research work in the best possible way as per my capability. I feel myself really lucky to be a part of his research group. During my PhD tenure in his lab, I not only got the opportunity to develop my research skills but he also taught me to remain humble in my best and worst situations. The kind of mentorship, guidance and freedom he has provided has developed immense confidence in me to become an independent researcher and utilize my skills for the betterment of my career. I can never express my gratitude towards Dr. Badiger in words and I whole heartedly owe all the achievements during my PhD to him.

I thank Council of Scientific and Industrial Research for financial support and also to Director, National Chemical Laboratory to allow me to utilize all the facilities without restrictions.

I would also like to thank Dr. P.R. Rajamohanan, Dr. Sapna, Dr. S.K. Bhat, Dr. Rathna, and my Doctoral advisory committee Dr. P.P. Wadgaonkar, Dr. Gopinath Chinnakonda and Dr. Ashootosh V. Ambade for their valuable inputs and guidance in my research projects. Their thoughtful inputs have immensely helped me to shape my thesis in the right direction. I am thankful to Prof Giyoong Tae, GIST, Korea for the guidance and exposure he has provided during my stay in his lab. I would also like to thank Dr. Sayam Sen Gupta for his guidance during the early phase of my PhD research.

I am grateful to all the lab members Suresha,Yogesh, Manjusha, Ashwini, Anumon, Pratiksh, Bhagyashree, Naresh, Lokanathan, Amarnath for their constant support and help. I would like to specially thank my labmate Arun and Dr. Aarti who not only help

me getting expertise in various instruments but also entertain and gave valuable suggestions whenever I needed the required help.

Obtaining PhD degree with the entire thick and thins was not possible without the constant support of my friends. I would like to thank my dearest friends Richa, Divya, Vikesh, Kundan, Neha, Jay, Anirudh, who always encouraged me to see the best in the worst situations. I would like to specially thank my two closest friends Noopur and Sayantan who stood as strong pillars during the difficult times. I could never imagine a better life in NCL full of happiness and positivity without both of them.

A special thanks to my lovely husband, Yogesh who was the biggest support system for me to materialize my dream of getting doctorate degree. His constant love and confidence in me has made the difficult tasks easier. I thank him to bear all my frustations and celebrate even the tiniest achievements. The kind of positivity and happiness he brings in my life has helped me to come so far. I would also like to thank my parents in law and my brother, Ketan for their immense love and support. I also thank another family member, my lovely dog, Pluto for his unconditional love.

Finally, I would like to thank my parents (S.D. Tiwari and Laxmi Tiwari) and my dearest sister, Bharti Tiwari for their immense faith in me. Without their support and love, I could never imagine obtaining PhD degree from such a prestigious Institute of India. They always encouraged me to see beyond the horizon and make me believe that nothing is impossible to achieve. I can never repay for the care, love and encouragement they provided throughout my academic career. Special thanks to my father who always see much more potential in me than anyone else. I dedicate my thesis and all the future achievements to my parents.

Neha Tiwari

Table of Contents

Abstract

Synthesis and Characterization of New Associating Polymers and Hydrogels for Biological Applications

The thesis work focuses on the design, synthesis and characterization of new associating polymers (APs), hydrogels and nanogels based on synthetic polymer poly(acrylic acid) and natural polymer, carboxymethyl cellulose.

Associating polymers (APs) or hydrophobically modified polymers (HMPs) are a class of partially ordered systems that have attracted a great deal of attention due to their unique rheological properties such as thermo associating, strain hardening, super viscosifying and shear thinning/ thickening. Therefore, they find wide range applications in paints, food, paper, textiles, thickeners for cosmetics and pharmaceutical industries. They contain large amount of hydrophilic polymer and a small percentage of hydrophobic moieties in their chemical structure still retaining the solubility in water. In an aqueous medium, the hydrophobic groups of the polymeric chains self-assemble/self-associate to form 3-D transient networks above a critical association concentration (CAC) resulting into dramatic increase in the viscosity of the overall solution.

Amongst APs, thermo associating polymers containing combination of both hydrophilic polymers and LCST polymers have become promising materials as injectables for drug delivery applications due to their response towards temperature as a stimulus. They show exceptional sol-gel transitions upon heating due to the formation of physical networks. In the thesis work, thermo associating graft polymers of PAA with LCST block copolymer, MPEG-*b*-PCL have been synthesized using dicyclo carbodiimide (DCC) coupling reaction between carboxylic groups of PAA and terminal hydroxyl groups of PCL in MPEG-*b*-PCL. The graft copolymer PAA-*g*-MPEG-*b*-PCL exhibited interesting irreversible thermo thickening behavior which was investigated using rheology, light scattering and NMR techniques. These thermo associating polymers

show great potential as injectables in controlled drug release systems and as rheology control agents for cosmetics creams/ ointments.

Hydrogels and nanogels based on both synthetic and natural polymers have been studied extensively especially for biomedical applications due to their biocompatibility and high water uptake that mimic the extracellular matrix (ECM). Various nanocarriers that have been studied in the past for drug delivery applications include liposomes, dendrimers, carbon nanotubes, metal nanoparticles, graphene etc. A few natural polymers explored are collagen, gelatin, alginate, agarose, chitosan, and hyaluronic acid. The advantages associated with natural polysaccharides is that they are biocompatible and biodegradable and can be easily functionalized due to the presence of various reactive groups like -NH_2, -COOH and -OH on the polymer chains. In our work, we synthesized nanogels based on Mesoporous Silica Nanoparticles (MSNs) functionalized with carboxy methyl cellulose (CMC) using an EDC coupling reaction between amine functionalized MSNs (MSN-NH_2) and the carboxylic groups of CMC. The pores of MSNs were used for the incubation of hydrophobic drug such as curcumin, which has both anticancer and antibacterial activity. The MSN-CMC hybrid nanogels were found to exhibit enhanced permeation of MSNs inside the tumor cells. The nanogels containing carboxymethyl cellulose grafted MSNs show potential in targeted drug delivery applications.

Hydrogels having control over the release of drug molecules at the required site has gained much attention towards drug delivery applications in the past few decades. The hydrogel structure and the degree of crosslinking play a major role in the swelling-controlled release of drugs. Amongst the synthetic polymers, polyacrylic acid (PAA) (FDA approved) has been proved to be a good candidate for both drug delivery and tissue engineering applications due to its biocompatibility in in-vivo conditions. In this thesis work, we have adopted a strategy of synthesizing double crosslinked Poly(acrylic acid) hydrogels using two different crosslinking agents namely, Jeffamine (jeff) and Cystamine (cys) in an aqueous medium. Jeffamine provides a good mechanical strength while, cystamine with disulphide bonds incorporates redox sensitivity to the hydrogels. We demonstrated the selective in-situ cleavage of one crosslinking (cys) by DTT and its

implications on the controlled release of an anticancer drug, Doxorubicin (Dox) and antimicrobial silver (Ag) nanoparticles.

In another study, we also synthesized PAA hydrogels using PEG-bismaleimide as cross linking agents by Furan-Maleimide “Click-Chemistry” approach. We studied the effect molecular weight of PEG on the gelation time and mechanical properties of the hydrogels. These hydrogels show great promise in biomedical applications both as injectables as well as scaffolds in tissue engineering.

Abbreviations & Symbols

Ag	Silver
APs	Associating Polymers
APTES	(3-aminopropyl)triethoxysilane
BET method	Brunauer–Emmett–Teller method
BJH method	Barrett-Joyner-Halenda method
CAC	Critical association concentration
CTAB	Cetyltrimethylammonium bromide
Cys	Cystamine
Cur	Curcumin
$CDCl_3$	Deuterated Chloroform
CMC	Critical micelle concentration
D_f	Diffusion coefficient
DCCI	N,N'-Dicyclohexylcarbodiimide
2-D NMR	2-dimensional Nuclear Magnetic Resonance
DLS	Dynamic Light Scattering
DSC	Differential scanning calorimetry
DMAP	4-Dimethylaminopyridine
DMSO-D_6	Deuterated dimethylsulphoxide
D_2O	Deuterated water
DOX.HCl	Doxorubicin hydrochloride
DTT	Dithiothreitol
DAPI	4',6-Diamidino-2-Phenylindole Dihydrochloride

ECM	Extracellular Matrix
EDC.HCl	1-ethyl-3-(3-dimethylaminopropyl)-carbodiimide hydrochloride
ET_3N	Triethylamine
FT-IR	Fourier-Transform Infrared Spectroscopy
G'	Storage Modulus
G''	Loss Modulus
GPC	Gel Permeation Chromatography
HSQC	Heteronuclear single quantum correlation spectroscopy
HMPs	Hydrophobically Modified Polymers
Jeff	Jeffamine
LCST	Lower Critical Solution Temperature
MPEG	Methoxy terminated poly(ethyleneglycol)
MSNs	Mesoporous Silica Nanoparticles
MTT	3-(4,5-dimethylthiazol-2-yl)-2,5-diphenyltetrazolium bromide
NMR	Nuclear magnetic Resonance
NHS	N-hydroxy succinimide
NOESY	Nuclear Overhauser Effect Spectroscopy
OD	Optical Density
PAA	Poly(acrylic acid)
PCL	Poly(caprolactone)
PEG	Poly(ethylene glycol)
Q_e	Equilibrium Swelling
ROP	Ring Opening Polymerization

R_h	Hydrodynamic radius
SEM	Scanning Electron Microscopy
SLS	Static Light Scattering
SAPs	Super Absorbant Polymers
$Sn(Oct)_2$	Stannous Octoate
TEM	Transmission Electron Microscopy
TEOS	Tetraethyl orthosilicate
Wt%	Weight percentage
WSPs	Water Soluble Polymers
XRD	X-Ray Diffraction
η_{sp}	Specific Viscosity

List of Schemes

List of Figures

List of Tables

Chapter-1

Introduction

This chapter gives an introduction to associating polymers, hydrogels and nanogels for drug delivery and tissue engineering applications along with their preparation and characterization techniques. It includes the literature survey on these materials followed by a brief description of the analytical techniques used in the thesis work.

1. Introduction

Associating polymers (APs) or hydrophobically modified polymers (HMPs) are a class of partially ordered polymer systems which have gained immense interest in the past few decades.[1, 2] The research towards APs mainly started to overcome the limitations associated with water soluble polymers which are adversely affected by the external conditions like temperature, pH, shear and the presence of salt.[3, 4] APs are water soluble polymers that consist of small number of hydrophobic groups attached to the hydrophilic polymer backbone. In aqueous media, these hydrophobic groups self assemble into micro structures to minimize their exposure to water molecules and form 3-D transient networks. The formation of network structures manifests into enhanced viscosity of the overall solution compared to their precursor polymer solutions. Therefore, they find applications as viscosity modifiers in paints, petroleum recovery, food and pharmaceutical industry etc.[5, 6]

The synthesis of HMPs along with their self assembling property was first explored by Strauss and co-workers in 1951.[7] They functionalized poly (2-vinyl pyridine) using n-dodecyl bromide groups to form a polyelectrolyte that shows self-association in aqueous media. Pluronics composed of poly(ethylene oxide)-*b*-poly(propylene oxide) (PEO-*b*-PPO) are the most studied amphiphilic polymers for drug delivery applications wherein the hydrophobic drugs can be effectively entrapped inside the hydrophobic core of PPO while the hydrophilic PEO forms hydrogen bonds with the aqueous surroundings and form a tight shell around the hydrophobic core.[8-11] PEO further helps in resisting protein or cellular adhesion thus preventing the amphiphiles against hydrolysis and enzymatic degradation. The copolymers in amphiphilic polymers can be chosen in order to prolong circulation time, introduction of targeting groups, drug solubilisation and to suppress multidrug resistance. A few of the hydrophobic groups in PEG based amphiphilic block copolymers explored are poly(amino acids) with functional groups [12-14], poly(ε-caprolactone) [15, 16], poly(lactic acid) (PLA)

[17, 18], copolymers of lactic and glycolic acid (PLGA) [19-21], poly(morpholine-2,5-dione) [22, 23], poly(trimethylene carbonate) [24, 25]etc. Hydrophilic polymers other than PEG explored for drug delivery applications are poly(l-glutamic acid) (PGA) [26, 27], poly(N-(2-hydroxypropyl)methacrylamide) (PHPMA) [28, 29], dextran [30], chitosan [31, 32], hyaluronic acid [33, 34]etc. Advantages associated with block copolymers are a control over the chemical composition, molecular weight, blocks length ratios which in turn allows one to have a control over the size and morphology of the associations.

The associating structures of APs/HMPs can also be induced by temperature and the resulting polymers are termed as "Thermo-associating Polymers". Thermo associating polymers consists of LCST polymers/stickers attached to the hydrophilic polymer back bone and undergo sol-gel transition in response to small external temperature change as shown in **Figure 1.1**.[35, 36]

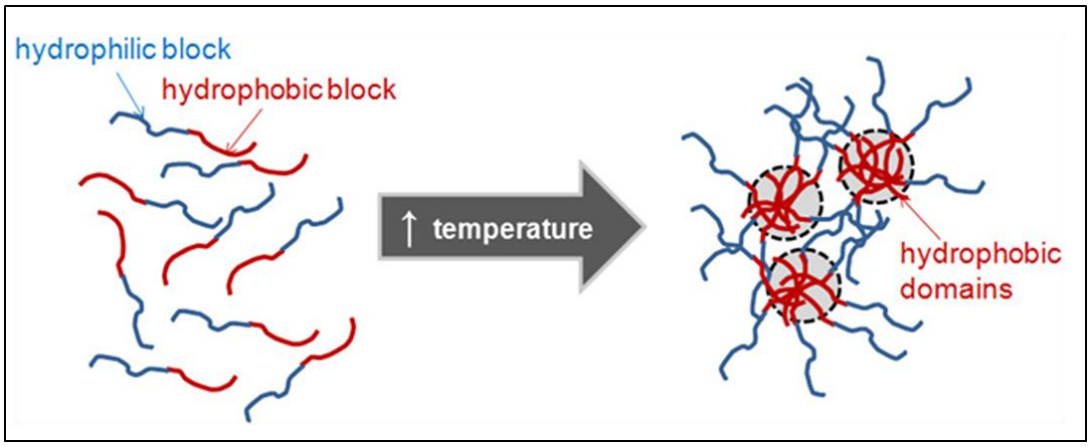

Figure 1.1. Thermogelation in amphiphilic polymer (Figure is adapted from Ref[37] with permission of Elsevier)

These polymers are becoming very important as injectables for controlled drug delivery systems. Bromberg and Hourdet et al have performed extensive studies on thermo associating polymers by grafting LCST polymers like poly(N-isopropylacrylamide) (PNIPAM), poly(ethylene oxide) (PEO) and poly(ethylene oxide)-b-poly(propylene oxide) (PEPO) to the hydrophilic synthetic polymer poly(acrylic acid).[38-43] Natural polymers like carboxymethyl cellulose exhibiting thermo associating behaviour have been explored by Bokias et al.[44] These polymers show inverse solubility with temperature and undergo phase separation in aqueous media above a characteristic LCST. Interestingly, when these LCST

polymers are grafted onto hydrophilic water-soluble polymers, the phase separation is prevented by the strong solubility of the backbone polymer which eventually leads to gelation. It has been demonstrated that thermo associating polymers have great potential either as in situ generated implants or they can be used in the form of liquids as injectables which forms gels at physiological temperature and can be used as controlled drug delivery systems.

1.1 Hydrogels/ Nanogels

Polymeric hydrogels or nanogels based on both synthetic and natural polymers have been studied extensively for biomedical applications due to their biocompatibility and high water uptake that mimic the extracellular matrix (ECM). Hence, they find wide range of applications as drug delivery vehicles [45], sensors [46], actuators [47], enzyme immobilizations [48] and scaffolds or implants for tissue engineering purposes.[49-51] Hydrogels have 3-dimensional polymer network structures which are either physically or chemically cross linked and are capable of holding copious amount of water (~90-95% and more than 500% in the case of Superabsorbent polymers, SAPs). The ability of the hydrogels to hold large amount of water arises from the presence of hydrophilic functional groups like $–NH_2$, -COOH, $-SO_3H$, -OH etc. The water holding capacity (i.e. swelling ratio) of a hydrogel is governed by the hydrophilicity of the polymer backbone and the crosslinking density. The mechanical strength of a hydrogel also depends on the swelling ratio and the crosslink density which can be tuned according to the area of application for making scaffolds in tissue engineering. This opens up a huge scope for developing new and precise hydrogels to suit the tissue engineering applications.

The term hydrogels was first coined by Wichterle and Lim in 1960s.[52] The first application of hydrogels was shown by scientists in Du Pont in 1960s who worked on poly (2-hydroxyethylmethacrylate) poly(HEMA) which is a highly water swollen, soft and elastic gel.[52] After their report, a lot of research has been carried out for application of hydrogels in pharmaceutical and biomedical field.[50, 53, 54] Hydrogels have structural similarity with extracellular matrix (ECM) in the body and thus allows easy diffusion of nutrients, growth factors and other biomolecules in the cells.[37] The high porosity in hydrogels enables them to incubate a larger amount of drug molecules and their release is controlled by

swelling of the hydrogel followed by diffusion of drug molecules. The cross linking in the polymeric hydrogels occurs via physical interactions, van der waals interactions, hydrogen bonding or through covalent interactions.[55] Hydrogels are generally classified depending on the type of crosslinking (physical or chemical), on the type of network (homopolymer, copolymer or interpenetrating networks), on the type of origin (natural or synthetic) and on the functional groups present (ionic or non-ionic). Both natural and synthetic polymers have been explored extensively for the synthesis of hydrogels for drug delivery and tissue engineering applications. A few of the synthetic polymers explored for synthesis of hydrogels are Polylactic acids, Polyglycolic acids, Polyhydroxyethyl methacrylate, Polyvinyl alcohol, Polyphosphazene, Polypeptides, etc. Amongst the synthetic polymers, polyacrylic acid (FDA approved) has been proved to be a good candidate for both drug delivery and tissue engineering applications due to its biocompatibility in in-vivo conditions.[56] On the other hand, natural based polymers explored are collagen, gelatin, alginate, agarose, chitosan, and hyaluronic acid among others. The advantages associated with natural polysaccharides is that they are biocompatible and biodegradable and can be easily functionalized due to the presence of various groups like $–NH_2$, -COOH and –OH on the polymer chains.

Hydrogels having control over the release of drug molecules or other active biomolecules at the required site has gained much attention towards drug delivery applications in past few decades.[57-59] Such smart hydrogels are sensitive towards various external stimuli like temperature, pH, magnetic and electric fields etc. One such stimulus is based on redox in which the volume transition in hydrogels is effected by breaking and reformation of crosslinks triggered by reduction and oxidation (which we have explored in our research work). These three dimensional hydrogels can be used as a scaffold for cell encapsulation[60], drug/ gene carriers[61] or they can be used as a barrier between material surfaces and tissues.[62]

Nanogels are nano sized hydrogels wherein the size varies from 1-1000 nm and are used as injectables for biomedical applications. Various nanocarriers that have been studied in the past for drug delivery applications are liposomes, dendrimers, carbon nanotubes, metal nanoparticles, graphene etc. The major drawback associated with the most of the above mentioned nanoparticles is

their stability in in-vivo conditions and enzymatic degradation leading to premature release of drug and other active biomolecules before reaching the targeted site. In order to overcome above mentioned limitations polymer-inorganic material nanoparticles come into picture. Inorganic materials like mesoporous silica nanoparticles having large surface area and good porosity help in the incubation of drug molecules and polymer coating on the surface of MSNs help in increasing the biocompatibility, stability and circulation time in the physiological environment along with preventing the drug molecules form premature release.[63-65] The internalization of these polymer functionalized mesoporous particles occur through a well known pathway, Enhanced Permeation and Retention (EPR) effect.[66] Literature survey reveals that both synthetic polymers (polyethylene glycol[67], folic acid[68], β-cyclodextrin[69], polyacrylic acid[70]) and natural polymers (polyamino acids and polysaccharides)[71] have been used for the surface modification of MSNs. Polysaccharides are naturally occurring molecules having inherent biocompatible and biodegradable properties that could be used to enhance the biocompatibility of the inorganic MSN without any side effects. Few of the naturally occurring polysaccharides that have been studied for encapsulation of hydrophobic drug molecules and enhanced permeation of the hybrid silica particles inside the tumour cells are chitosan[72], hyaluronic acid[73], mannose[74] and alginate[75]. Polysaccharides are associated with excellent hydrophilicity and hence they possess gel like properties which enhance the blood circulation of the particles tremendously. Polysaccharides being biodegradable by various enzymatic actions inside the cells could be used for surface coating of the drug loaded silica particles and the release could be achieved by natural phenomenon of the degradation of the polysaccharide layer inside the tumour cells.

1.2 Polymers in Drug Delivery

Conventional drug delivery systems (DDS) such as oral route and intravenous have contributed greatly towards the treatment of various diseases in the past. However, the drawbacks associated with them like premature drug release and toxicity to healthy cells lead to major research focus on designing intelligent drug delivery systems. The major challenge however, is to limit the dosage of drugs at the targeted site with minimal side effects. During the past few decades, controlled drug delivery

systems at the targeted site have become major area of research to limit toxicity to the normal cells. Modern drug delivery systems begin with the use of polymers having inherent biocompatibility for both drug delivery and tissue engineering applications.[76] They have potential for additional modification and can be easily prepared at industrial scale. Polymers have played a significant part in the advancement of drug delivery technology by having a control over the release of both hydrophilic and hydrophobic drugs and other biomolecules in desired dosages over a long period of time.[77] Synthesis of new polymeric systems having inherent biocompatibility and stimuli-responsive property has attracted a lot of attention in recent years.[78] Polymers must possess the following properties in order to be used as an efficient drug delivery system:

1. Biocompatibility
2. Easy functionalization
3. Mimic biological environment
4. Efficient cellular uptake or cell adhesion
5. High drug loading efficiency
6. Control over the drug release for a long period of time

These polymeric systems act as a carrier for the drug molecules preventing their premature release or degradation in physiological environment before reaching the targeted site.[79] Both synthetic and natural polymers have been explored extensively towards drug delivery applications.

Table 1.1: Natural polymers used in Drug Delivery

Natural Polymers	
Protein-based	**Polysaccharides**
Gelatin [80, 81]	Alginate [82, 83]
Albumin [84, 85]	Agarose [86, 87]
Collagen [88, 89]	Hyaluronic acid [90, 91]
Silk [92, 93]	Dextran [94, 95]
	Cyclodextrins [96, 97]
	Chitosan [98, 99]
	Carrageenans [100, 101]

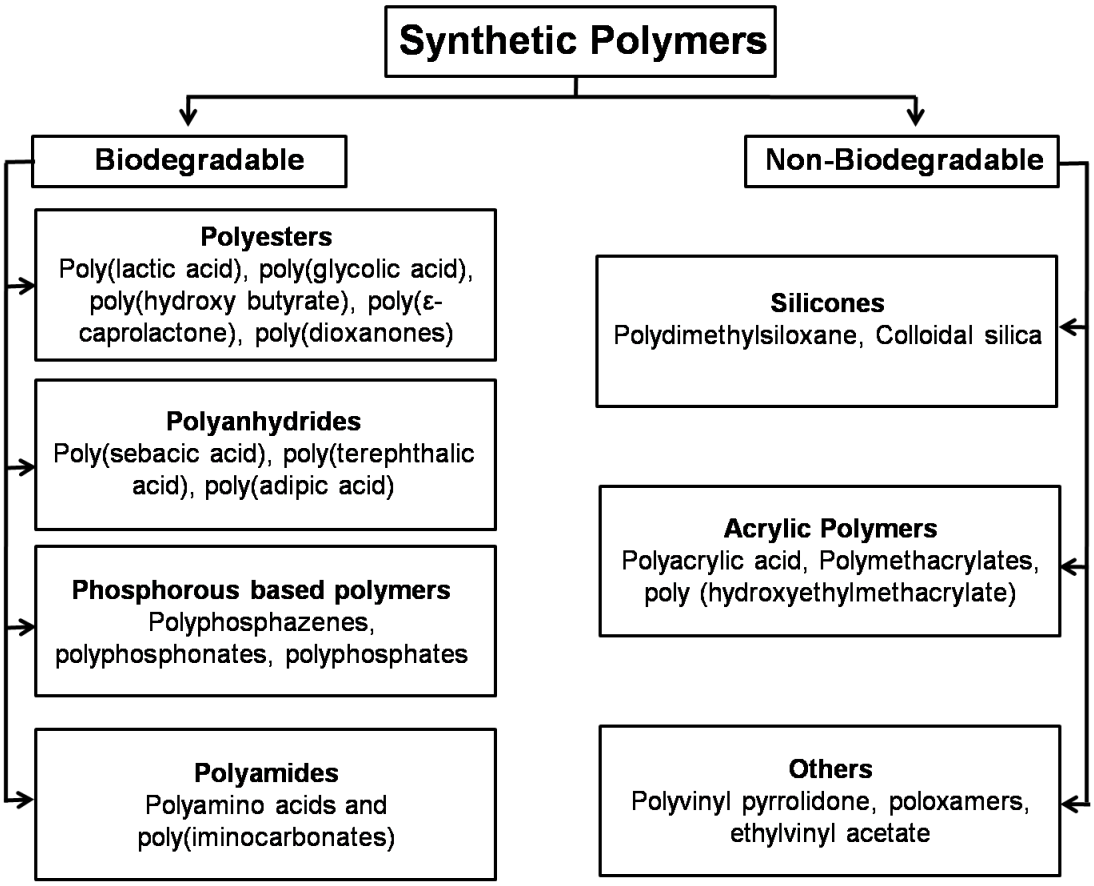

Figure 1.2. Synthetic polymers used in Drug Delivery[78, 102]

A few examples of natural and synthetic polymers are given in **Table 1.1** and **Figure 1.2** respectively. While natural polymers have an added advantage of inherent biodegradability and biocompatibility, a varied level of heterogeneity has led to the exploration of synthetic polymers for biological applications. These polymeric systems further can be used either in the form of implants or in the form of nano or micro particles/ assemblies that can be loaded with large amount of drug molecules. The drug molecules can be loaded in the polymeric systems either physically through diffusion or by covalent linking with functional groups present in the polymer backbone. The covalently linked drug can be released by the cleavage of covalent linkages after reaching the target site in certain conditions.

Smart or intelligent polymers have stimuli-responsive property wherein their properties such as volume, shape, size, colour, the hydrophilic/hydrophobic balance respond to various stimuli like, pH[103, 104], temperature[105, 106], redox[107], light, magnetic[108, 109] and electrical field[110, 111] etc. The stimuli- responsive property helps in the controlled release

of drugs at the desired rate..[112] Polymers that are responsive towards various stimuli are given in **Table 1.2**.

Table 1.2: Smart Polymeric Drug Delivery Systems

Stimulus	**Polymers**	**Ref**
Temperature	PLGA-PEG-PLGA, Chitosan-beta-glycerophosphate, lonoleic acid coupled with pluronic F-127, polybenzofulvene	[113-116]
pH	PEO-b-PPO-b-PEO, alginate with carboxymethyl chitosan, Poly(acrylamide)-g carrageenan and sodium alginate, Poly(n-isopropylacrylamide-copropylacrylic acid-co-butylacrylate)	[117-120]
Glucose responsive	Methacrylate derivatives of dextran and concanavellin, N,N-(dimethylacrylamide) and sulfadimethoxine monomer	[121, 122]
Light	poly(lactide-co-glycolide), N-isopropylacrylamide and sodium acrylate, pluronic F-127	[123-125]
Redox	Polymethacrylic acid, poly(ethylene glycol)–SS–poly(2-(N,N-dimethylamino) ethyl methacrylate) with α-cyclodextrin (PRX–SS–PDMAEMA), poly(ethylene glycol)-b-poly(lysine)-b-poly(caprolactone), poly(ethylene glycol)-bl-poly(propylene sulfide)	[126-129]
Ultrasound	Poly DL lactide-co-glycolide, pluronic P105, PLA-b-PEG	[130-132]
Magnetic Field	Polyvinyl alcohol containing Fe_3O_4, Alginate with iron oxide particles, poly(ethylene glycol)/ methacrylic acid with Fe_3O_4	[133-135]
Electric Field	poly(2-acrylamido-2-methylpropane sulfonic acid-co-n-butylmethacrylate), sodium alginate/ polyacrylic acid composites, polyvinyl alocohol/ polyacrylic acid	[111, 136, 137]

2. Characterization Techniques used in the thesis work

2.1 Rheology

The rheological properties such as, solution viscosity, linear visco-elasticity, stress relaxation of APs/HMPs and hydrogels can be measured using rheometer. In rheometry, the sample is subjected to either dynamic (sinusoidal) or steady (linear) shear force and the response of the torque is measured by the transducer. Different geometries are used depending upon the consistency of the polymer solution viscosity. For example, parallel plate and cone and plate geometries are used for viscosity, $\eta > 10$ m Pa.s, couette (cup-bob) geometry is used when the $\eta < 10$ m Pa.s, and double wall couette is used when the $\eta < 1$ m Pa.s.

According to Hook's law for a perfectly elastic solid material the stress (σ) is related to the deformation (γ, strain) via a constant, elastic modulus (G), and is given as:

$$\sigma = G\gamma \quad (1)$$

Whereas, for a perfectly viscous fluid, Newton's law states that, shear stress (σ) is related to the deformation (γ, strain) via a constant, viscosity coefficient (η), and is given as:

$$\sigma = \eta\gamma \quad (2)$$

APs/HMPs containing long molecular chains exhibit properties of both elastic solids as well as Newtonian fluids and thus possess visco-elastic properties. Depending upon the concentration of APs/HMPs, different rheological properties can be studied. In dilute solution regime (C<C*), intramolecular associations are more dominant and in high polymer concentrations (C*>C), i.e. above overlap concentration, the polymer chains forms loops and bridges. Shear thinning/ thickening behaviour and zero shear viscosity can be obtained from steady shear experiments.

In dynamic experiments, such as oscillatory shear flow, a sinusoidal varying strain of amplitude, γ_o is applied to the sample, which is explained with the equation:

$$\gamma(t) = \gamma_o \sin(\omega t) \quad (3)$$

Where γ is the shear strain, γ_o is the amplitude, ω is the frequency of oscillation and t is time. It is possible to measure the viscoelastic properties of the polymer without

affecting the networks at very low amplitude of strain and this regime is known as linear viscoelastic regime (LVR). Stress generated due to sinusoidal shear will again be sinusoidal and is expressed as:

$$\tau(t) = \tau_o \sin(\omega t + \delta) \quad (4)$$

Where τ_o is the stress amplitude and δ is phase angle. For a perfectly elastic solid, both stress and strain will be in phase ($\delta = 0^o$), while for a perfectly viscous material, stress and strain will be completely out of phase ($\delta = 90^o$). When a viscoelastic material is subjected to sinusoidal oscillatory stress, there exist a phase lag between strain and stress wave, which is defined by a phase angle (δ) and it varies from 0 to 90 °. An oscillating stress and strain response (**Figure 1.3**) for a viscoelastic material is as shown in expressed as:

$$\tau(t) = \gamma_o [G'(\omega) \sin(\omega t) + G''(\omega)\cos(\omega t)] \quad (5)$$

Where,

$$G' = \frac{\tau_o}{\gamma_o}\cos(\delta)$$

$$G'' = \frac{\tau_o}{\gamma_o}\sin(\delta)$$

Where G' is elastic or storage modulus and G" is loss modulus. The two moduli are generally used to study the viscoelastic property of the polymer solutions. The moduli depend only on the frequency in linear range of deformation whereas they depend upon both strain and frequency in the non linear regime. The complex viscosity (η*) is given by the equation:

$$\eta^*(\omega) = \frac{G^*}{\omega} = \sqrt{(\frac{G'}{\omega})^2 + (\frac{G''}{\omega})^2} \quad (6)$$

Where, G* is the complex modulus and is given as $G^* = \sqrt{G'^2 + G''^2}$ and ω is the frequency of deformation. In viscoelastic material, at lower frequencies liquid-like response is observed where the loss modulus (G") is higher than the storage modulus (G') while at higher frequencies, the storage modulus (G') dominates over the loss modulus (G").

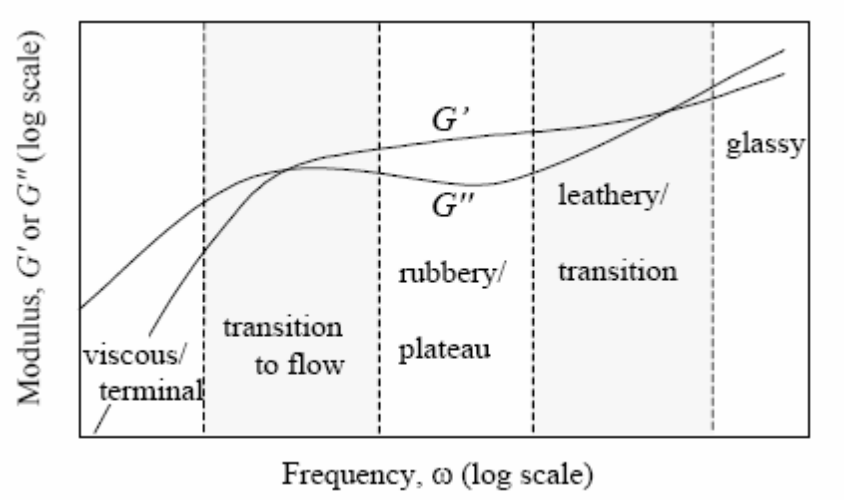

Figure 1.3. Oscillatory test response of viscoelastic material at a range of frequencies

The viscoelastic properties of APs/HMPs provide valuable information about the associating behaviour which helps in designing APs for suitable applications.

2.2 Light Scattering

When light passes through a solution containing solute particles of size higher than the wavelength of light, then part of the light changes its path or get scattered. In such a case, the transmitted light intensity decreases exponentially depending upon the thickness of the particles it passes through. The scattered light is analysed either in terms of the fluctuations or in terms of the intensity. The light detector is used to measure the scattered light at specified scattering angles.

2.2.1 *Static Light Scattering (SLS)*

It measures the intensity of the light scattered by the solution at a single time. Information like molecular weight, size of the particles and interaction between the particles can be obtained from SLS. Zimm derived the relationship between the concentration and intensity of the scattered light as:

$$\frac{KC}{R_\theta^O} = \frac{1}{M_w} + 2\,A_2\,c \qquad (7)$$

Where, C = concentration, M_w = weight average molecular weight, R_θ^O = Rayleigh ratio, A_2 = second virial coefficient, constant K which is defined as:

$$K = \frac{4\Pi^2 n^2 (\frac{dn}{dc})^2}{N_A \lambda_o^4} \quad (8)$$

Where, n = refractive index, dn/dc = refractive index increment, λ_0 = wavelength of the incident light. P (θ) describes the large particle size effect and it is a ratio of actual scattering (i_θ) and the scattering that would occur off small particles (i_θ^0) as:

$$P(\Theta) = \frac{i_\theta}{i_\theta^0} = \frac{R_\theta}{R_\theta^0} \quad (9)$$

Where in R_θ^0 is the Rayleigh ratio and is defined as :

$$R_\theta^0 = \frac{r^2 i_\theta^0}{I_0} \quad (10)$$

Here, I_0 is the incident polarized light. Substituting all the values in Zimm equation (7), one can calculate the value of second virial (A_2) coefficient from the slope and the intercept gives the value of the molecular weight (M_w).

2.2.2 *Dynamic Light Scattering (DLS)*

Dynamic light scattering gives the information related to the size of the particles. Here, the measurement is performed generally at one scattering angle. Diffusion coefficient can be calculated from the DLS experiments which are a measure of the movement of the particles in a solution due to Brownian motion which in turn is

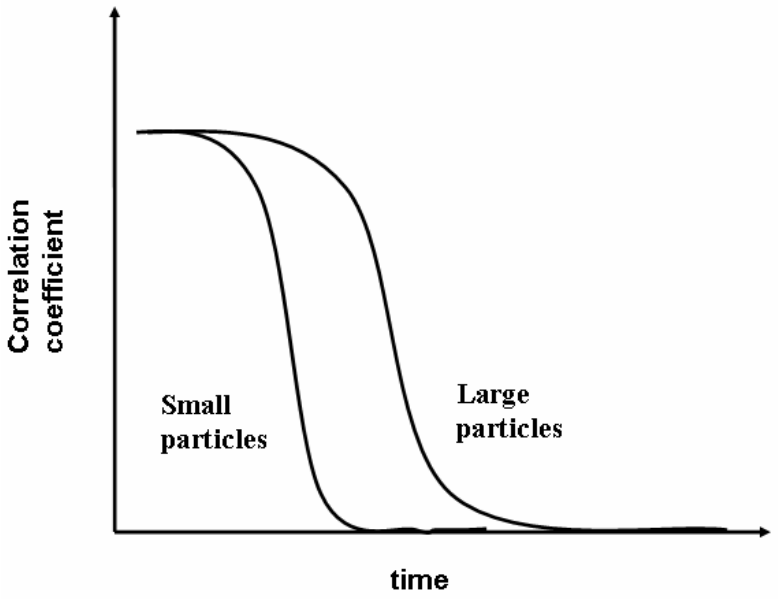

Figure 1.4. Autocorrelation function as a function of particle size

related to the size of the particles. This is performed by measuring the rate at which the intensity of the scattered light fluctuates, measured using digital autocorrelator and the rate of the intensity fluctuation depends upon the size of the particles. The smaller particles leads to intensity to fluctuate faster compared to the larger particles. The decay in the correlation indicates the mean size of the particles. For instance, if the size of the particles is larger, the correlation will persist for a longer time. On the other hand, the smaller particles diffuse rapidly and the correlation will decrease more quickly. **Figure 1.4** shows the decay of correlation coefficient with time for smaller and larger particles. The monodisperse samples show steeper lines whereas polydispersity is indicated by the extended decay. The wave vector that determines the length scale of the molecular motions is given by:

$$q = \frac{2\Pi n sin\left(\frac{\theta}{2}\right)}{\pi} \tag{11}$$

Where, n= refractive index, $\boldsymbol{\lambda}$= wavelength of radiation and Θ is the scattering angle. The correlation function is defined as:

$$G(\tau) = \int \frac{I(t)I(t+\tau)}{\langle I(t)\rangle^2} dt \tag{12}$$

The correlation function shows single exponential decay under ideal conditions and is expressed as:

$$G(\tau) = 1 + \beta \exp(-D_q^2 \tau) \tag{13}$$

Where D_q^2 is the diffusion coefficient of the molecule and β is the ratio of coherent signal to incoherent noise. The Stokes-Einstein relation relates the diffusion coefficient to the hydrodynamic diameter (d_H) of the particle as:

$$D = \frac{K_B T}{3\pi\eta\, d_H} \tag{14}$$

Where η = viscosity, K_B = Boltzmann constant and T = absolute temperature

2.3 2-D NMR Spectroscopy

NMR techniques have been explored extensively for the study of polymer structures, their assemblies and interactions among various groups.[138] Jeener in 1971 first proposed the 2D NMR spectroscopy[139] and the first experiments were performed

by Ernst et al in 1976.[140] 2D NMR spectroscopy provides much more detailed information about the molecules compared to that of 1D NMR spectroscopy especially in large molecules like polymers, proteins and other macromolecules.[141-143] As compared to 1D NMR spectroscopy having single frequency scale in horizontal direction, 2D NMR spectra contains two frequency scales at right angle to each other.[144] Different 2D experiments contain different radiofrequency pulses and delays. In 1D NMR studies a pulse of 90^{o} is applied in a plane perpendicular to the magnetic field and the time dependent voltage is measured and the data is acquired in a single time period and thus the final spectrum has a single frequency scale. In a 2D NMR spectrum, in addition to the free induction decay a second variable is introduced. With respect to the second time variable the data are transformed to obtain spectrum having two frequency coordinates.[145] Correlation experiments are one of the common forms of 2D NMR spectroscopy which shows the chemical shift positions of nuclei that interact with each other. The interactions could be due to chemical exchange, J coupling or through dipole-dipole interactions. They are further divided in to Homonuclear 2D NMR spectroscopy and Heteronuclear 2D NMR spectroscopy depending on the interaction between the same kinds of nuclei (^{1}H-^{1}H) or interaction between different nuclei (^{1}H-^{13}C).[144, 146] A few examples of Homonuclear 2D NMR spectroscopy techniques are Nuclear Overhauser effect spectroscopy (NOESY), Correlation Spectroscopy (COSY), Exclusive correlation spectroscopy (ECOSY) and examples of Heteronuclear 2D NMR Spectroscopy are Heteronuclear Overhauser Effect spectroscopy (HOESY), Heteronuclear single-quantum correlation spectroscopy (HSQC) etc.[146, 147] In this thesis work, we have performed two important 2D NMR spectroscopy experiments that revealed the details of interactions among the various groups in thermo-associating polymers which we have synthesised.

2.3.1 *NOESY*

NOESY (Nuclear Overhauser Effect Spectroscopy) make use of the nuclear Overhauser effect in which the spin-spin coupling takes place among atoms that are present in close proximity to each other through space rather than through bond coupling.[148] In NOESY spectrum, the ^{1}H nuclei interacting with each other

through dipole relaxation will appear as cross peaks. This is very similar to COSY spectrum (interactions between the nuclei chemically bonded to each other) with an exception that additional cross peaks will appear that arises from the interaction between nuclei through space. Generally, nuclei which are present within a distance of 5 Å could take place in spatial interaction in NOESY spectrum. NOESY spectroscopy is more useful for the study of large molecules like polymers as they tend to tumble slowly in solution thereby giving more time for the nuclear Overhauser effect to develop.[149] Whereas, in the case of small molecules this phenomenon is seldom observed since tumbling takes place very quickly to allow any significant development of interactions through space. As the cross peaks in NOESY arises through special interactions, it is used to study the configurations and conformations of molecules.[150] In our study, we have used this technique to show the development of strong hydrophobic interactions in thermo-associating polymers as a function of temperature.

2.3.2 *HSQC*

HSQC (Heteronuclear single quantum correlation spectroscopy) is used to determine proton-carbon single bond correlations. It is a 2D spectrum in which one of the coordinate is plotted with one type of nucleus (^{1}H) and the other coordinate with a other type of nucleus (^{13}C or ^{15}N) coupled with each other.[151] In this experiment, two different nuclei spin coupled with each other which facilitates identifying carbons and protons that are directly bonded to each other. Here, the transfer of magnetization form proton to the carbon takes place via INEPT (Insensitive nuclei enhanced by polarization transfer) and after a delay time (t_1), the magnetization is transferred back to the proton via retro-INEPT step wherein the signal is then recorded.[149, 152]

2.4 MTT Assay

MTT (3-(4,5-dimethylthiazol-2-yl)-2,5-diphenyl tetrazolium bromide) is a tetrazolium based colorimetric assay which is used to evaluate the metabolic activity of the cells in contact with the material. NAD(P)H cellular oxidoreductases enzymes present inside the living cells reduce the tetrazolium dye MTT to insoluble formazan crystals (**Figure 1.5**) which are purple in color which in turn denotes the cell

viability. The formazan crystals when dissolved in DMSO give an absorbance maximum at 570 nm. We have performed MTT assay on MDA-MB-231 breast cancer cell line. The cells were incubated at 37 °C in air with 5 % CO_2 for a minimum of 24 h. Confluent monolayer were trypsinize and were seeded into 96 well plate with a density of $1x10^5$ cells/well. Growth medium and the nanoparticles were added for another 24 h. MTT reagent was added and the formazan crystals formed after 4 h were dissolved in DMSO and the absorbance was recorded at 570 nm immediately to calculate cell viability.

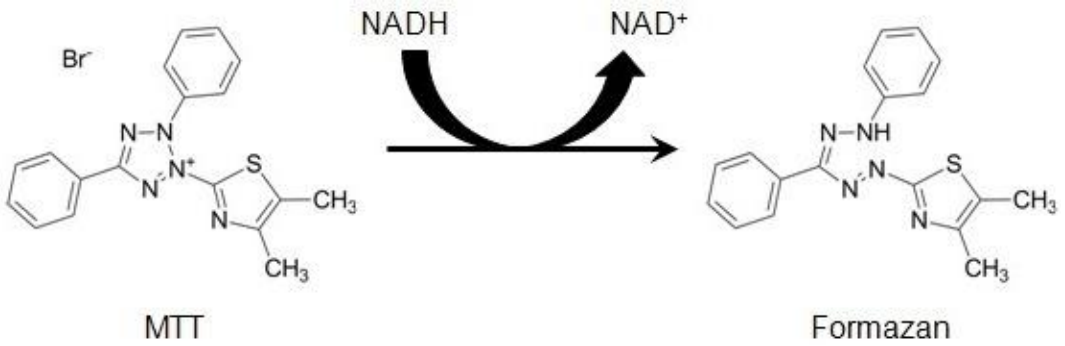

Figure 1.5. Conversion of MTT to formazan

References

[1] J.E. Glass, Polymers in aqueous media: performance through association, ACS Publications, 1989.

[2] J.E. Glass, Hydrophilic polymers: performance with environmental acceptance, ACS Publications, 1996.

[3] A. Shedge, Hydrophobically modified Water soluble polymers: syntheses, characterization & rheology, in, CSIR-National Chemical Laboratory, Pune, India, 2012.

[4] A.S. Shedge, A.K. Lele, P.P. Wadgaonkar, D. Hourdet, P. Perrin, C. Chassenieux, M.V. Badiger, Hydrophobically Modified Poly (acrylic acid) Using 3-Pentadecylcyclohexylamine: Synthesis and Rheology, Macromolecular chemistry and Physics, 206 (2005) 464-472.

[5] P. Rey, R. Varsanik, Water Soluble Polymers: Beauty with Performance, Advance in Chemistry Series, 213 (1986).

[6] G.A. Stahl, D. Schulz, Water-soluble polymers for petroleum recovery, Springer Science & Business Media, 2012.

[7] U.P. Strauss, E.G. Jackson, Polysoaps. I. Viscosity and solubilization studies on an n-dodecyl bromide addition compound of poly-2-vinylpyridine, Journal of Polymer Science Part A: Polymer Chemistry, 6 (1951) 649-659.

[8] I.W. Hamley, V. Castelletto, J. Fundin, Z. Yang, C. Price, C. Booth, A Small-Angle X-ray Scattering Study of the Structure of Gels Formed by Poly (oxyethylene)− Poly (oxypropylene) Diblock Copolymers in Water, Langmuir, 18 (2002) 1051-1055.

[9] G. Wanka, H. Hoffmann, W. Ulbricht, Phase diagrams and aggregation behavior of poly (oxyethylene)-poly (oxypropylene)-poly (oxyethylene) triblock copolymers in aqueous solutions, Macromolecules, 27 (1994) 4145-4159.

[10] P. Alexandridis, T.A. Hatton, Poly (ethylene oxide)瑎poly (propylene oxide)瑎poly (ethylene oxide) block copolymer surfactants in aqueous solutions and at interfaces: thermodynamics, structure, dynamics, and modeling, Colloids and Surfaces A: Physicochemical and Engineering Aspects, 96 (1995) 1-46.

[11] K. Mortensen, Cubic Phase in a Connected Micellar Network of Poly (propylene oxide)− Poly (ethylene oxide)− Poly (propylene oxide) Triblock Copolymers in Water, Macromolecules, 30 (1997) 503-507.

[12] S. Caillol, S. Lecommandoux, A.-F. Mingotaud, M. Schappacher, A. Soum, N. Bryson, R. Meyrueix, Synthesis and Self-Assembly Properties of Peptide− Polylactide Block Copolymers, Macromolecules, 36 (2003) 1118-1124.

[13] A. Harada, S. Cammas, K. Kataoka, Stabilized α-helix structure of poly (l-lysine)-block-poly (ethylene glycol) in aqueous medium through supramolecular assembly, Macromolecules, 29 (1996) 6183-6188.

[14] A. Lavasanifar, J. Samuel, G.S. Kwon, Poly (ethylene oxide)-block-poly (L-amino acid) micelles for drug delivery, Advanced drug delivery reviews, 54 (2002) 169-190.

[15] C. Allen, J. Han, Y. Yu, D. Maysinger, A. Eisenberg, Polycaprolactone–b-poly (ethylene oxide) copolymer micelles as a delivery vehicle for dihydrotestosterone, Journal of Controlled Release, 63 (2000) 275-286.

[16] Z. Gan, T.F. Jim, M. Li, Z. Yuer, S. Wang, C. Wu, Enzymatic biodegradation of poly (ethylene oxide-b-ε-caprolactone) diblock copolymer and its potential biomedical applications, Macromolecules, 32 (1999) 590-594.

[17] S. Hagan, A. Coombes, M. Garnett, S. Dunn, M. Davies, L. Illum, S. Davis, S. Harding, S. Purkiss, P. Gellert, Polylactide− poly (ethylene glycol) copolymers as drug delivery systems. 1. characterization of water dispersible micelle-forming systems, Langmuir, 12 (1996) 2153-2161.

[18] J. Lee, E.C. Cho, K. Cho, Incorporation and release behavior of hydrophobic drug in functionalized poly (D, L-lactide)-block–poly (ethylene oxide) micelles, Journal of Controlled Release, 94 (2004) 323-335.

[19] C. Deng, H. Tian, P. Zhang, J. Sun, X. Chen, X. Jing, Synthesis and characterization of RGD peptide grafted poly (ethylene glycol)-b-poly (L-lactide)-b-poly (L-glutamic acid) triblock copolymer, Biomacromolecules, 7 (2006) 590-596.

[20] K.M. Huh, Y.W. Cho, K. Park, PLGA-PEG block copolymers for drug formulations, Drug Deliv Technol, 3 (2003) 42-44.

[21] C. Hoskins, P.K. Thoo-Lin, W.P. Cheng, A review on comb-shaped amphiphilic polymers for hydrophobic drug solubilization, (2011).

[22] Y. Kimura, K. Shirotani, H. Yamane, T. Kitao, Copolymerization of 3-(S)-[(benzyloxycarbonyl) methyl]-1, 4-dioxane-2, 5-dione and L-lactide: a facile synthetic method for functionalized bioabsorbable polymer, Polymer, 34 (1993) 1741-1748.

[23] Y. Kimura, K. Shirotani, H. Yamane, T. Kitao, Ring-opening polymerization of 3 (S)-[(benzyloxycarbonyl) methyl]-1, 4-dioxane-2, 5-dione: a new route to a poly (. alpha.-hydroxy acid) with pendant carboxyl groups, Macromolecules, 21 (1988) 3338-3340.

[24] Z. Zhang, D.W. Grijpma, J. Feijen, Thermo-sensitive transition of monomethoxy poly (ethylene glycol)-block-poly (trimethylene carbonate) films to micellar-like nanoparticles, Journal of controlled release, 112 (2006) 57-63.

[25] X. Zhang, H. Mei, C. Hu, Z. Zhong, R. Zhuo, Amphiphilic triblock copolycarbonates with poly (glycerol carbonate) as hydrophilic blocks, Macromolecules, 42 (2009) 1010-1016.

[26] J.W. Singer, B. Baker, P. De Vries, A. Kumar, S. Shaffer, E. Vawter, M. Bolton, P. Garzone, Poly-(l)-glutamic acid-paclitaxel (CT-2103)[XYOTAX™], a biodegradable polymeric drug conjugate, in: Polymer drugs in the clinical stage, Springer, (2004) 81-99.

[27] E. Auzenne, N.J. Donato, C. Li, E. Leroux, R.E. Price, D. Farquhar, J. Klostergaard, Superior therapeutic profile of poly-L-glutamic acid-paclitaxel copolymer compared with taxol in xenogeneic compartmental models of human ovarian carcinoma, Clinical cancer research, 8 (2002), 573-581.

[28] N. Schoemaker, C. Van Kesteren, H. Rosing, S. Jansen, M. Swart, J. Lieverst, D. Fraier, M. Breda, C. Pellizzoni, R. Spinelli, A phase I and pharmacokinetic study of MAG-CPT, a water-soluble polymer conjugate of camptothecin, British journal of cancer, 87 (2002), 608-614.

[29] R. Duncan, M. Vicent, F. Greco, R. Nicholson, Polymer–drug conjugates: towards a novel approach for the treatment of endrocine-related cancer, Endocrine-related cancer, 12 (2005), 189-199.

[30] T. Nakanishi, S. Fukushima, K. Okamoto, M. Suzuki, Y. Matsumura, M. Yokoyama, T. Okano, Y. Sakurai, K. Kataoka, Development of the polymer micelle carrier system for doxorubicin, Journal of Controlled Release, 74 (2001) 295-302.

[31] M.B. Dowling, R. Kumar, M.A. Keibler, J.R. Hess, G.V. Bochicchio, S.R. Raghavan, A self-assembling hydrophobically modified chitosan capable of reversible hemostatic action, Biomaterials, 32 (2011) 3351-3357.

[32] O. Inta, R. Yoksan, J. Limtrakul, Hydrophobically modified chitosan: A bio-based material for antimicrobial active film, Materials Science and Engineering: C, 42 (2014) 569-577.

[33] X. Dong, C. Liu, Preparation and characterization of self-assembled nanoparticles of hyaluronic acid-deoxycholic acid conjugates, Journal of Nanomaterials, 2010 (2010) 12.

[34] S. Ganesh, A.K. Iyer, D.V. Morrissey, M.M. Amiji, Hyaluronic acid based self-assembling nanosystems for CD44 target mediated siRNA delivery to solid tumors, Biomaterials, 34 (2013) 3489-3502.

[35] D. Roy, W.L. Brooks, B.S. Sumerlin, New directions in thermoresponsive polymers, Chemical Society Reviews, 42 (2013) 7214-7243.

[36] M.A. Ward, T.K. Georgiou, Thermoresponsive polymers for biomedical applications, Polymers, 3 (2011) 1215-1242.

[37] T.R. Hoare, D.S. Kohane, Hydrogels in drug delivery: progress and challenges, Polymer, 49 (2008) 1993-2007.

[38] A. Durand, D. Hourdet, Synthesis and thermoassociative properties in aqueous solution of graft copolymers containing poly (N-isopropylacrylamide) side chains, Polymer, 40 (1999) 4941-4951.

[39] D. Hourdet, F. L'alloret, R. Audebert, Reversible thermothickening of aqueous polymer solutions, Polymer, 35 (1994) 2624-2630.

[40] D. Hourdet, F. L'alloret, R. Audebert, Synthesis of thermoassociative copolymers, Polymer, 38 (1997) 2535-2547.

[41] L. Bromberg, Scaling of rheological properties of hydrogels from associating polymers, Macromolecules, 31 (1998) 6148-6156.

[42] L. Bromberg, Self-assembly in aqueous solutions of polyether-modified poly (acrylic acid), Langmuir, 14 (1998) 5806-5812.

[43] L. Bromberg, Polyether-modified poly (acrylic acid): synthesis and applications, Industrial & engineering chemistry research, 37 (1998) 4267-4274.

[44] G. Bokias, Y. Mylonas, G. Staikos, G. Bumbu, C. Vasile, Synthesis and aqueous solution properties of novel thermoresponsive graft copolymers based on a carboxymethylcellulose backbone, Macromolecules, 34 (2001) 4958-4964.

[45] H. Zhang, A. Patel, A.K. Gaharwar, S.M. Mihaila, G. Iviglia, S. Mukundan, H. Bae, H. Yang, A. Khademhosseini, Hyperbranched polyester hydrogels with controlled drug release and cell adhesion properties, Biomacromolecules, 14 (2013) 1299-1310.

[46] D. Buenger, F. Topuz, J. Groll, Hydrogels in sensing applications, Progress in Polymer Science, 37 (2012) 1678-1719.

[47] L. Ionov, Hydrogel-based actuators: possibilities and limitations, Materials Today, 17 (2014) 494-503.

[48] B. Kim, Y. Lee, K. Lee, W.-G. Koh, Immobilization of enzymes within hydrogel microparticles to create optical biosensors for the detection of organophosphorus compounds, Current Applied Physics, 9 (2009), 225-228.

[49] K.Y. Lee, D.J. Mooney, Hydrogels for tissue engineering, Chemical reviews, 101 (2001) 1869-1880.

[50] A.S. Hoffman, Hydrogels for biomedical applications, Advanced drug delivery reviews, 64 (2012) 18-23.

[51] J.A. Hunt, R. Chen, T. van Veen, N. Bryan, Hydrogels for tissue engineering and regenerative medicine, Journal of Materials Chemistry B, 2 (2014) 5319-5338.

[52] O. Wichterle, D. Lim, Hydrophilic gels for biological use, Nature, 185 (1960) 117-118.

[53] N. Kashyap, N. Kumar, M.R. Kumar, Hydrogels for pharmaceutical and biomedical applications, Critical Reviews™ in Therapeutic Drug Carrier Systems, 22 (2005).

[54] S. Venkatesh, M.E. Byrne, N.A. Peppas, J.Z. Hilt, Applications of biomimetic systems in drug delivery, Expert opinion on drug delivery, 2 (2005) 1085-1096.

[55] Y. Qiu, K. Park, Environment-sensitive hydrogels for drug delivery, Advanced drug delivery reviews, 53 (2001) 321-339.

[56] P. Gupta, K. Vermani, S. Garg, Hydrogels: from controlled release to pH-responsive drug delivery, Drug discovery today, 7 (2002) 569-579.

[57] S.-Y. Choh, D. Cross, C. Wang, Facile synthesis and characterization of disulfide-cross-linked hyaluronic acid hydrogels for protein delivery and cell encapsulation, Biomacromolecules, 12 (2011) 1126-1136.

[58] J. Zhang, F. Yang, H. Shen, D. Wu, Controlled formation of microgels/nanogels from a disulfide-linked core/shell hyperbranched polymer, ACS Macro Letters, 1 (2012) 1295-1299.

[59] A.N. Zelikin, Q. Li, F. Caruso, Disulfide-stabilized poly (methacrylic acid) capsules: formation, cross-linking, and degradation behavior, Chemistry of materials, 20 (2008) 2655-2661.

[60] C. Wang, R.R. Varshney, D.-A. Wang, Therapeutic cell delivery and fate control in hydrogels and hydrogel hybrids, Advanced drug delivery reviews, 62 (2010) 699-710.

[61] E.J. Oh, K. Park, K.S. Kim, J. Kim, J.-A. Yang, J.-H. Kong, M.Y. Lee, A.S. Hoffman, S.K. Hahn, Target specific and long-acting delivery of protein, peptide, and nucleotide therapeutics using hyaluronic acid derivatives, Journal of Controlled Release, 141 (2010) 2-12.

[62] I. Strehin, Z. Nahas, K. Arora, T. Nguyen, J. Elisseeff, A versatile pH sensitive chondroitin sulfate–PEG tissue adhesive and hydrogel, Biomaterials, 31 (2010) 2788-2797.

[63] S. Wang, Ordered mesoporous materials for drug delivery, Microporous and mesoporous materials, 117 (2009) 1-9.

[64] M. Bouchoucha, M.-F. Côté, C. René, M.-A. Fortin, F. Kleitz, Size-controlled functionalized mesoporous silica nanoparticles for tunable drug release and enhanced anti-tumoral activity, Chem. Mater, 28 (2016) 4243-4258.

[65] J.L. Vivero-Escoto, I.I. Slowing, B.G. Trewyn, V.S.Y. Lin, Mesoporous silica nanoparticles for intracellular controlled drug delivery, Small, 6 (2010) 1952-1967.

[66] J. Lu, M. Liong, Z. Li, J.I. Zink, F. Tamanoi, Biocompatibility, biodistribution, and drug-delivery efficiency of mesoporous silica nanoparticles for cancer therapy in animals, Small, 6 (2010) 1794-1805.

[67] L. Ma'mani, S. Nikzad, H. Kheiri-Manjili, S. al-Musawi, M. Saeedi, S. Askarlou, A. Foroumadi, A. Shafiee, Curcumin-loaded guanidine functionalized PEGylated I3ad mesoporous silica nanoparticles KIT-6: Practical strategy for the breast cancer therapy, European journal of medicinal chemistry, 83 (2014) 646-654.

[68] J. Lu, Z. Li, J.I. Zink, F. Tamanoi, In vivo tumor suppression efficacy of mesoporous silica nanoparticles-based drug-delivery system: enhanced efficacy by folate modification, Nanomedicine: Nanotechnology, Biology and Medicine, 8 (2012) 212-220.

[69] Q. Zhang, K.G. Neoh, L. Xu, S. Lu, E.T. Kang, R. Mahendran, E. Chiong, Functionalized mesoporous silica nanoparticles with mucoadhesive and sustained drug release properties for potential bladder cancer therapy, Langmuir, 30 (2014) 6151-6161.

[70] L. Yuan, Q. Tang, D. Yang, J.Z. Zhang, F. Zhang, J. Hu, Preparation of pH-responsive mesoporous silica nanoparticles and their application in controlled drug delivery, The Journal of Physical Chemistry C, 115 (2011) 9926-9932.

[71] M. Kar, N. Tiwari, M. Tiwari, M. Lahiri, S.S. Gupta, Poly-L-Arginine Grafted Silica Mesoporous Nanoparticles for Enhanced Cellular Uptake and their Application in DNA Delivery and Controlled Drug Release, Particle & Particle Systems Characterization, 30 (2013) 166-179.

[72] M. Zhu, Y. Zhu, L. Zhang, J. Shi, Preparation of chitosan/mesoporous silica nanoparticle composite hydrogels for sustained co-delivery of biomacromolecules and small chemical drugs, Science and technology of advanced materials, 14 (2013) 045005.

[73] Q. Zhao, H. Geng, Y. Wang, Y. Gao, J. Huang, Y. Wang, J. Zhang, S. Wang, Hyaluronic acid oligosaccharide modified redox-responsive mesoporous silica nanoparticles for targeted drug delivery, ACS applied materials & interfaces, 6 (2014) 20290-20299.

[74] M. Gary-Bobo, Y. Mir, C. Rouxel, D. Brevet, I. Basile, M. Maynadier, O. Vaillant, O. Mongin, M. Blanchard-Desce, A. Morère, Mannose-functionalized mesoporous silica nanoparticles for efficient two-photon photodynamic therapy of solid tumors, Angewandte Chemie, 123 (2011) 11627-11631.

[75] L. Hu, C. Sun, A. Song, D. Chang, X. Zheng, Y. Gao, T. Jiang, S. Wang, Alginate encapsulated mesoporous silica nanospheres as a sustained drug delivery system for the poorly water-soluble drug indomethacin, asian journal of pharmaceutical sciences, 9 (2014) 183-190.

[76] W.B. Liechty, D.R. Kryscio, B.V. Slaughter, N.A. Peppas, Polymers for drug delivery systems, Annual review of chemical and biomolecular engineering, 1 (2010) 149-173.

[77] D. Jones, Pharmaceutical applications of polymers for drug delivery, iSmithers Rapra Publishing, 2004.

[78] O. Pillai, R. Panchagnula, Polymers in drug delivery, Current opinion in chemical biology, 5 (2001) 447-451.

[79] P. Agrawal, Significance of polymers in drug delivery system, J Pharmacovigil, 3 (2014) 127.

[80] M. Foox, M. Zilberman, Drug delivery from gelatin-based systems, Expert opinion on drug delivery, 12 (2015) 1547-1563.

[81] M. Santoro, A.M. Tatara, A.G. Mikos, Gelatin carriers for drug and cell delivery in tissue engineering, Journal of controlled release, 190 (2014) 210-218.

[82] H.H. Tønnesen, J. Karlsen, Alginate in drug delivery systems, Drug development and industrial pharmacy, 28 (2002) 621-630.

[83] A. Sosnik, Alginate particles as platform for drug delivery by the oral route: state-of-the-art, ISRN pharmaceutics, 2014.

[84] M.T. Larsen, M. Kuhlmann, M.L. Hvam, K.A. Howard, Albumin-based drug delivery: harnessing nature to cure disease, Molecular and cellular therapies, 4 (2016) 3.

[85] Y. Ishima, T. Maruyama, Human serum albumin as carrier in drug delivery systems, Yakugaku zasshi: Journal of the Pharmaceutical Society of Japan, 136 (2016) 39-47.

[86] T. Marras-Marquez, J. Peña, M. Veiga-Ochoa, Agarose drug delivery systems upgraded by surfactants inclusion: critical role of the pore architecture, Carbohydrate polymers, 103 (2014) 359-368.

[87] N. Wang, X.S. Wu, Preparation and characterization of agarose hydrogel nanoparticles for protein and peptide drug delivery, Pharmaceutical development and technology, 2 (1997) 135-142.

[88] M.G. Albu, I. Titorencu, M.V. Ghica, Collagen-based drug delivery systems for tissue engineering, in: Biomaterials Applications for Nanomedicine, InTech, 2011.

[89] R. Khan, M.H. Khan, Use of collagen as a biomaterial: an update, Journal of Indian Society of Periodontology, 17 (2013) 539.

[90] G. Tripodo, A. Trapani, M.L. Torre, G. Giammona, G. Trapani, D. Mandracchia, Hyaluronic acid and its derivatives in drug delivery and imaging: recent advances and challenges, European Journal of Pharmaceutics and Biopharmaceutics, 97 (2015) 400-416.

[91] A.K. Yadav, P. Mishra, G.P. Agrawal, An insight on hyaluronic acid in drug targeting and drug delivery, Journal of drug targeting, 16 (2008) 91-107.

[92] T. Yucel, M.L. Lovett, D.L. Kaplan, Silk-based biomaterials for sustained drug delivery, Journal of Controlled Release, 190 (2014) 381-397.

[93] T. Wongpinyochit, B.F. Johnston, F.P. Seib, Manufacture and drug delivery applications of silk nanoparticles, JoVE (Journal of Visualized Experiments), (2016) 54669-54669.

[94] J. Varshosaz, Dextran conjugates in drug delivery, Expert Opinion on Drug Delivery, 9 (2012) 509-523.

[95] S.S. Dhaneshwar, K. Mini, N. Gairola, S. Kadam, Dextran: A promising macromolecular drug carrier, Indian journal of pharmaceutical sciences, 68 (2006) 705.

[96] R. Challa, A. Ahuja, J. Ali, R. Khar, Cyclodextrins in drug delivery: an updated review, Aaps Pharmscitech, 6 (2005) E329-E357.

[97] B. Gidwani, A. Vyas, A comprehensive review on cyclodextrin-based carriers for delivery of chemotherapeutic cytotoxic anticancer drugs, BioMed research international, 2015.

[98] C. Saikia, P. Gogoi, T. Maji, Chitosan: A promising biopolymer in drug delivery applications, J. Mol. Genet. Med. S, 4 (2015) 006.

[99] A. Bernkop-Schnürch, S. Dünnhaupt, Chitosan-based drug delivery systems, European Journal of Pharmaceutics and Biopharmaceutics, 81 (2012) 463-469.

[100] L. Li, R. Ni, Y. Shao, S. Mao, Carrageenan and its applications in drug delivery, Carbohydrate polymers, 103 (2014) 1-11.

[101] A. Kalsoom Khan, A.U. Saba, S. Nawazish, F. Akhtar, R. Rashid, S. Mir, B. Nasir, F. Iqbal, S. Afzal, F. Pervaiz, Carrageenan based bionanocomposites as drug delivery tool with special emphasis on the influence of ferromagnetic nanoparticles, Oxidative Medicine and Cellular Longevity, 2017 (2017).

[102] A.J. Gavasane, H.A. Pawar, Synthetic biodegradable polymers used in controlled drug delivery system: an overview, Clin Pharmacol Biopharm, 3 (2014) 2.

[103] J.E. Elliott, M. Macdonald, J. Nie, C.N. Bowman, Structure and swelling of poly (acrylic acid) hydrogels: effect of pH, ionic strength, and dilution on the crosslinked polymer structure, Polymer, 45 (2004) 1503-1510.

[104] Y. Xu, S. Bolisetty, M. Drechsler, B. Fang, J. Yuan, M. Ballauff, A.H. Müller, pH and salt responsive poly (N, N-dimethylaminoethyl methacrylate) cylindrical brushes and their quaternized derivatives, Polymer, 49 (2008) 3957-3964.

[105] J. Kobayashi, T. Okano, Fabrication of a thermoresponsive cell culture dish: a key technology for cell sheet tissue engineering, Science and technology of advanced materials, 11 (2010) 014111.

[106] T. Takezawa, Y. Mori, K. Yoshizato, Cell culture on a thermo-responsive polymer surface, Nature Biotechnology, 8 (1990) 854-856.

[107] R.L. McCarley, Redox-responsive delivery systems, Annual review of analytical chemistry, 5 (2012) 391-411.

[108] C. Plank, O. Zelphati, O. Mykhaylyk, Magnetically enhanced nucleic acid delivery. Ten years of magnetofection—Progress and prospects, Advanced drug delivery reviews, 63 (2011) 1300-1331.

[109] T.-Y. Liu, S.-H. Hu, T.-Y. Liu, D.-M. Liu, S.-Y. Chen, Magnetic-sensitive behavior of intelligent ferrogels for controlled release of drug, Langmuir, 22 (2006) 5974-5978.

[110] J. Ge, E. Neofytou, T.J. Cahill III, R.E. Beygui, R.N. Zare, Drug release from electric-field-responsive nanoparticles, ACS nano, 6 (2011) 227-233.

[111] I.C. Kwon, Y.H. Bae, T. Okano, S.W. Kim, Drug release from electric current sensitive polymers, Journal of Controlled Release, 17 (1991) 149-156.

[112] H.P. James, R. John, A. Alex, K. Anoop, Smart polymers for the controlled delivery of drugs–a concise overview, Acta Pharmaceutica Sinica B, 4 (2014) 120-127.

[113] K. Li, L. Yu, X. Liu, C. Chen, Q. Chen, J. Ding, A long-acting formulation of a polypeptide drug exenatide in treatment of diabetes using an injectable block copolymer hydrogel, Biomaterials, 34 (2013) 2834-2842.

[114] C.L. Hastings, H.M. Kelly, M.J. Murphy, F.P. Barry, F.J. O'brien, G.P. Duffy, Development of a thermoresponsive chitosan gel combined with human mesenchymal stem cells and desferrioxamine as a multimodal pro-angiogenic therapeutic for the treatment of critical limb ischaemia, Journal of controlled release, 161 (2012) 73-80.

[115] W.K. Bae, M.S. Park, J.H. Lee, J.E. Hwang, H.J. Shim, S.H. Cho, D.-E. Kim, H.M. Ko, C.-S. Cho, I.-K. Park, Docetaxel-loaded thermoresponsive conjugated linoleic acid-incorporated poloxamer hydrogel for the suppression of peritoneal metastasis of gastric cancer, Biomaterials, 34 (2013) 1433-1441.

[116] M. Licciardi, G. Amato, A. Cappelli, M. Paolino, G. Giuliani, B. Belmonte, C. Guarnotta, G. Pitarresi, G. Giammona, Evaluation of thermoresponsive properties and biocompatibility of polybenzofulvene aggregates for leuprolide delivery, International journal of pharmaceutics, 438 (2012) 279-286.

[117] L. Zhao, L. Zhu, F. Liu, C. Liu, Q. Wang, C. Zhang, J. Li, J. Liu, X. Qu, Z. Yang, pH triggered injectable amphiphilic hydrogel containing doxorubicin and paclitaxel, International journal of pharmaceutics, 410 (2011) 83-91.

[118] I.M. El-Sherbiny, Enhanced pH-responsive carrier system based on alginate and chemically modified carboxymethyl chitosan for oral delivery of protein drugs: preparation and in-vitro assessment, Carbohydrate Polymers, 80 (2010) 1125-1136.

[119] R.V. Kulkarni, R. Boppana, G.K. Mohan, S. Mutalik, N.V. Kalyane, pH-responsive interpenetrating network hydrogel beads of poly (acrylamide)-g-carrageenan and sodium alginate for intestinal targeted drug delivery: Synthesis, in vitro and in vivo evaluation, Journal of colloid and interface science, 367 (2012) 509-517.

[120] J.C. Garbern, E. Minami, P.S. Stayton, C.E. Murry, Delivery of basic fibroblast growth factor with a pH-responsive, injectable hydrogel to improve angiogenesis in infarcted myocardium, Biomaterials, 32 (2011) 2407-2416.

[121] R. Yin, Z. Tong, D. Yang, J. Nie, Glucose and pH dual-responsive concanavalin A based microhydrogels for insulin delivery, International journal of biological macromolecules, 49 (2011) 1137-1142.

[122] S.I. Kang, Y.H. Bae, A sulfonamide based glucose-responsive hydrogel with covalently immobilized glucose oxidase and catalase, Journal of Controlled Release, 86 (2003) 115-121.

[123] J. You, R. Shao, X. Wei, S. Gupta, C. Li, Near-infrared light triggers release of paclitaxel from biodegradable microspheres: photothermal effect and enhanced antitumor activity, Small, 6 (2010) 1022-1031.

[124] A. Suzuki, T. Ishii, Y. Maruyama, Optical switching in polymer gels, Journal of Applied Physics, 80 (1996) 131-136.

[125] A.P. Goodwin, J.L. Mynar, Y. Ma, G.R. Fleming, J.M. Fréchet, Synthetic micelle sensitive to IR light via a two-photon process, Journal of the American Chemical Society, 127 (2005) 9952-9953.

[126] Y. Yan, Y. Wang, J.K. Heath, E.C. Nice, F. Caruso, Cellular association and cargo release of redox-responsive polymer capsules mediated by exofacial thiols, Advanced Materials, 23 (2011) 3916-3921.

[127] W. Yuan, H. Zou, W. Guo, T. Shen, J. Ren, Supramolecular micelles with dual temperature and redox responses for multi-controlled drug release, Polymer Chemistry, 4 (2013) 2658-2661.

[128] T. Thambi, V. Deepagan, H. Ko, D.S. Lee, J.H. Park, Bioreducible polymersomes for intracellular dual-drug delivery, Journal of Materials Chemistry, 22 (2012) 22028-22036.

[129] A.J. Van Der Vlies, U. Hasegawa, J.A. Hubbell, Reduction-sensitive tioguanine prodrug micelles, Molecular pharmaceutics, 9 (2012) 2812-2818.

[130] M. Enayati, D.a. Mohazey, M. Edirisinghe, E. Stride, Ultrasound-stimulated drug release from polymer micro and nanoparticles, Bioinspired, Biomimetic and Nanobiomaterials, 2 (2013) 3-10.

[131] G.A. Husseini, N.Y. Rapoport, D.A. Christensen, J.D. Pruitt, W.G. Pitt, Kinetics of ultrasonic release of doxorubicin from pluronic P105 micelles, Colloids and Surfaces B: Biointerfaces, 24 (2002) 253-264.

[132] H. Zhang, H. Xia, J. Wang, Y. Li, High intensity focused ultrasound-responsive release behavior of PLA-b-PEG copolymer micelles, Journal of controlled release, 139 (2009) 31-39.

[133] M. Zrınyi, D. Szabó, H.-G. Kilian, Kinetics of the shape change of magnetic field sensitive polymer gels, Polymer Gels and Networks, 6 (1998) 441-454.

[134] X. Zhao, J. Kim, C.A. Cezar, N. Huebsch, K. Lee, K. Bouhadir, D.J. Mooney, Active scaffolds for on-demand drug and cell delivery, Proceedings of the National Academy of Sciences, 108 (2011) 67-72.

[135] H.M. Nizam El-Din, A.W.M. El-Naggar, Radiation synthesis of magnetic sensitive ferrogels from poly (ethylene glycol) and methacrylic acid as drug delivery matrices for vitamin B12, Designed Monomers and Polymers, 17 (2014) 322-333.

[136] S.H. Yuk, S.H. Cho, H.B. Lee, Electric current-sensitive drug delivery systems using sodium alginate/polyacrylic acid composites, Pharmaceutical research, 9 (1992) 955-957.

[137] S.Y. Kim, Y.M. Lee, Drug release behavior of electrical responsive poly (vinyl alcohol)/poly (acrylic acid) IPN hydrogels under an electric stimulus, Journal of applied polymer science, 74 (1999) 1752-1761.

[138] W. Aue, E. Bartholdi, R.R. Ernst, Two-dimensional spectroscopy. Application to nuclear magnetic resonance, The Journal of Chemical Physics, 64 (1976) 2229-2246.

[139] J. Jeener, Ampere international summer school, Basko Polje, Yugoslavia, 197 (1971).

[140] W. Aue, J. Karhan, R. Ernst, Homonuclear broad band decoupling and two-dimensional J-resolved NMR spectroscopy, The Journal of Chemical Physics, 64 (1976) 4226-4227.

[141] T. Öman, M.-B. Tessem, T.F. Bathen, H. Bertilsson, A. Angelsen, M. Hedenström, T. Andreassen, Identification of metabolites from 2D 1 H-13 C HSQC NMR using peak correlation plots, BMC bioinformatics, 15 (2014) 413.

[142] K. Wüthrich, NMR with Proteins and Nucleic Acids, Europhysics News, 17 (1986) 11-13.

[143] G. Torri, M. Guerrini, Quantitative 2D NMR analysis of glycosaminoglycans, NMR Spectroscopy in Pharmaceutical Analysis, (2008) 407.

[144] R.R. Ernst, G. Bodenhausen, A. Wokaun, Principles of nuclear magnetic resonance in one and two dimensions, 1987.

[145] M. Zoonens, L.J. Catoire, F. Giusti, J.-L. Popot, NMR study of a membrane protein in detergent-free aqueous solution, Proceedings of the National Academy of Sciences of the United States of America, 102 (2005) 8893-8898.

[146] P.A. Mirau, 2D NMR STUDIES OF SYNTHETIC POLYMERS.

[147] M.D. Bruch, F.A. Bovey, R.E. Cais, Microstructure analysis of poly (vinyl fluoride) by fluorine-19 two-dimensional J-correlated NMR spectroscopy, Macromolecules, 17 (1984) 2547-2551.

[148] A. Kumar, R. Ernst, K. Wüthrich, A two-dimensional nuclear Overhauser enhancement (2D NOE) experiment for the elucidation of complete proton-proton cross-relaxation networks in biological macromolecules, Biochemical and biophysical research communications, 95 (1980) 1-6.

[149] D.L. Pavia, G.M. Lampman, G.S. Kriz, J.A. Vyvyan, Introduction to spectroscopy, Cengage Learning, 2008.

[150] R.S. Macomber, A complete introduction to modern NMR spectroscopy, Wiley New York, 1998.

[151] S.W. Fesik, E.R. Zuiderweg, Heteronuclear three-dimensional NMR spectroscopy. A strategy for the simplification of homonuclear two-dimensional NMR spectra, Journal of Magnetic Resonance (1969), 78 (1988) 588-593.

[152] T.J. Norwood, Product Operator Formalism in NMR A2 - Lindon, John C, in: G.E. Tranter, D.W. Koppenaal (Eds.) Encyclopedia of Spectroscopy and Spectrometry (Third Edition), Academic Press, Oxford, 2017, pp. 732-739.

Chapter-2

Scope and Objectives

Hydrogels/ nanogels continue to attract immense attention in the field of drug delivery and tissue engineering due to high hydrophilicity, biocompatibility and their similarity to the extra cellular matrix (ECM).[1-3] Hydrogels are three dimensional polymer networks that are insoluble in water due to the presence of cross linking between the polymers chains either physically or chemically. They can hold large amount of water (even up to thousand times of their dry weight in the case of super absorbant polymers) depending upon the hydrophilicity and degree of crosslinking in the polymer chains.[4, 5] A variety of hydrogels based on the natural and synthetic polymers have been studied in the past few decades for drug delivery applications. The natural polymers include chitosan, alginate, collagen, gelatin etc. whereas, a few biocompatible synthetic polymers explored for the synthesis of hydrogels are poly(ethylene glycol) (PEG), poly(aspartic acid), poly(glycolic acid) (PGA), poly(L-lactic acid) (PLLA) among others.[6-8] Recently, polysaccharides like carboxymethyl tamarind [9], carboxymethyl guar [10] and carboxymethyl cellulose[11] have been explored for biomedical application owing to their bulk availability, inherent biocompatibility and biodegradability. However, their full potential is yet to be explored. In the present thesis work, we have synthesized and characterized carboxymethyl cellulose grafted MSN nanogels as potential drug delivery carriers inside the cancer cells. Although the natural polymers are desired for biomedical applications, some of the disadvantages associated with natural polymers are their difficulty in modification (due to incompatibility with organic solvents) and their batch to batch variation that affects the overall properties of the polymers. Synthetic biocompatible polymers on the other hand can be easily modified with wide variety of functional groups.[8] Poly(acrylic acid) for example, is one such biocompatible synthetic polymer (FDA approved) that has been studied extensively for biomedical applications.[12] Also, hydrogels prepared from synthetic polymers have shown better mechanical strengths compared to that of natural polymers. Large number of synthetic hydrogels is becoming important as Smart /Intelligent hydrogels wherein their properties such as swelling, volume-transitions, size, shape, optical, colour etc. respond to various stimuli like pH, temperature, redox, light etc. The swelling property of hydrogels strongly depends on the degree of crosslinking which has large implications in the controlled drug delivery from hydrogels. The swelling-controlled release of drug or other

biomolecules incubated inside the hydrogels can be affected by controlling the degree of cross linking. Accordingly, in this thesis work, we have synthesized double crosslinked poly(acrylic acid) hydrogels using two different crosslinking agents namely, Jeffamine (jeff) (amine terminated copolymer of PEO-PPO) and Cystamine (cys). The cystamine with disulphide linkages can be selectively cleaved using dithiothreitol (DTT). By selective cleaving of one crosslinking and enhancing the swelling of hydrogel, we have demonstrated the controlled release of an anticancer drug, Doxorubicin (Dox) and an antimicrobial Ag nanoparticle from the PAA hydrogel. Recently, "Click-Chemistry" approach has become important and considered as Green Chemistry since it does not utilize hazardous chemicals in the reactions. With this approach, we have synthesized poly(acrylic acid) hydrogels using furan-maleimide click chemistry approach and showed the in situ encapsulation of cells or other biomolecules in the hydrogels which have potential in bio-medical applications.

Besides, chemically crosslinked hydrogels, associating polymers (APs) or hydrophobically modified polymers (HMPs) undergo physical gelation due to the self-assembly of hydrophobic groups in an aqueous media and exhibit interesting rheological properties such as thermo-gelation, shear thickening/thinning, strain hardening, super viscosification etc. Therefore, they find large number of applications in areas such as creams, pharmaceutical formulations, paints, textile, paper, oil recovery etc [13, 14] as thickeners. Different molecular architectures of APs/HMPs are reported in the literature.[15] Particularly, polymers which undergo thermo-gelation with temperature as stimuli have become important as injectables in controlled drug delivery systems.[16] There has been a growing interest in designing and synthesizing new injectables which are efficient in controlled release technology. In this context, we have synthesized PAA-*g*-MPEG-*b*-PCL polymer and studied the thermo-thickening behaviour using rheology, light scattering and NMR techniques. The results revealed the unusual irreversible nature of the thermo-thickening behaviour which was attributed to the formation of ordered microdomains in the structure leading to permanent gelation.

The main objectives of the thesis are:

1. To design and synthesize carboxymethyl cellulose grafted MSN nanogels for drug delivery applications. The focus of the work is to incubate curcumin, an anticancer and antibacterial drug inside the pores of MSNs and coat the surface with CMC to prevent the premature release of curcumin.

2. To study the drug loaded nanogels in cancer cell line, MDA-MB-231 for their biocompatibility, cellular uptake and drug release.

3. To synthesize PAA-*g*-MPEG-*b*-PCL thermo-associating polymers and study their thermo-thickening behavior using rheology, light scattering and NMR spectroscopy.

4. To synthesize double cross linked PAA hydrogels and subsequently in-situ cleave one crosslinking to enhance the swelling of the hydrogel. The increased swelling of the hydrogel could be utilized for the controlled release of the incorporated drug in the hydrogel.

5. To design and synthesize PAA based hydrogels with different degree of crosslinking using furan-maleimide click chemistry approach in the absence of any organic solvents and catalyst. These hydrogels show great promise in in-situ loading of drug molecules and cells for tissue engineering applications.

References

[1] A.C. Jen, M.C. Wake, A.G. Mikos, Hydrogels for cell immobilization, Biotechnology and bioengineering, 50 (1996) 357-364.

[2] B. Říhová, Immunocompatibility and biocompatibility of cell delivery systems, Advanced drug delivery reviews, 42 (2000) 65-80.

[3] J.E. Babensee, J.M. Anderson, L.V. McIntire, A.G. Mikos, Host response to tissue engineered devices, Advanced drug delivery reviews, 33 (1998) 111-139.

[4] T. Yoshimura, K. Matsuo, R. Fujioka, Novel biodegradable superabsorbent hydrogels derived from cotton cellulose and succinic anhydride: Synthesis and characterization, Journal of Applied Polymer Science, 99 (2006) 3251-3256.

[5] F.L. Buchholz, N.A. Peppas, Superabsorbent polymers: science and technology, ACS Publications, 1994.

[6] T. Kimura, N. Yasui, S. Ohsawa, K. Ono, Chondrocytes embedded in collagen gels maintain cartilage phenotype during long-term cultures, Clin Orthop, 186 (1984) 231-239.

[7] D.L. Wise, Encyclopedic Handbook of Biomaterials and Bioengineering: v. 1-2. Applications, CRC Press, 1995.

[8] K.Y. Lee, D.J. Mooney, Hydrogels for tissue engineering, Chemical reviews, 101 (2001) 1869-1880.

[9] S. Jana, R. Sharma, S. Maiti, K.K. Sen, Interpenetrating hydrogels of O-carboxymethyl Tamarind gum and alginate for monitoring delivery of acyclovir, International journal of biological macromolecules, 92 (2016) 1034-1039.

[10] A. Giri, M. Bhowmick, S. Pal, A. Bandyopadhyay, Polymer hydrogel from carboxymethyl guar gum and carbon nanotube for sustained trans-dermal release of diclofenac sodium, International journal of biological macromolecules, 49 (2011) 885-893.

[11] H. Kono, Characterization and properties of carboxymethyl cellulose hydrogels crosslinked by polyethylene glycol, Carbohydrate Polymers, 106 (2014) 84-93.

[12] Y.-C. Nho, J.-S. Park, Y.-M. Lim, Preparation of poly (acrylic acid) hydrogel by radiation crosslinking and its application for mucoadhesives, Polymers, 6 (2014) 890-898.

[13] J.E. Glass, Polymers in aqueous media: performance through association, ACS Publications, 1989.

[14] J.E. Glass, Hydrophilic polymers: performance with environmental acceptance, ACS Publications, 1996.

[15] M.A. Winnik, A. Yekta, Associative polymers in aqueous solution, Current opinion in colloid & interface science, 2 (1997) 424-436.

[16] M.A.C. Stuart, W.T. Huck, J. Genzer, M. Müller, C. Ober, M. Stamm, G.B. Sukhorukov, I. Szleifer, V.V. Tsukruk, M. Urban, Emerging applications of stimuli-responsive polymer materials, Nature materials, 9 (2010) 101-113.

Chapter-3

Carboxymethyl Cellulose Grafted Mesoporous Silica Nanogels

3.1 Introduction

Cancer has become a major concern worldwide as most of the drugs effective towards its treatment are hydrophobic in nature and thus have less bioavailability at the required site. Chemotherapy, although is a widely accepted treatment towards cancer wherein high dosages of chemotherapeutic agents are used is associated with major side effects like insufficient drug concentrations at the tumor site leading to toxicity to the healthy cells along with cancer cells. [1, 2] Developing controlled-release technology to avoid premature drug release with targeted drug delivery may provide more efficient and less harmful solution compared to conventional chemotherapy. The major challenge however is to limit the dosage of drugs at the targeted site with minimal side effects. In this context, nanotechnology has emerged as one of the major areas of research for drug delivery towards cancer treatment to overcome the above mentioned problems.[3, 4] Various efforts have been made in recent years towards the synthesis of nanocarriers for drug delivery and preventing the premature release of drugs before reaching the targeted site. The nanocarriers for drug delivery must possess certain desired properties like biocompatibility, bioavailability, and improved circulation half time, chemical stability in in-vivo conditions, inertness towards enzymatic degradation, tissue specificity and controlled drug release. Although various nanocarriers like liposomes [5], polymeric micelles [6, 7], dendrimers [8, 9], carbon nanotubes [10] etc. have been studied, they lack stability in in-vivo conditions and are prone to various enzymatic degradation before reaching the targeted site and results in premature drug release.[11] Recently, inorganic mesoporous silica nanoparticles (MSNs) have attracted increasing attention in bio-medical applications due to their stability in in-vivo conditions, biocompatibility and ease of synthesis.[12, 13] The particle and pore size of MSNs can be controlled depending on their applications which make them highly versatile in nature.[14, 15] With large surface area, porosity and tunable pore size, control over the functionalization of surface, ordered mesopores, biocompatibility and stability, MSNs have great advantages over other nanocarriers.[15] The template synthesis is one of the strategies to make mesopores in silica particles which has proven to be a potential route to achieve desired nano architectures.[16] The ordered porous structure in MSNs is

important in wide range of applications such as catalysis, adsorption, optics, photochemistry etc. [17] The control over the dimensions, morphologies, composition and porosity of MSNs has been exploited for synthesizing integrated nanocrystals (INCs) in catalytic applications.[18] MSNs have been successfully explored for various biological applications like drug delivery [19-21], biosensors [22], gene transfection [23, 24] etc. Particularly, porous MSNs have become important since their porosity can be successfully utilized for the encapsulation of hydrophobic drugs [25, 26] and other bio-molecules. The highly porous structure of MSNs facilitates loading of large amounts of drugs so that minimum amount of the carrier is sufficient for drug delivery at the cancer site by enhanced cell permeability (EPR) without any potential side effects. Well established EPR theory postulates that MSNs tend to accumulate at the cancer site more effectively as compared to normal cells.[27, 28] Further, both the outer surface and the pores of MSNs can be selectively functionalized with organic moieties to enhance their biocompatibility and increased circulation time in blood.[29] The functionalization of MSNs can also help in preventing the drug or other bio-molecules present inside the porous structure from enzymatic degradation before reaching the targeted site. Surface functionalization could be achieved by modification of the surface of MSNs with organic moieties that are biocompatible.

A literature review reveals that surface modifications have been carried out using both synthetic molecules like polyethylene glycol [30], folic acid [31], β-cyclodextrin [32] and polyacrylic acid [33] as well as naturally occurring molecules like amino acids (poly-L-lysine and poly-L-arginine) [34] which are biocompatible with the cell environment. Polysaccharides are another class of naturally occurring polymers with inherent biocompatible and biodegradable properties which can be used to enhance the biocompatibility of MSNs without any potential side effects. For example, chitosan [35, 36], hyaluronic acid [37], mannose [38] and alginate [39] are a few of the naturally occurring polysaccharides that have been studied extensively for encapsulation of hydrophobic drug molecules and enhanced permeation of hybrid silica particles inside the tumor cells. Other potential polysaccharides like carboxymethyl cellulose (CMC), carboxymethyl tamarind (CMT) and guar gum (GG) in combination with MSNs are yet

to be fully explored for drug delivery applications. Another advantage of the polysaccharides is their degradability by enzymes, they can be coated onto drug loaded MSNs and the drug can be released by polysaccharide degradation.

In the present work, we carried out the functionalization of MSNs with a polysaccharide, namely, carboxy methyl cellulose (CMC) using an EDC coupling reaction between amine functionalized MSNs (MSN-NH_2) and the carboxylic groups of CMC. The pores of MSNs were incubated with the hydrophobic drug curcumin, which has both anticancer and antibacterial activity. It was observed that CMC modified MSNs helped in the enhanced permeation of MSNs inside the tumor cells. MTT assay of both MSN-NH_2 and MSN-CMC shows high biocompatibility of the nanoparticles in MDA-MB-231 breast cancer cell line. Also, MTT assay of breast cancer cell line, MDA-MB-231 revealed that curcumin loaded and CMC coated MSNs (MSN-cur-CMC) showed better cell inhibition compared to the curcumin loaded MSN-cur-NH_2 Therefore, CMC grafted MSNs show great promise in enhanced internalization of drug molecules inside the cancer cell lines.

3.2 Experimental

3.2.1 Materials

Tetraethylorthosilicate (TEOS) (99%), (3-aminopropyl) triethoxysilane (APTES), hexadecyltrimethylammonium bromide (CTAB) (99%), 1-ethyl-3-(3-dimethylaminopropyl)-carbodiimide hydrochloride (EDC.HCl), N-hydroxy succinimide (NHS), sodium lauryl sulphate (SLS), Potassium Bromide (KBr), Polytetrafluoroethylene (PTFE) filters and carboxymethyl cellulose (CMC) were obtained from Sigma Aldrich, St. Louis, MO, USA. Curcumin was a gift sample from Arjuna Natural Extracts, Kerala, India. Dulbecco's modified Eagle's medium (DMEM) high glucose, fetal bovine serum (FBS), L-15 medium, Trypsin (0.25% EDTA), annexin-V FITC, 4',6-Diamidino-2-Phenylindole Dihydrochloride (DAPI), propidium iodide (PI), RNAse A, 4-(2-hydroxyethyl)-1-piperazineethanesulfonic acid (HEPES) buffer, paraformaldehyde (4.7%) and 3-(4,5-dimethylthiazol-2-yl)-2,5-diphenyltetrazolium bromide (MTT) were procured from Invitrogen, Bangalore, India.

All chemicals were used as received. The required cell lines for this work (MDA-MB-231) were purchased from National Center for Cell Science (NCCS), Pune, India.

3.2.2 Synthesis of Mesoporous Silica Nanoparticles

One gram of Cetyltrimethylammonium bromide (CTAB) was dissolved in 480 mL of deionized water using an overhead stirrer at room temperature followed by the addition of 2 M NaOH solution (3.5 mL). The solution was allowed to stir for 30 min at 80 °C. 5 mL of tetraethyl orthosilicate (TEOS) was added drop wise to the above mixture. The mixture was stirred at 6000 rpm for another 2 h at 80 °C. The resultant white precipitate was collected by vacuum filtration and washed with copious amount of water. The precipitate was dried in vacuum oven overnight to obtain mesoporous silica in powder form.

3.2.3 Outer Surface Functionalization of MSNs with amino groups

For the outer surface functionalization of MSNs, 1 g of MSNs were dispersed in 100 mL anhydrous toluene followed by the addition of 200 μL of 3-aminopropyltriethoxysilane (APTES) in the presence of catalytic amount of triethylamine (Et_3N). The reaction mixture was refluxed for 18 h under argon atmosphere. The product was obtained using vacuum filtration, washed with toluene (to remove any unreacted APTES) and finally with ethanol. The template (CTAB) was removed by refluxing the material in acidic methanol solution for 6 h. The amine grafted and template removed MSNs were finally washed with methanol and vacuum dried. The obtained material was denoted as MSN-NH_2.

3.2.4 Loading of Curcumin inside the pores of MSNs

To load curcumin into the pores of MSN-NH_2, 200 mg of MSN-NH_2 was dispersed in 20 mL of methanol using probe sonicator. To this dispersion, 30 mg of curcumin dissolved in 10 mL methanol was added. The dispersion was stirred for overnight at 25 °C. Methanol was then evaporated under vacuum at 50 °C. The curcumin loaded MSNs were then dispersed in water using a sonicator. The MSNs were centrifuged at 12,000

rpm for 10 min and washed several times with water in order to remove any curcumin adsorbed on the surface of MSNs. The particles were then dried under vacuum overnight to obtain curcumin loaded MSNs. The obtained material was denoted as MSN-cur-NH_2.

3.2.5 Functionalization of MSN-NH_2 and MSN-cur-NH_2 with Carboxymethyl Cellulose

One hundred milligram of MSN-NH_2 and MSN-cur-NH_2 were dispersed in 100 mL deionized water using sonication. To this, a premixed solution of NHS (0.4 g), EDC (0.2 g) and carboxymethyl cellulose (150 mg) in 20 mL deionized water were added. [37] The pH of the solution was then adjusted to 9 with an addition of triethylamine. The solution was stirred overnight at 40 °C. The product was centrifuged at 12,000 rpm for 10 min followed by 3 times washing with deionized water to remove any unreacted reactants. The precipitate was then dried under vacuum overnight to obtain curcumin loaded CMC grafted MSN particles. The material was denoted as MSN-cur-CMC (with curcumin) and MSN-CMC (without curcumin).

3.2.6 In vitro Curcumin Release Studies

The in vitro release of curcumin from MSN-Cur-NH_2 and MSN-Cur-CMC were performed in 0.5 % SLS solution. Both MSN-cur-NH_2 and MSN-cur-CMC equivalent to 1 mg of curcumin were suspended in 10 ml 0.5 % SLS solution and kept at shaking water bath preset at 37 °C. 1 ml of the supernatant was collected at predetermined time intervals and immediately replaced with equal amount of dissolution medium in order to maintain the sink conditions. The supernatant collected was centrifuged to remove any solid particles and appropriately diluted before taking the absorbance at 432 nm using UV-Vis spectrophotometer. The release profile of curcumin from MSN-cur-NH_2 and MSN-cur-CMC was compared in the same dissolution medium under same conditions. The release profile was performed at 37 °C on a shaking water bath for 72 h.

3.2.7 In vitro Cytotoxicity assay

The sensitivity of MDA-MB-231 cells to the curcumin loaded MSNs was determined by MTT dye uptake as described previously. Briefly, 1×10^5 cells/mL was seeded in a flat bottomed 96-well plate. Next day, the cells were treated with increasing concentrations of blank (3.125–200 µg/mL final concentrations) and curcumin loaded MSNs (0.12–16 µg/mL final drug concentrations) in sterilized MilliQ water and incubated at 37 °C with 5 % CO_2 for 24 h. An untreated group was kept as a negative control and cells treated with free curcumin (0.12–16 µg/mL) were used as positive control. Wells containing culture medium and MTT but no cells acted as blank. After incubation, the MTT solution (5 mg/mL solution in PBS) was added to each well and the cells were incubated for another 3.5 h at 37 °C in 5 % CO_2 incubator. The formazan crystals formed were dissolved by addition of 200 µL of 0.04 N acidified isopropanol. After 15 min, the amount of colored formazan derivative formed was determined by measuring optical density (OD) using the microplate reader at 570 nm. All experiments were conducted in triplicates and the results were presented as average with ± standard deviation. The percentage inhibition was calculated as:

$$\% \text{ Inhibition} = \frac{(OD \text{ of control well} - OD \text{ of treated well})}{(OD \text{ of control well} - OD \text{ of blank})} \times 100 \quad (1)$$

3.2.8 Intracellular uptake of MSN particles in cancer cells

The fluorescence of curcumin was used to determine the uptake of curcumin loaded MSNs inside the breast cancer cell line MDA-MB-231. Briefly, 1×10^5 cells/mL was seeded in a glass bottomed black 96-well plate. Next day, cells were treated with MSN-NH_2 and MSN-CMC (200 µg/mL), curcumin (16 µg/mL) and MSN-cur-NH_2 and MSN-cur-CMC (GI_{50}= 7 and 1.5 µg/mL final drug concentrations respectively) in sterilized MilliQ water (Merck, Darmstadt, Germany) and incubated at 37 °C with 5% CO_2 for 1 hr. Following incubation, the cells were washed with PBS and stained with DAPI. An alteration in released curcumin level was detected using Laser Scanning Confocal Microscope (LSCM) (Thermo Fischer, Waltham, MA, USA) by measuring the green fluorescence (excitation 490 nm, emission 530 nm).

3.2.9 Apoptosis by Annexin V-FITC /PI staining

Apoptosis was evaluated by binding of annexin V-FITC to phosphatidylserine that gets externalized to the outer leaflet of the plasma membrane, followed by high content screening. After 48 h of incubation of the cells with MSN-NH_2 and MSN-CMC (200 µg/mL), curcumin (16 µg/mL) and MSN-cur-NH_2 and MSN-cur-CMC (GI_{50}= 7 and 1.5 µg/mL final drug concentrations respectively), the cells were harvested and subsequently treated with annexin V-binding buffer comprising annexin V-FITC (3 µg/mL), DAPI (1 µM) and propidium iodide (10 µg/mL). The number of cells undergoing apoptosis were examined using LSCM (20× magnification, Olympus FV1000) (Olympus, Melville, NY, USA and Thermo Scientific™ HCS studio™ 2.0 software (Thermo Fischer Scientific, Waltham, USA) was used for three-dimensional multichannel-image processing. The apoptotic ratio was calculated as:

$$\% \text{ Apoptotic ratio} = \frac{(Number\ \ of\ cells\ positive\ \ for\ Annexin\ \ V-FITC)}{(Number\ \ of\ cells\ positive\ \ for\ DAPI)} \text{ x } 100 \qquad (2)$$

3.3 Characterizations

3.3.1 Structural Characterization

3.3.1.1 *FT-IR*

FT-IR spectra were recorded on Perkin Elmer FT-IR spectrum GX instrument (Perkin Elmer, Waltham, MA, USA) using KBr pellets. Pellets were prepared by mixing 3 mg of sample with 97 mg of KBr.

3.3.1.2 *Thermo Gravimetric Analysis*

Thermo gravimetric analysis (TGA) of the MSNs were carried out using a TA Instrument SDT Q600 analyzer (TA Instruments, New Castle, DE, USA) between 50 and 800 °C in air (flow 50 $mL.min^{-1}$) at an heating rate of 10 $°C.min^{-1}$. All samples were dried under vacuum at 80 °C overnight prior to TGA runs (to remove all traces of water). The graft density of the grafted moiety on the silica surface was determined by thermo gravimetric analysis (TGA) as described before.

3.3.1.3 *Nitrogen Adsorption/Desorption*

Nitrogen adsorption/desorption studies at -196 °C were carried out using Quadrasorb SI instrument (Quantachrome Instruments, Burlington, ON, Canada). The samples were degassed overnight under vacuum using FloVac Degasser (Quantachrome Instruments, Burlington, ON, Canada) at 100 °C before nitrogen adsorption measurements. Multi-point Brunauer-Emmett-Teller (BET) surface area was obtained from the nitrogen adsorption isotherm in the relative pressure range from 0.1 to 0.3. Pore sizes were calculated using the Barrett, Joyner and Halenda (BJH) method from adsorption branch of the isotherm in the relative pressure range from 0.3 to 0.99 units and total pore volume was calculated at P/P_o of 0.99.

3.3.1.4 *ζ Potential and Size Determination*

The hydrodynamic diameters of dilute aqueous solutions of the MSNs, MSN-NH_2 and MSN-CMC were determined by dynamic light scattering (DLS) (Brookhaven Instruments, Holtsville, NY, USA) equipped with a He–Ne laser operating at 632 nm. The particle size was calculated using 90 Plus particle Sizing Software Ver. 3.94 (Brookhaven Instruments). Sample solutions 1 mg/mL were dispersed in water and were filtered using a 0.8 μm Polytetrafluoroethylene (PTFE) filter.

Aqueous electrophoretic data for the above mentioned MSNs were obtained using Brookhaven Instruments. For each sample three measurements were taken and the average value is reported. ζ potentials were calculated using PALS ζ Potential Analyzer Software Ver. 3.54 (Brookhaven Instruments).

3.3.2 Morphological Analysis

3.3.2.1 *Scanning electron microscopy (SEM)*

Scanning electron Microscopy (SEM) was used to investigate the morphology of the MSNs using Quanta 200 3D (FEI) dual beam having electron source of tungsten (W) filament with emission at resolution of 20 kV in high vacuum. All the samples were sputter-coated with a thin layer of gold.

3.3.2.2 *Transmission electron microscopy (TEM)*

HR-TEM images were taken on a FEI Technai F30 operating (FEI, Hillsboro, OR, USA) at 300 kV with Field Emission Gun (FEG). The samples were prepared by dispersing a 0.1 mg/mL of MSNs in methanol by sonication, dropping the resulting suspension on a copper grid of 400 meshes for 30 s and allowing it to dry in air.

3.4 Results and discussion

3.4.1 Synthesis and functionalization of Mesoporous Silica Nanoparticles (MSNs)

Mesoporous silica nanoparticles (MSNs) were synthesized according to the previous reports.[20, 40] The synthetic route of MSNs and its functionalization with amine moieties and carboxymethyl cellulose is given in **Scheme 3.1**. Briefly, the synthesis of MSNs was carried out by sol-gel method using cetyltrialkyl ammonium bromide (CTAB) as a structure-directing agent and tetraethyl orthosilicate (TEOS) as a silica precursor in the presence of base as a catalyst.[34, 41]

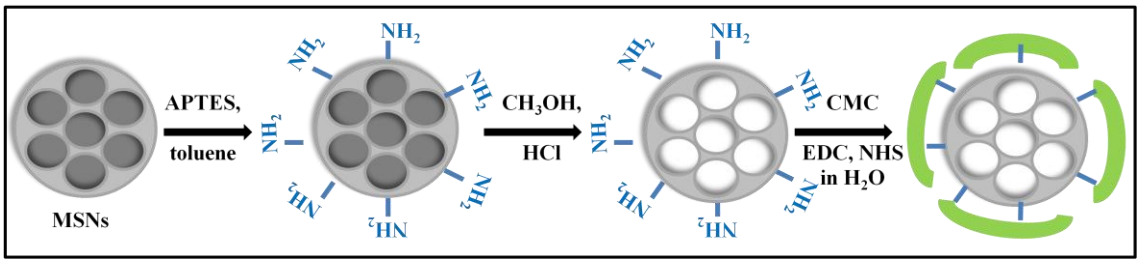

Scheme 3.1. Synthesis of CMC grafted MSNs

Functionalization of the outer surface of MSNs with amine moieties was performed using aminopropyl triethoxysilane (APTES) in the presence of a catalytic amount of triethylamine. The amino groups were introduced to further functionalize the MSN surface with carboxymethyl cellulose (CMC). The amine groups on MSNs covalently react with the –COOH groups of CMC to form amide linkages in the presence of N-hydroxy succinimide (NHS) using EDC coupling chemistry. TEM images of as-prepared MSNs show uniform discrete spherical nanoparticles with particle sizes in the diameter range of 120±20 nm for MSN, MSN- NH_2 and MSN-CMC. The images also show that MSNs and amine-functionalized MSNs have a porous structure under high

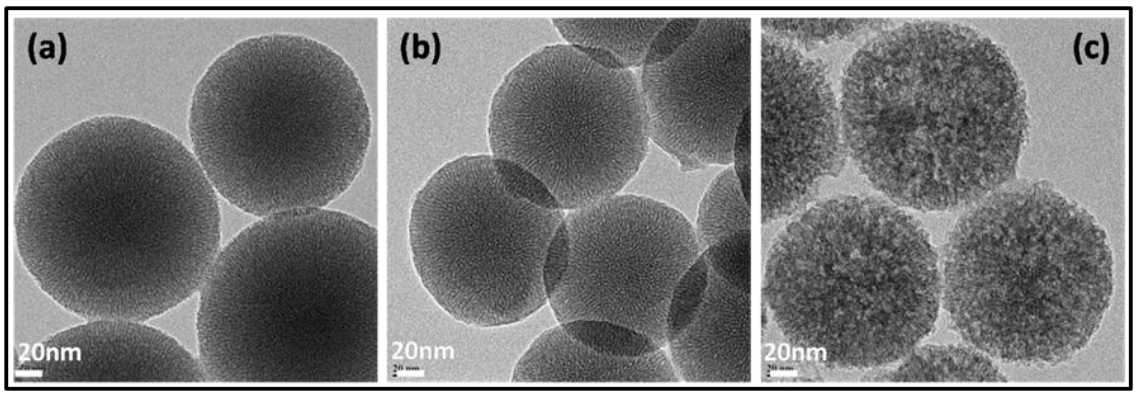

Figure 3.1. Transmission electron microscopy (TEM) images of (a) MSN, (b) MSN-NH_2 and (c) MSN-CMC

magnification (**Figure 3.1 (a&b)**). However, this porous structure is completely disappeared upon subsequent CMC grafting on to the surface of MSNs which is evident from **Figure 3.1(c)**. The observed particle size form TEM is in agreement with the sizes obtained from Scanning Electron Microscopy (SEM) (**Figure 3.2**) which shows a uniform size of particles over a long range order.

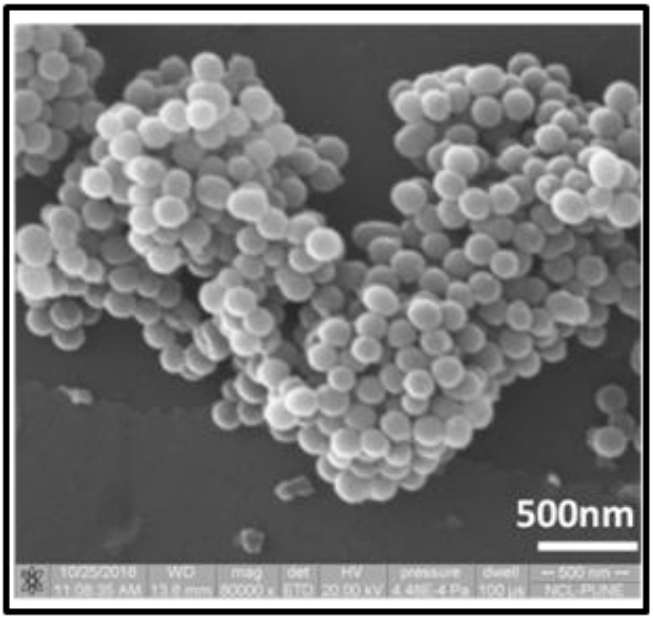

Figure 3.2. SEM image of as synthesized MSNs

Further, the particle size distribution and multimodal size distribution of MSNs with and without functionalization was determined using dynamic light scattering (DLS) experiments (**Figure 3.3 (a&b)**). As shown in **Table 3.1**, the

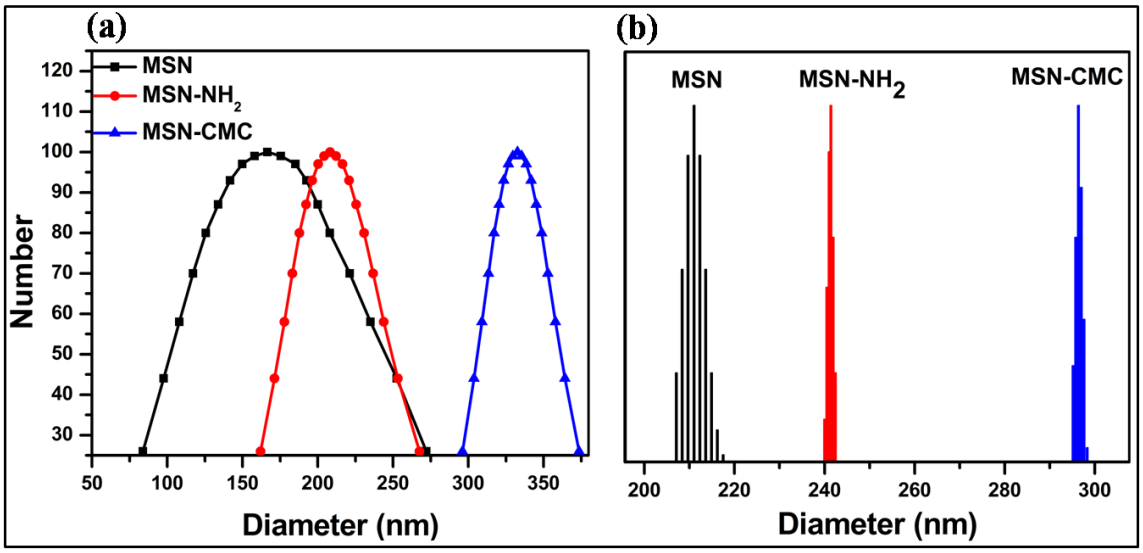

Figure 3.3. Particle (a) and Particle size distribution (b) of MSN and functionalized MSNs obtained by DLS experiments

diameters of MSNs were found to be larger as compared to diameters observed from TEM which could be due to the presence of a hydrated layer in the aqueous environment. The MSN-CMC showed a larger diameter of ~333 nm since CMC undergoes gelation and swelling in aqueous medium.

Aqueous electrophoresis experiments were performed on MSNs to determine their ζ potential. It was observed that ζ potential changed from a negative to a positive value upon amine functionalization and later changed to negative value after CMC grafting. This clearly indicated the successful reaction between the $–NH_2$ groups on MSNs and the –COOH groups of CMC (**Table 3.1**).

Table 3.1: Physical properties of various MSNs

Sample Name	Weight Loss (%)	Hydrodynamic Diameter (nm)	Mean Zeta Potential (mV) in water
MSN	7.3	167	-34.2±2
MSN-NH_2	17.5	210	38.48±3
MSN-CMC	30.7	333	-3.07±2

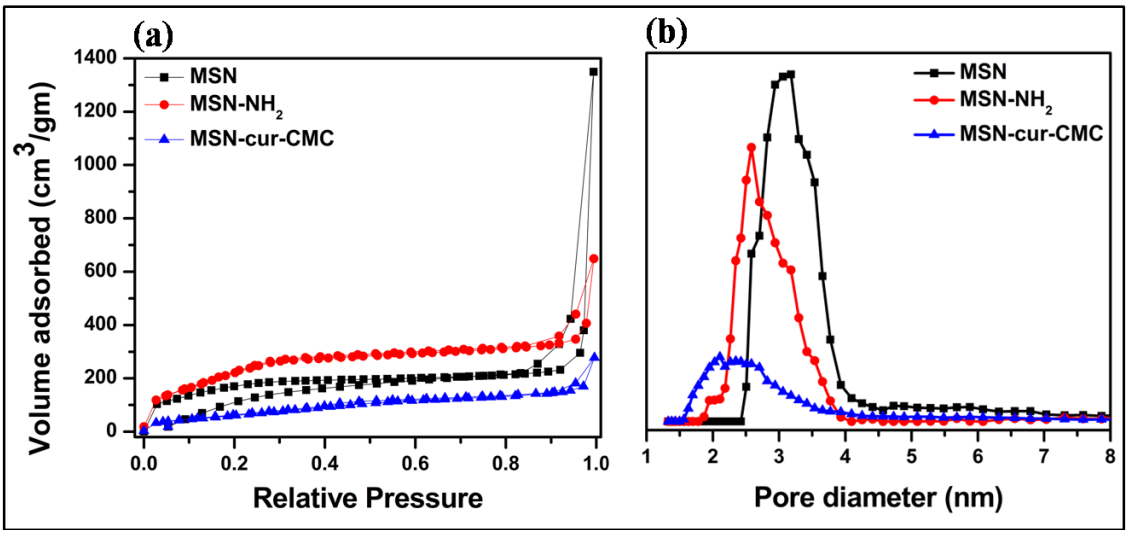

Figure 3.4. (a) Nitrogen adsorption-desorption isotherms of MSN, MSN-NH_2 and MSN-cur-CMC and (b) Pore diameter of MSN, MSN-NH_2 and MSN-cur-CMC using BJH method from N_2-adsorption desorption studies

Nitrogen adsorption desorption isotherms of MSN, MSN-NH_2 and MSN-cur-CMC showed type IV isotherms, which indicated the mesoporous nature of MSNs as shown in **Figure 3.4(a)**. Barrett, Joyner and Halenda (BJH) method was used for the pore size analysis (**Figure 3.4(b)**).[42] MSNs showed a pore size of ~3 nm, which decreased to 2.7 nm on amine functionalization. This small decrease in the pore size could be due to the presence of some amine groups inside the pores of MSNs. The pore size was further reduced to 2 nm in the case of MSN-cur-CMC as a result of the successful incorporation of curcumin inside the pores of MSNs. The curcumin incorporation also resulted in the decrease of surface area and the pore volume of MSNs as shown in **Table 3.2**. The XRD studies of MSNs and MSN-NH_2 showed a well resolved diffraction peak at 2Θ of 2.44 assigned as 100 plane confirming the mesoporous structure of MSNs (**Figure 3.5(a)**).

Further confirmation of the functionalization of MSNs with amine groups and CMC was indicated in the TGA analysis. **Figure 3.5(b)** shows the percentage mass loss profiles as a function of temperature for MSN-NH_2 and MSN-CMC. It can be seen that after heating the samples up to 800 °C, MSNs, MSN-NH_2 and MSN-CMC show a mass loss of ~7.3 %, 17.5 % and 30.7 % respectively (**Table 3.1**).

Table 3.2: Nitrogen adsorption-desorption analysis of MSNs

Sample Name	Surface Area (m^2/gm)	Pore Diameter (nm)	Pore Volume (cm^3/gm)
MSN	939.618	3	0.738
MSN-NH_2	659.111	2.6	0.642
MSN-cur-CMC	262.981	2	0.339

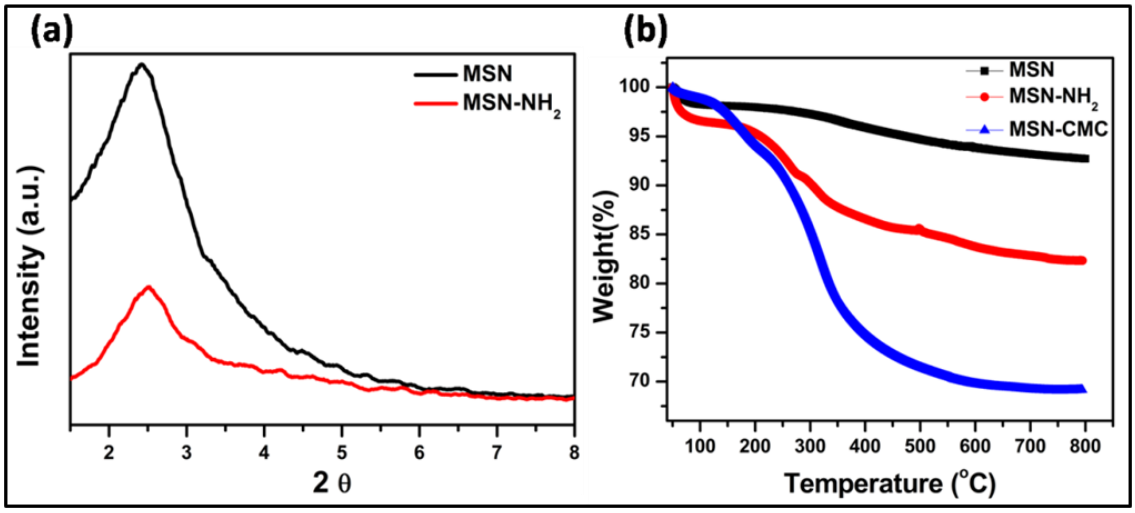

Figure 3.5. (a) X -Ray Diffraction (XRD) patterns of MSN and MSN-NH_2 and (b) Thermo gravimetric Analysis (TGA) curves of MSN, MSN-NH_2 and MSN-CMC

From these results, the percentage grafting of CMC onto MSNs was calculated to be ~13.2 %. We also show in **Figure 3.6**, the FT-IR spectra of MSNs, MSN-NH_2 and MSN-CMC. All the samples showed characteristic peaks at 1650 and 800 cm^{-1} due to Si–O stretching and at 480 cm^{-1} due to Si–O–Si bending. The broad peak at 3400–3500 cm^{-1} corresponds to –OH groups in the samples. MSN-NH_2 showed a peak at 2907 cm^{-1} due to the C– H stretching of the poly-amino groups and 1508 cm^{-1} due to the –NH bending. However, the peak at 1508 cm^{-1} disappeared in MSN-CMC due to the functionalization of amine groups with CMC. Further, an additional peak appears in MSN-CMC at 1570 cm^{-1} due to the amide bending which is absent in MSN-NH_2. This further confirms the successful functionalization of MSNs surface with CMC.

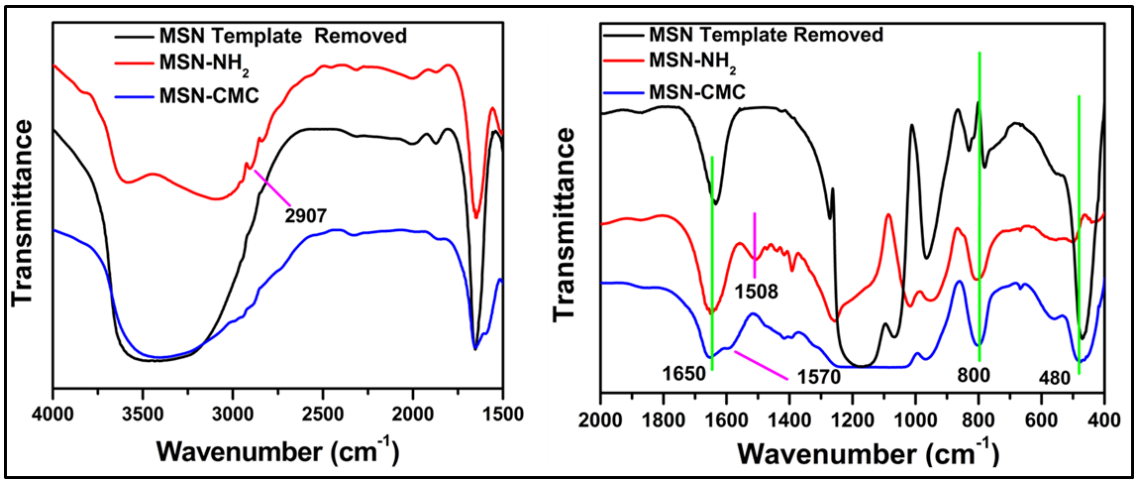

Figure 3.6. Fourier Transform Infrared Spectroscopy (FT-IR) Spectra of MSN, MSN-NH_2 and MSN-CMC

3.4.2 Synthesis of curcumin loaded MSN-CMC nanoparticles

Curcumin, an anticancer drug was effectively loaded in the pores of MSNs in order to increase its bioavailability (since it is hydrophobic in nature) and also to prevent its enzymatic degradation before reaching the cancer cells by EPR effect. For curcumin incubation, MSNs surface was first grafted with amine moieties using APTES.

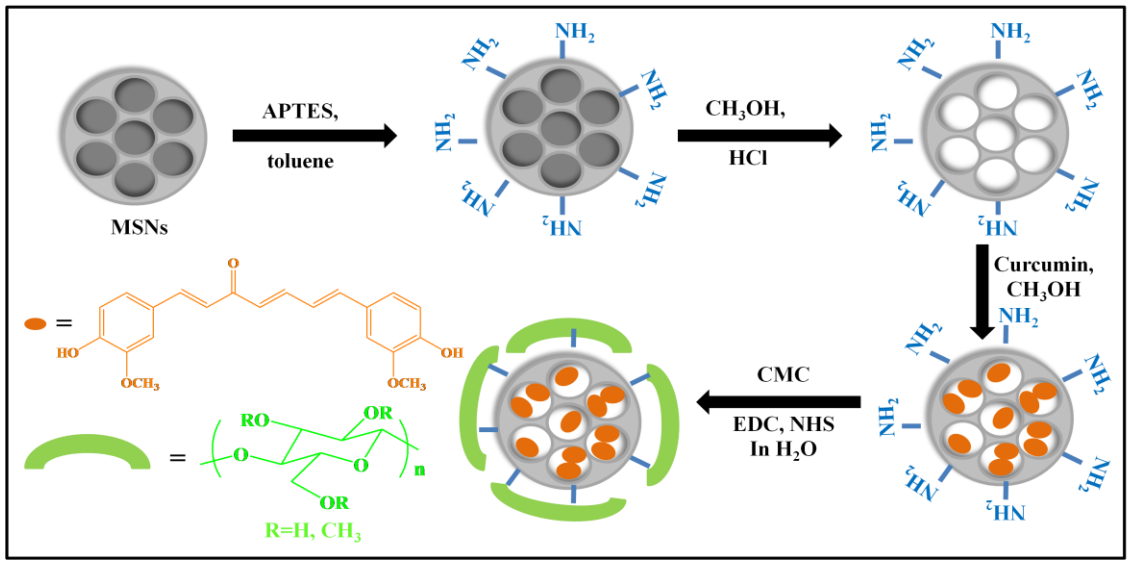

Scheme 3.2. Synthesis of curcumin loaded carboxymethyl cellulose grafted MSN

Curcumin was then physically incubated into the pores of MSN-NH_2 by stirring MSN-NH_2 in methanol containing curcumin overnight. The curcumin adsorbed on the surface

was removed by washing with excess water multiple times. The incorporation of curcumin inside the pores of MSNs was confirmed from the reduction in the pore diameter of MSNs from N_2 adsorption-desorption isotherms (**Table 2**). In the next step, CMC was grafted onto the surface of curcumin-loaded MSN-NH_2 by EDC coupling reaction between –NH_2 groups of MSN-NH_2 and –COOH groups of CMC. The unreacted reactants and side products if any were removed by washing with distilled water. The synthetic pathway for the curcumin incorporation in MSN-CMC is shown in **Scheme 3.2**. In order to calculate the amount of curcumin loaded into MSN-NH_2 and MSN-CMC, 1mg of each material was dispersed in methanol and sonicated for 20 min using probe sonicator. Nanoparticles were then centrifuged and UV absorbance of the supernatant was carried out at 430 nm. The amount of drug loaded in the MSN nanoparticles is given in **Table 3.3**. The drug loading content and the drug entrapment efficiency were calculated using the following equations [30]:

$$\text{Drug loading content (\%)} = \frac{\text{Weight of curcumin in MSNs}}{\text{Total weight of loaded MSNs}} \times 100 \quad (3)$$

$$\text{Drug Entrapment Efficiency (\%)} = \frac{\text{Weight of curcumin in MSNs}}{\text{Initial weight of curcumin added}} \times 100 \quad (4)$$

Table 3.3: Curcumin loading in functionalized MSNs

Sample Name	Drug Loading Content (%)	Drug Entrapment Efficiency (%)
MSN-cur-NH_2	10.7	71.3
MSN-cur-CMC	80.0	53.3

3.4.3 Release Study of Curcumin from MSNs in 0.5 % Sodium Lauryl Sulphate solution

The in vitro release of curcumin from MSN-cur-NH_2 and MSN-cur-CMC was studied by dispersing curcumin loaded MSNs (with same amount of drug loading) in 10 mL of 0.5 % sodium lauryl sulphate (SLS) solution at 37 °C in a water bath with continuous shaking. The SLS (0.5 %) was used as a drug-releasing medium since curcumin is known to degrade in neutral to basic solutions within a few hours.[23] An aliquot was

taken out at fixed time interval and UV absorbance of curcumin at 432 nm was measured. A total of 45 % curcumin release was observed in MSN-cur-NH_2 whereas; only 15 % curcumin could be released from MSN-cur-CMC over a period of 72 h

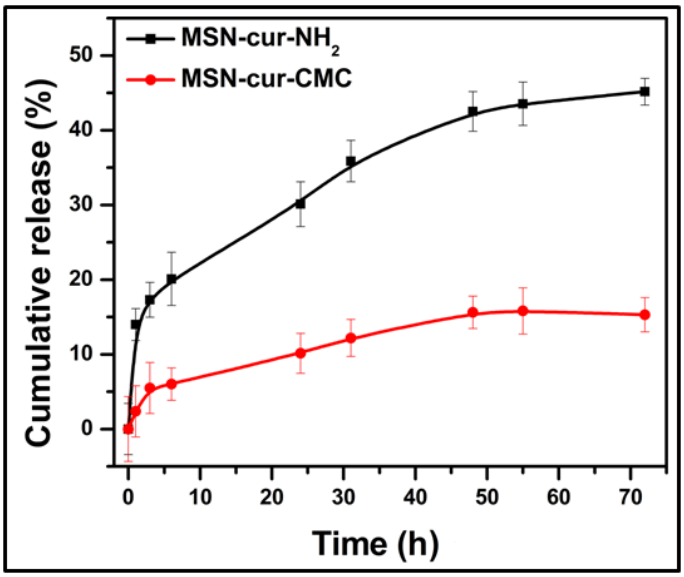

Figure 3.7. In vitro cumulative release (%) of curcumin from MSN-cur-NH_2 and MSN-cur-CMC in 0.5 % sodium lauryl sulphate (SLS)

(**Figure 3.7**). A relatively slower release of curcumin from MSN-cur-CMC could be attributed to the presence of CMC on the surface which creates a barrier to the curcumin molecules to release from the pores of MSN. The slower release of curcumin from MSN-cur-CMC is beneficial since the drug molecules are protected inside the pores of MSNs for a longer period and will be released only after reaching the targeted cancer cells by EPR effect. The drug molecules inside the cells could be easily released by the cleavage of amide linkages (between CMC and MSN-NH_2) by enzymatic action.

3.4.4 In vitro Cytotoxicity Assay

The in vitro cell cytotoxicity of MSN-NH_2, MSN-CMC, MSN-cur-NH_2, MSN-cur-CMC and free curcumin to MDA-MB-231 cells was investigated using MTT assay. It can be seen from **Figure 3.8 (a)** that the MSN-NH_2 and MSN-CMC show almost no toxic effect to the cancer cells up to a concentration of 200 µg/mL after incubation for 24 h. The results indicate that MSN-NH_2 and MSN-CMC are highly biocompatible with the cancer cell line used. **Figure 3.8 (b)** showed the in vitro cellular toxicity of MSN-

cur-NH_2, MSN-cur-CMC and free curcumin in MDA-MB-231 cells at different concentrations. It is observed that free curcumin showed negligible cytotoxicity to the cancer cells. This could be due to curcumin being hydrophobic in nature and has very less solubility in the dispersed medium that might affect least contact with the

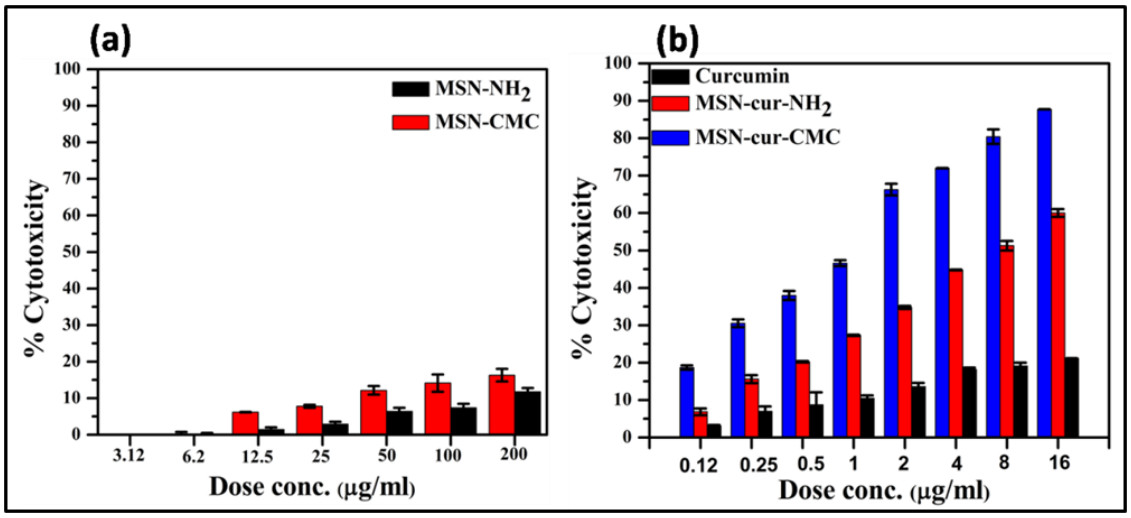

Figure 3.8.(a) % Cytotoxicity of MDA-MB-231 cells incubated with MSN-NH_2 and MSN-CMC and (b) % Cytotoxicity of MDA-MB-231 cells incubated with free curcumin, MSN-cur-NH_2 and MSN-cur-CMC keeping the amount of curcumin same in all the samples (x axis represents concentration of free curcumin and curcumin incubated in MSN-NH_2 and MSN-CMC)

cancer cells. A comparison of the MTT results of MSN-cur-NH_2 and MSN-cur-CMC with the same concentration of curcumin inside the pores indicated that MSN-cur-CMC has higher cell inhibitory effect as compared to that of MSN-cur-NH_2. The GI_{50} of MSN-cur-NH_2 and MSN- cur-CMC are found to be 7 and 1.5 µg/mL respectively (**Figure 3.8 (b)**). This clearly indicates that CMC functionalization helps with better internalization of curcumin-loaded MSNs, resulting in better inhibition of the cancer cells as compared to MSN-cur-NH_2.

3.4.5 Intracellular Uptake of MSN Particles

For the cellular uptake studies, breast cancer cell line MDA-MB-231 was incubated with free curcumin (16 µg/mL), MSN-cur-NH_2 and MSN-cur-CMC (GI_{50} conc. of ~7 and 1.5 µg/mL respectively). The GI_{50} concentrations were selected to ensure that the same amount of drug enters the cells (as calculated from MTT assay). Similarly, MSNs

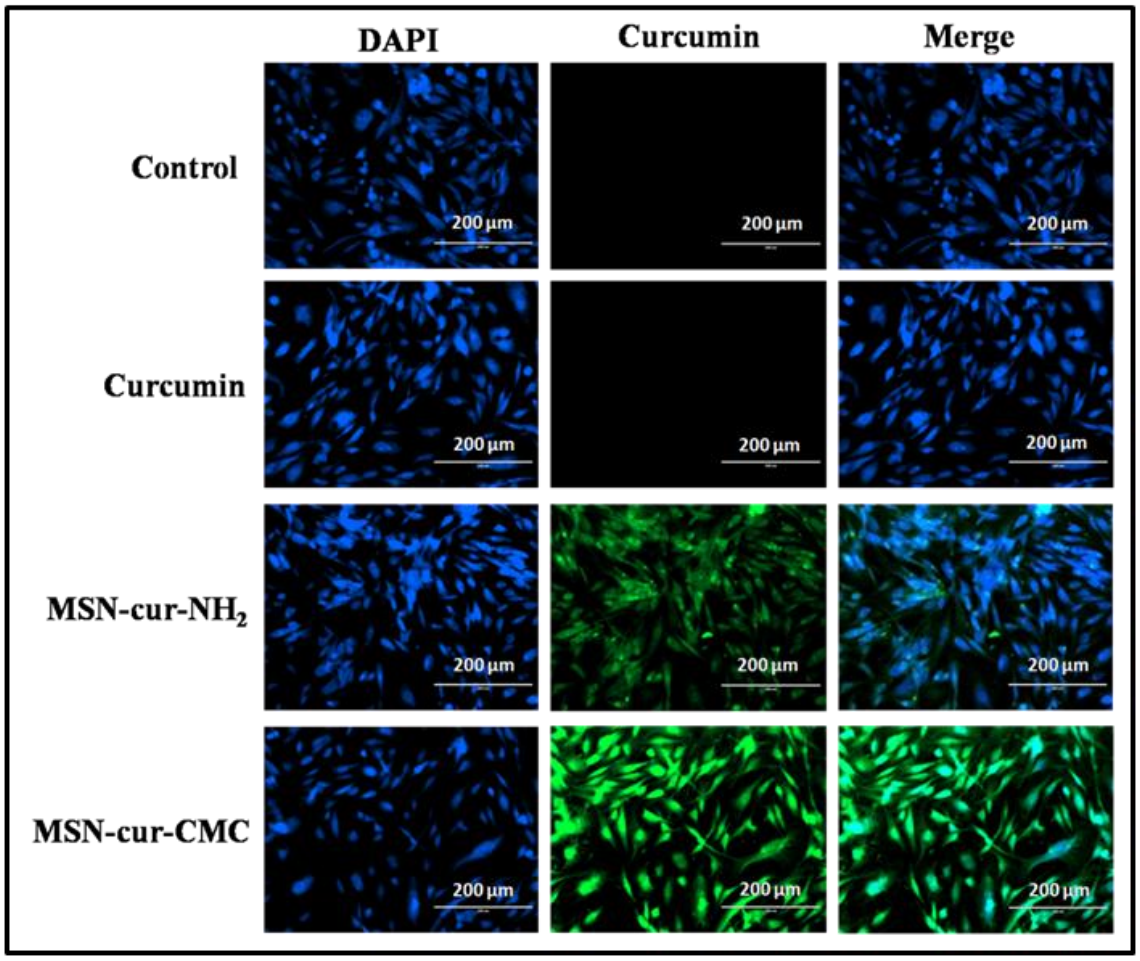

Figure 3.9. Intracellular uptake of $–NH_2$ and –CMC functionalized MSNs using fluorescence microscopy. Images of MDA-MB-231 incubated with 16 µg/mL of free curcumin, MSN-cur-NH_2 (GI_{50}= 7 µg/mL) and MSN-cur-CMC (GI_{50}= 1.5 µg/mL). Control refers to the non-treated MDA-MB-231 cells. Blue fluorescence is due to nucleus staining of cells with 4', 6-Diamidino-2-Phenylindole Dihydrochloride (DAPI) and green is due to fluorescence of curcumin release inside the cells effectively in MDA-MB-231 cancer cells, which is also in agreement with the MTT assay where the comparable % cytotoxicity in the cells is absent

without curcumin (MSN-NH_2 and MSN-CMC) were used as a control at a concentration of 200 µg/mL. The fluorescence of curcumin inside the cells was captured after 1 h of incubation of the MSNs (with and without curcumin) and free curcumin. It was observed that free curcumin does not show any fluorescence after 1 h, whereas MSN-cur-NH_2 and MSN-cur-CMC showed fluorescence of curcumin molecules indicating that curcumin molecules are not able to entre inside the cells in the absence of carriers. It was also evident from the images that MSN-cur-CMC showed much better fluorescence due to curcumin as compared to that of MSN-cur-NH_2

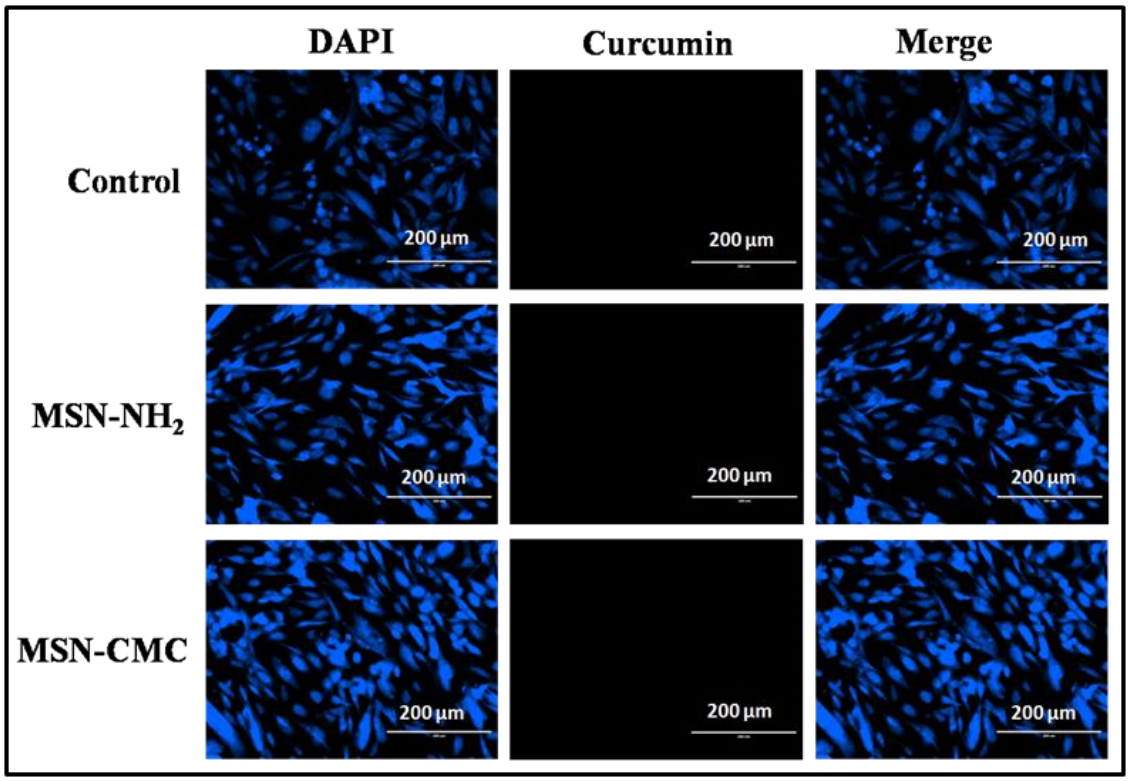

Figure 3.10. Intracellular uptake of MSN-NH_2 and MSN-CMC without curcumin using fluorescence microscopy. Images are at a magnification of 200 µm of MDA-MB-231 incubated with a concentration of 200 µg/ml. Blue fluorescence is due to nuclei staining of cell with DAPI

(**Figure 3.9**). This confirms that CMC-grafted MSNs help with better internalization of curcumin inside the cells as compared to MSN-NH_2 since the GI_{50} of MSN-cur-CMC is much lower compared to that of MSN-cur-NH_2. The control experiments with MSN-NH_2 and MSN-CMC do not show any fluorescence, as expected (**Figure 3.10**). The results indicate that the CMC-coated MSNs are internalized inside the cells more effectively as compared to MSN-cur-NH_2.

3.4.6 Apoptosis by Fluorescein Isothiocyanate (FITC)-Labelled Annexin V (Annexin V-FITC)/ Propidium Iodine Iodide (PI) Staining

In order to find out whether the curcumin-loaded MSNs mediate decreases in cell growth due to apoptosis, we investigated apoptosis in MDA-MB-231 cells using annexin fluorescein isothiocyanate (FITC)-labelled annexin V (annexin V-FITC)/propidium iodide (PI) and 4',6-Diamidino-2-Phenylindole Dihydrochloride

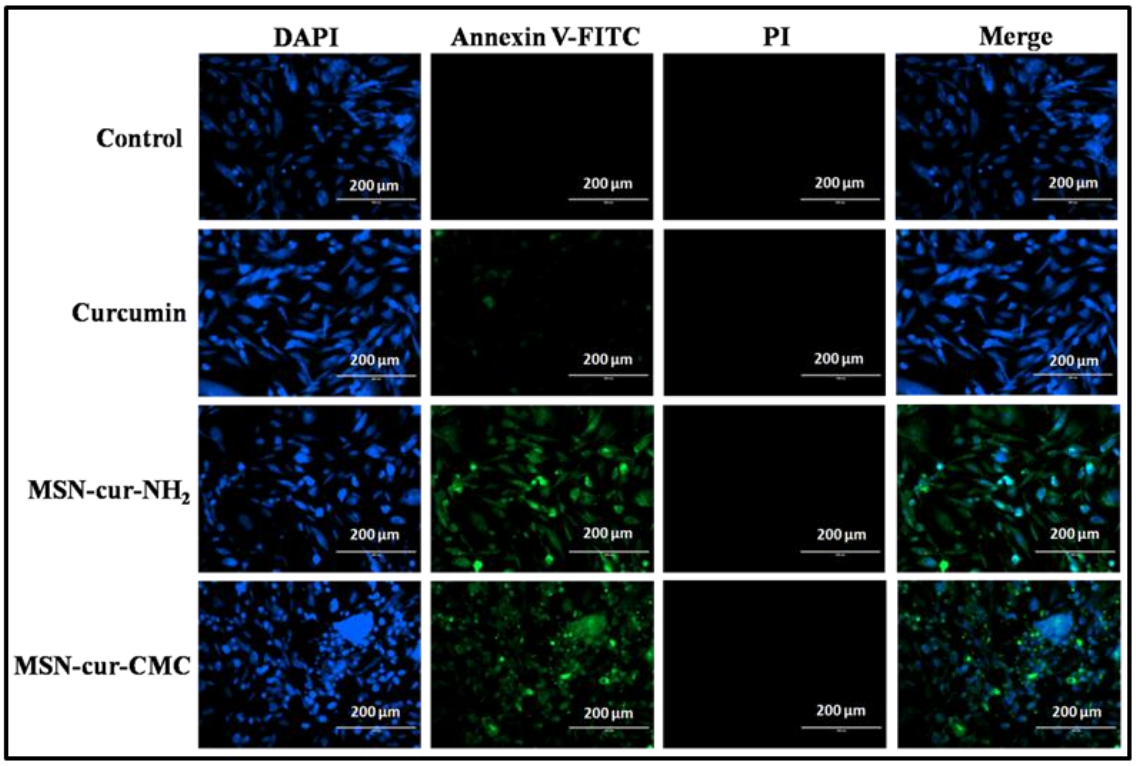

Figure 3.11. Apoptosis of MDA-MB-231 cells using fluorescence microscopy. Images of MDA-MB-231 incubated with 16 µg/mL of free curcumin, MSN-cur-NH_2 (GI_{50} = 7 µg/mL) and MSN-cur-CMC (GI_{50} =1.5 µg/mL). Control refers to the non-treated MDA-MB-231 cells. Blue fluorescence is due to nucleus staining of cells with DAPI and green fluorescence is due to staining of cells by annexin V-FITC

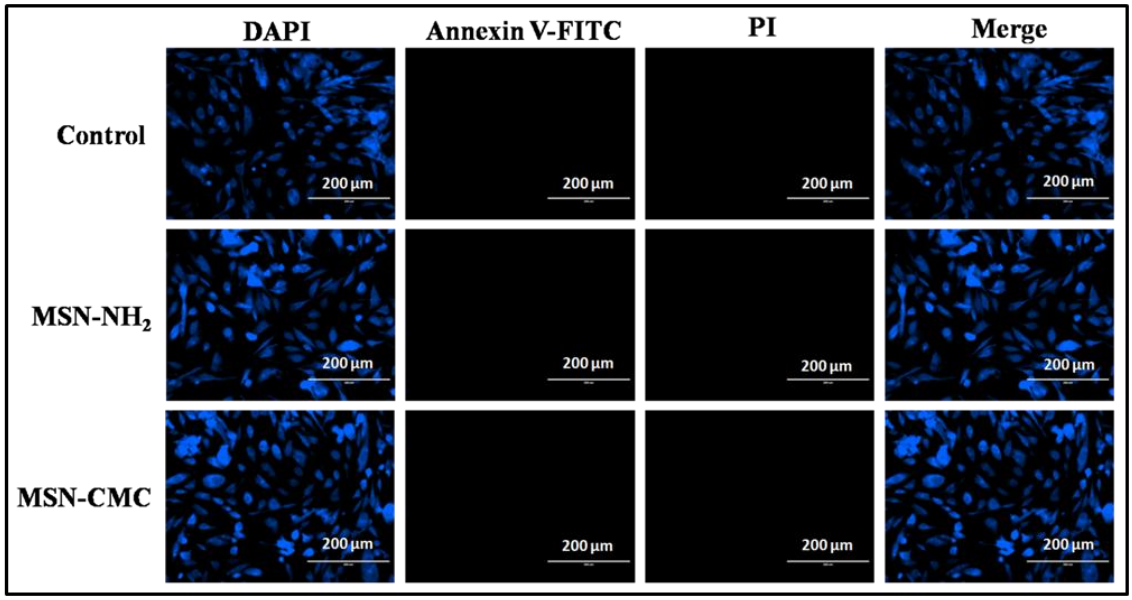

Figure 3.12. Apoptosis of MDA-MB-231 cells using fluorescence microscopy. Images are at a magnification of 200 µm of MDA-MB-231 incubated with 200 µg/ml of MSN-NH_2 and MSN-CMC. Blue fluorescence is due to nuclei staining of cell with DAPI

(DAPI) as the staining agents. We observed that treatment of cells with free curcumin (16 µg/mL) and GI_{50} concentrations of MSN-cur-NH_2 (7 µg/mL) and MSN-cur-CMC (1.5 µg/mL) resulted in an increase in the apoptotic cells in 48 h (**Figure 3.11**). The MSNs without curcumin, taken as a control, did not show any green fluorescence due to annexin V-FITC/PI, indicating no apoptosis in the cells, and are thus biocompatible (**Figure 3.12**). The calculated apoptotic ratios in 48 h for control, curcumin, MSN-cur-NH_2 and MSN-cur-CMC were found to be 2.5 %, 9.7 %, 49 % and 69 % respectively

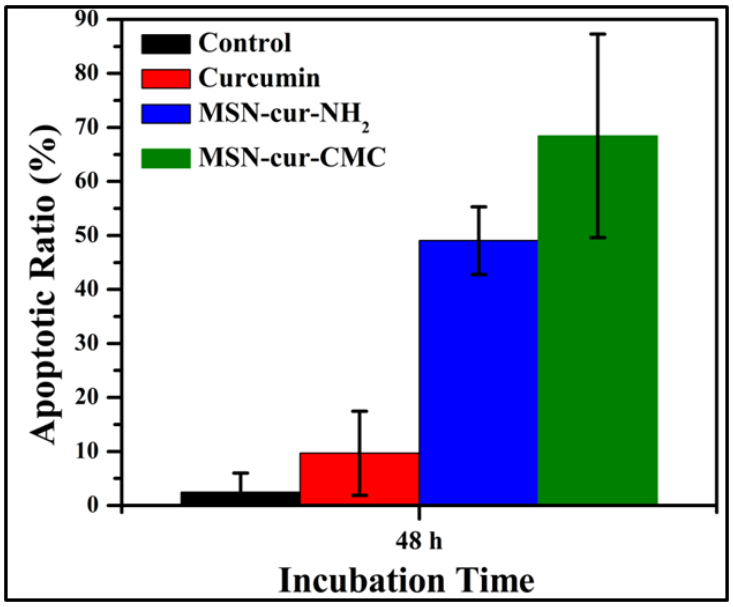

Figure 3.13. Apoptotic ratios of free curcumin, MSN-cur-NH_2 and MSN-cur-CMC in 48 h

(Figure 3.13). The high apoptotic value of MSN-cur-CMC compared to free curcumin and MSN-cur-NH_2 further confirmed that CMC coating on the MSN surface helps with better uptake of MSNs inside the cells and hence more curcumin molecules are released effectively at the targeted site.

We also observed that PI positive cells were not observed in the experiment suggesting the absence of necrosis. In order to prove that the green fluorescence observed in the cells after treatment with MSN-cur-NH_2 and MSN-cur-CMC is due to staining of the cells with annexin V-FITC and not due to fluorescence due to curcumin molecules, we performed the imaging of the cells without annexin V-FITC after 48 h (**Figure 3.14**). We observed that in absence of annexin V-FITC, green

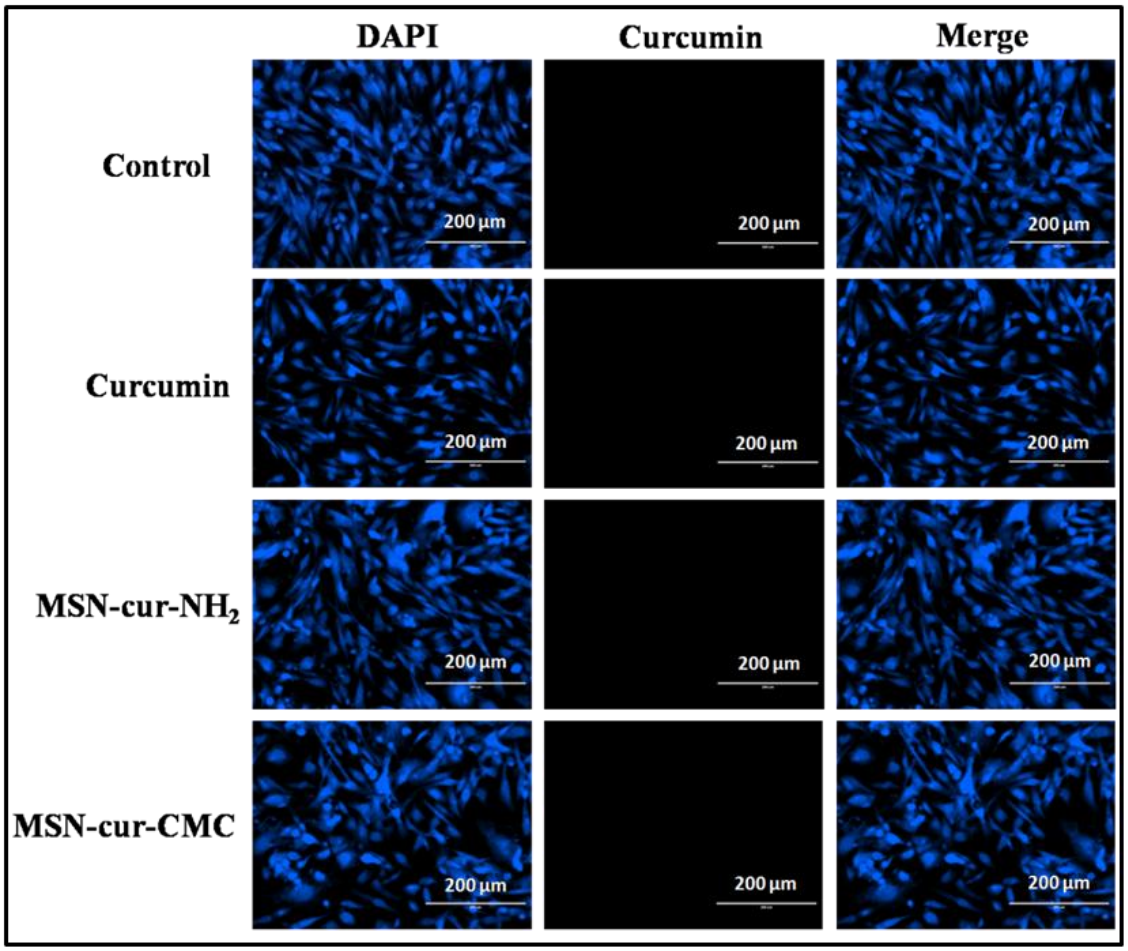

Figure 3.14. Intracellular uptake of $–NH_2$ and –CMC functionalized MSNs using fluorescence microscopy after 48 h. Images of MDA-MB-231 incubated with 16 µg/ml of free curcumin, MSN-cur-NH_2 (GI_{50}= 7 µg/ml) and MSN-cur-CMC (GI_{50}= 1.5 µg/ml). Control refers to the non treated MDA-MB-231 cells. Blue fluorescence is due to nuclei staining of cell with DAPI and green due to fluorescence of curcumin release inside the cells

fluorescence was absent in the cells as the fluorescence due to curcumin do not last for longer time due to quenching (i.e., degradation of curcumin).[23] This experiment proves that MSN-cur-CMC induces cell death in the MDA-MB-231 cell line via apoptotic pathway.

3.5 Conclusion

In conclusion, we have successfully synthesized MSNs with particle sizes in the range of 120–130 nm and pore size of 2–3 nm as confirmed by TEM, SEM and N_2 adsorption–desorption studies. The grafting of MSNs with $–NH_2$ and CMC moieties on

the surface was confirmed by a decrease in the surface area by N_2– adsorption data and weight loss by TGA data. Also, the zeta potential showed a change in the sign of the charge from positive to negative upon grafting with $–NH_2$ and CMC, which also confirmed the functionalization. The drug release profile in 0.5 % SLS solution showed only a 15 % release of curcumin molecules from MSN-cur-CMC as compared to 45 % from MSN-cur-NH_2 over a period of 72 h. The release profile indicated that CMC helped in preventing curcumin molecules from experiencing premature release over a longer period of time. An MTT assay showed the negligible toxic effects of MSN-NH_2 and MSN-CMC on breast cancer cell line MDA-MB-231 up to a concentration of 200 µg/mL, thus indicating biocompatibility of the functionalized MSNs. MSN-cur-CMC showed enhanced cellular uptake and percent cytotoxicity as compared to MSN-cur-NH_2 as observed in the MTT assay (from GI_{50} values) on MDA-MB-231 breast cancer cell line. Apoptosis studies performed over a period of 48 h showed that MSN-cur-CMC induces cell death in the MDA-MB-231 cell line via apoptotic pathway. All the above-mentioned observations indicate that CMC grafting on the surface of MSNs enhanced the cellular uptake and cytotoxicity of the cells at remarkably lower concentrations of the curcumin drug. These studies demonstrate that MSN-CMC nanogels could be used as model systems for enhanced cellular uptake and drug delivery applications.

References

[1] K.N. Yang, C.Q. Zhang, W. Wang, P.C. Wang, J.P. Zhou, X.J. Liang, pH-responsive mesoporous silica nanoparticles employed in controlled drug delivery systems for cancer treatment, Cancer biology & medicine, 11 (2014) 34-43.

[2] B.A. Chabner, T.G. Roberts, T.G. Roberts Jr, Timeline: Chemotherapy and the war on cancer, Nature Reviews Cancer, 5 (2005).

[3] M. De, P.S. Ghosh, V.M. Rotello, Applications of Nanoparticles in Biology, Advanced Materials, 20 (2008) 4225-4241.

[4] A.H. Faraji, P. Wipf, Nanoparticles in cellular drug delivery, Bioorganic & medicinal chemistry, 17 (2009) 2950-2962.

[5] K. Ninomiya, S. Kawabata, H. Tashita, N. Shimizu, Ultrasound-mediated drug delivery using liposomes modified with a thermosensitive polymer, Ultrasonics sonochemistry, 21 (2014) 310-316.

[6] J. Ding, L. Chen, C. Xiao, L. Chen, X. Zhuang, X. Chen, Noncovalent interaction-assisted polymeric micelles for controlled drug delivery, Chemical communications, 50 (2014) 11274-11290.

[7] X.-Y. Ke, V.W.L. Ng, S.-J. Gao, Y.W. Tong, J.L. Hedrick, Y.Y. Yang, Co-delivery of thioridazine and doxorubicin using polymeric micelles for targeting both cancer cells and cancer stem cells, Biomaterials, 35 (2014) 1096-1108.

[8] B. Yavuz, S.B. Pehlivan, İ. Vural, N. Ünlü, In vitro/in vivo evaluation of dexamethasone—PAMAM dendrimer complexes for retinal drug delivery, Journal of pharmaceutical sciences, 104 (2015) 3814-3823.

[9] C. Zhang, D. Pan, K. Luo, W. She, C. Guo, Y. Yang, Z. Gu, Peptide Dendrimer–Doxorubicin Conjugate-Based Nanoparticles as an Enzyme-Responsive Drug Delivery System for Cancer Therapy, Advanced healthcare materials, 3 (2014) 1299-1308.

[10] H. Wu, H. Shi, H. Zhang, X. Wang, Y. Yang, C. Yu, C. Hao, J. Du, H. Hu, S. Yang, Prostate stem cell antigen antibody-conjugated multiwalled carbon nanotubes for targeted ultrasound imaging and drug delivery, Biomaterials, 35 (2014) 5369-5380.

[11] S. Kwon, R.K. Singh, R.A. Perez, E.A. Abou Neel, H.W. Kim, W. Chrzanowski, Silica-based mesoporous nanoparticles for controlled drug delivery, Journal of tissue engineering, 4 (2013) 2041731413503357.

[12] S. Wang, Ordered mesoporous materials for drug delivery, Microporous and Mesoporous Materials, 117 (2009) 1-9.

[13] M. Vallet-Regí, L. Ruiz-González, I. Izquierdo-Barba, J.M. González-Calbet, Revisiting silica based ordered mesoporous materials: medical applications, J. Mater. Chem., 16 (2006) 26-31.

[14] M. Bouchoucha, M.-F. Côté, R. C.-Gaudreault, M.-A. Fortin, F. Kleitz, Size-Controlled Functionalized Mesoporous Silica Nanoparticles for Tunable Drug Release and Enhanced Anti-Tumoral Activity, Chemistry of Materials, 28 (2016) 4243-4258.

[15] J. Morell, M. Güngerich, G. Wolter, J. Jiao, M. Hunger, P.J. Klar, M. Fröba, Synthesis and characterization of highly ordered bifunctional aromatic periodic mesoporous organosilicas with different pore sizes, J. Mater. Chem., 16 (2006) 2809-2818.

[16] V. Malgras, Q. Ji, Y. Kamachi, T. Mori, F.-K. Shieh, K.C.-W. Wu, K. Ariga, Y. Yamauchi, Templated Synthesis for Nanoarchitectured Porous Materials, Bull. Chem. Soc. Jpn., 88 (2015) 1171–1200.

[17] E. Yamamoto, K. Kuroda, Colloidal Mesoporous Silica Nanoparticles, Bull. Chem. Soc. Jpn., 89 (2016) 501-539.

[18] G. Zhan, HuaChunZeng, Integrated nanocatalystswithmesoporoussilica/silicateand microporous MOFmaterials, Coordination ChemistryReviews, 320-321 (2016) 181-192.

[19] J.L. Vivero-Escoto, Slowing, II, B.G. Trewyn, V.S. Lin, Mesoporous silica nanoparticles for intracellular controlled drug delivery, Small, 6 (2010) 1952-1967.

[20] F. Tang, L. Li, D. Chen, Mesoporous silica nanoparticles: synthesis, biocompatibility and drug delivery, Adv Mater, 24 (2012) 1504-1534.

[21] M. Karimi, H. Mirshekari, M. Aliakbari, P. Sahandi-Zangabad, M.R. Hamblin, Smart mesoporous silica nanoparticles for controlled-release drug delivery, Nanotechnology Reviews, 5 (2016) 195-207.

[22] B.G. Trewyn, S. Giri, Slowing, II, V.S. Lin, Mesoporous silica nanoparticle based controlled release, drug delivery, and biosensor systems, Chemical communications, (2007) 3236-3245.

[23] Y.-J. Wang, M.-H. Pan, A.-L. Cheng, L.-I. Lin, Y.-S. Ho, C.-Y. Hsieh, J.-K. Lin, Stability of curcumin in buffer solutions and characterization of its degradation products, Journal of Pharmaceutical and Biomedical Analysis, 15 (1997) 1867-1876.

[24] Slowing, II, J.L. Vivero-Escoto, C.W. Wu, V.S. Lin, Mesoporous silica nanoparticles as controlled release drug delivery and gene transfection carriers, Advanced drug delivery reviews, 60 (2008) 1278-1288.

[25] J. Lu, M. Liong, J.I. Zink, F. Tamanoi, Mesoporous silica nanoparticles as a delivery system for hydrophobic anticancer drugs, Small, 3 (2007) 1341-1346.

[26] C.H. Lee, S.H. Cheng, I.P. Huang, J.S. Souris, C.S. Yang, C.Y. Mou, L.W. Lo, Intracellular pH-responsive mesoporous silica nanoparticles for the controlled release of anticancer chemotherapeutics, Angewandte Chemie, 49 (2010) 8214-8219.

[27] J. Lu, M. Liong, Z. Li, J.I. Zink, F. Tamanoi, Biocompatibility, biodistribution, and drug-delivery efficiency of mesoporous silica nanoparticles for cancer therapy in animals, Small, 6 (2010) 1794-1805.

[28] Q. He, Z. Zhang, Y. Gao, J. Shi, Y. Li, Intracellular localization and cytotoxicity of spherical mesoporous silica nano- and microparticles, Small, 5 (2009) 2722-2729.

[29] A.S. Johann Kecht, and Thomas Bein, Selective Functionalization of the Outer and Inner Surfaces in MSN, Chemistry of Materials, 20 (2008) 7207-7214.

[30] L. Ma'mani, S. Nikzad, H. Kheiri-Manjili, S. Al-Musawi, M. Saeedi, S. Askarlou, A. Foroumadi, A. Shafiee, Curcumin-loaded guanidine functionalized PEGylated I3ad mesoporous silica nanoparticles KIT-6: practical strategy for the breast cancer therapy, European journal of medicinal chemistry, 83 (2014) 646-654.

[31] J. Lu, Z. Li, J.I. Zink, F. Tamanoi, In vivo tumor suppression efficacy of mesoporous silica nanoparticles-based drug-delivery system: enhanced efficacy by folate modification, Nanomedicine : nanotechnology, biology, and medicine, 8 (2012) 212-220.

[32] Q. Zhang, K.G. Neoh, L. Xu, S. Lu, E.T. Kang, R. Mahendran, E. Chiong, Functionalized mesoporous silica nanoparticles with mucoadhesive and sustained drug release properties for potential bladder cancer therapy, Langmuir : the ACS journal of surfaces and colloids, 30 (2014) 6151-6161.

[33] L. Yuan, Q. Tang, D. Yang, J.Z. Zhang, F. Zhang, J. Hu, Preparation of pH-Responsive Mesoporous Silica Nanoparticles and Their Application in Controlled Drug Delivery, The Journal of Physical Chemistry C, 115 (2011) 9926-9932.

[34] M. Kar, N. Tiwari, M. Tiwari, M. Lahiri, S.S. Gupta, Poly-L-Arginine Grafted Silica Mesoporous Nanoparticles for Enhanced Cellular Uptake and their Application in DNA Delivery and Controlled Drug Release, Particle & Particle Systems Characterization, 30 (2013) 166-179.

[35] M. Gulfam, B.G. Chung, Development of pH-Responsive Chitosan-Coated Mesoporous Silica Nanoparticl, Macromolecular Research, 22 (2014) 412-417.

[36] M. Zhu, Y. Zhu, L. Zhang, J. Shi, Preparation of chitosan/mesoporous silica nanoparticle composite hydrogels for sustained co-delivery of biomacromolecules and small chemical drugs, Science and technology of advanced materials, 14 (2013) 045005.

[37] Q. Zhao, H. Geng, Y. Wang, Y. Gao, J. Huang, Y. Wang, J. Zhang, S. Wang, Hyaluronic acid oligosaccharide modified redox-responsive mesoporous silica nanoparticles for targeted drug delivery, ACS applied materials & interfaces, 6 (2014) 20290-20299.

[38] M. Gary-Bobo, Y. Mir, C. Rouxel, D. Brevet, I. Basile, M. Maynadier, O. Vaillant, O. Mongin, M. Blanchard-Desce, A. Morère, M. Garcia, J.-O. Durand, L. Raehm,

Mannose-Functionalized Mesoporous Silica Nanoparticles for Efficient Two-Photon Photodynamic Therapy of Solid Tumors, Angewandte Chemie International Edition, 50 (2011) 11425-11429.

[39] L. Hu, C. Sun, A. Song, D. Chang, X. Zheng, Y. Gao, T. Jiang, S. Wang, Alginate encapsulated mesoporous silica nanospheres as a sustained drug delivery system for the poorly water-soluble drug indomethacin, Asian Journal of Pharmaceutical Sciences, 9 (2014) 183-190.

[40] B.G. TREWYN, I.I. SLOWING, S. GIRI, H.-T. CHEN, V.S.-Y. LIN, Synthesis and Functionalization of a Mesoporous Silica Nanoparticle Based on the Sol–Gel Process and Applications in Controlled Release, Acc. Chem. Res., 40 (2007) 846-853.

[41] F. Hoffmann, M. Cornelius, J. Morell, M. Froba, Silica-based mesoporous organic-inorganic hybrid materials, Angewandte Chemie, 45 (2006) 3216-3251.

[42] X. Huang, N.P. Young, H.E. Townley, Characterization and Comparison of Mesoporous Silica Particles for Optimized Drug Delivery, Nanomaterials and Nanotechnology, 4 (2014) 2.

Chapter-4

Thermothickening Behavior of MPEG-b-PCL Grafted Poly(acrylic acid)

4.1 Introduction

Water soluble polymers (WSPs) and hydrophobically modified water soluble polymers (HMPs)/ Associating polymers (APs) are important class of materials and find extensive applications as thickening/ rheology control agents in paints, coatings, textiles pastes, pharmaceutical creams and ointments, food formulations etc.[1] However, the viscosity of these polymer solutions decreases with increase in temperature which is in line with the Arrhenius law for flow. This can be a severe drawback especially for their high temperature applications. Therefore, it becomes important to use polymers where the viscosity of their solutions remain independent of temperature or even increase upon heating. In this context, thermo thickening polymers are attracting increasing attention recently in which the viscosity of aqueous solutions of these polymers increase upon heating and undergo sol-to-gel transition at certain critical temperature and polymer concentration. The basic requirement of the thermo thickening polymer is the co-presence of a highly water soluble hydrophilic polymer and the partial hydrophobic polymer exhibiting the thermodynamic lower critical solution temperature (LCST) property. Owing to their LCST property, the hydrophobic moiety of the polymer self associate reversibly into micro domains when the temperature is raised above the LCST. But the ultimate phase separation in the solution is prevented by the hydrophilic polymer which eventually leads the polymer solution to undergo sol-to-gel transition.

Thermo thickening polymers have great potential as injectables in controlled release technology (CRT).[2-5] These polymers do not require surgical operations for implantation and both hydrophilic and hydrophobic drugs can be incorporated by simple physical mixing. Extensive work on thermo thickening polymers has been reported in the literature. For example, Hourdet et al [1] have developed a whole family of thermo thickening polymers by grafting LCST side chains like PEO, PNIPAM, and PEPO on to a hydrophilic polymer, sodium polyacrylate (PAA-Na). An excellent review on thermo thickening polymers with fundamental aspects and applications has been reported in the literature.[6] The thermo thickening behaviour of amphiphilic systems based on diblock, triblock and multi block copolymers of PEG and PCL have also been studied extensively.[7-10] These block

copolymers in aqueous medium can form micelles at certain polymer concentration due to the hydrophobic associations of PCL chains when the temperature is increased. The tendency of partial crystallization of PCL chains which contributes to the gelation is also reported in the literature.[11-13] Although, extensive studies have been performed on the sol-gel transition of these polymers, a molecular insight in the thermo thickening behaviour of MPEG-*b*-PCL grafted poly(acrylic acid)(PAA) has not been made. Besides synthetic polymers, some of the natural polymers like polysaccharides namely chitosan [14], hyaluronic acid [15], carboxymethyl cellulose [16], alginate [17], pullulan [18] and dextran [19] have been used along with LCST polymers for the synthesis of thermo thickening polymers.

In the present work, we have studied the thermo thickening behaviour of MPEG-*b*-PCL grafted poly(acrylic acid) aqueous solutions using rheology, light scattering and NMR techniques. The controlled synthesis of block copolymers of MPEG-*b*-PCL with equal molecular weights was carried out by ring opening polymerization (ROP) taking a known molecular weight of MPEG as an initiator. Subsequently, the grafting reaction of MPEG-*b*-PCL onto PAA was carried out between the carboxylic groups of PAA and terminal hydroxyl groups of PCL in MPEG-*b*-PCL. The structural characterization of the obtained thermo thickening polymers was performed using NMR spectroscopy and gel permeation chromatography. The results from multiple experimental techniques give insights into the molecular level mechanism of the thermo thickening process.

4.2 Experimental

4.2.1 Materials

Poly(acrylic acid) (PAA) solution (80% in water, MW= 2,50,000 g/mol), ε-caprolactone (CL), stannous octoate ($Sn(Oct)_2$), polyethylene glycol mono methyl ether (MW=2,000 g/mol) (MPEG), dicyclohexyl carbodiimide (DCCI) and N, N-dimethyl amino pyridine (DMAP) were procured from Sigma Aldrich, USA. Dry dimethyl sulphoxide (DMSO), diethyl ether and sodium bicarbonate ($NaHCO_3$) were purchased from Merck, India. All the chemicals were of analytical grade and used as received.

4.2.2 Synthesis of block copolymer of MPEG-*b*-PCL

The block copolymer MPEG-*b*-PCL was synthesized via ring opening polymerization in a bulk state, using ε-caprolactone (CL) as a monomer, MPEG as a macro initiator and stannous octoate ($Sn(Oct)_2$) as a catalyst. All glasswares were dried at 80 °C for 12 h to avoid any moisture contamination. In a typical synthesis, 4 g (3.5 mmol) of MPEG was dissolved in anhydrous toluene (100 ml) and toluene was distilled off completely under vacuum in order to remove moisture present in the polymer. To the above solution, CL (0.0175 mmol) and $Sn(Oct)_2$ (0.874 mmol) was added and the reaction mixture was stirred at 100 °C for 24 h under N_2 atmosphere. The product obtained was then dissolved in chloroform and precipitated in diethylether. The precipitation was carried out twice in diethyl ether to obtain the pure product. The product obtained was finally dried in a vacuum oven at 50 °C. (Yield = 95 %)

^{1}H NMR ($CDCl_3$) of MPEG-*b*-PCL copolymer: δ 1.38 (-OCH_2CH_2**CH_2**CH_2CH_2CO-), δ 1.65 (-OCH_2**CH_2**CH_2**CH_2**CH_2CO-), δ 2.31 (-$OCH_2CH_2CH_2CH_2$**CH_2**CO-), δ 3.38 (terminal –CH_3 of MPEG), δ 3.65 (-O**CH_2CH_2**O-), δ 4.06 (-O**CH_2**$CH_2CH_2CH_2CH_2CO$).

4.2.3 Grafting of MPEG-*b*-PCL block copolymer onto PAA (PAA-*g*-MPEG-*b*-PCL)

The PAA powder was obtained by lyophilization of PAA solution received from Sigma Aldrich. PAA (5 g, 69.4 mmol) was dissolved in 100 ml dry DMSO in a 250 ml two necked round bottomed flask. The dissolution was carried out by stirring the solution for 2 h at room temperature under N_2 atmosphere. To this solution, DCC (6.94 mmol) and DMAP (6.94 mmol) pre-dissolved in 10 ml dry DMSO were added and the reaction mixture was stirred for an additional 4 h at room temperature for the complete activation of carboxylic groups in PAA. After 4 h, MPEG-*b*-PCL (0.694 mmol, 1 mol%) solution in dry DMSO was added drop wise to the reaction mixture under stirring in N_2 atmosphere. The reaction mixture was allowed to stir for 24 h at 40 °C. The product obtained was precipitated in $CHCl_3$, filtered and dried under vacuum at 50

°C for further purification. The dry product obtained was further dissolved in distilled water, dialyzed for 48 h with frequent changes of distilled water. Finally, the solution was neutralized using sodium bicarbonate and lyophilized to get the pure product, PAA-*g*-MPEG-*b*-PCL-1 (1mol% grafting) in the powder form. (Yield = 90 %)

The same procedure was followed to obtain PAA-*g*-MPEG-*b*-PCL-1.5 with 1.5 mol% grafting (Yield = 92 %). PAA was also neutralized using $NaHCO_3$ in order to have similar conditions in all experiments unless otherwise mentioned.

^{1}H NMR (D_2O:CD_3OD, 70:30) of PAA: δ 1.57 (-**CH_2**CH(COOH)-) and δ 2.18 (-CH_2**CH**(COOH)-).

^{1}H NMR (D_2O:CD_3OD, 70:30) of PAA-*g*-MPEG-*b*-PCL (1mol% grafting): δ 0.5-2.8 (-OCH_2CH_2**CH_2**CH_2CH_2CO-), (-OCH_2**CH_2**CH_2**CH_2**CH_2CO-), (-$OCH_2CH_2CH_2CH_2$**CH_2**CO-), (-**CH_2**CH(COOH)-), (-CH_2**CH**(COOH)-), δ 3.66 (-O**CH_2CH_2**O-), δ 4.07 (-O**CH_2**$CH_2CH_2CH_2CH_2CO$-).

^{1}H NMR (D_2O:CD_3OD, 70:30) of PAA-*g*-MPEG-*b*-PCL (1.5 mol% grafting): δ 0.5-2.8 (-OCH_2CH_2**CH_2**CH_2CH_2CO-), (-OCH_2**CH_2**CH_2**CH_2**CH_2CO-), (-$OCH_2CH_2CH_2CH_2$**CH_2**CO-), (-**CH_2**CH(COOH)-), (-CH_2**CH**(COOH)-), δ 3.66 (-O**CH_2CH_2**O-), δ 4.07 (-O**CH_2**$CH_2CH_2CH_2CH_2CO$-).

4.2.4 Sample Preparation

Polymer solutions (g/L) of desired concentrations were prepared by dissolving a known amount of polymer in de-ionized water. All solutions were gently stirred at room temperature for 24 h to obtain homogenous solutions.

4.3 Characterizations

4.3.1 NMR Spectroscopy

^{1}H NMR spectra for characterization of mono methoxy terminated PEG (MPEG), PAA, MPEG-*b*-PCL and PAA-*g*-MPEG-*b*-PCL-1 and PAA-*g*-MPEG-*b*-PCL-1.5 were recorded on Bruker AV-200, AV-500 NMR spectrometers operating at ^{1}H frequency of

200 and 500 MHz, respectively. ^{1}H spectra of MPEG and MPEG-*b*-PCL were recorded in $CDCl_3$, whereas PAA and PAA-*g*-MPEG-*b*-PCL-1 and PAA-*g*-MPEG-*b*-PCL-1.5 samples were recorded in D_2O:CD_3OD (70:30) mixtures (concentration of polymer =100 mg mL^{-1}). The samples were homogenized for 24 h before recording the NMR spectra.

Variable temperature NMR, spin-lattice and spin-spin relaxation time (T_1, T_2) measurements and 2D NMR experiments were carried out on Bruker Avance 500 and Avance III HD 700 spectrometers using 5 mm BBO probes with z-axis gradients. Experiments were carried out on PAA-*g*-MPEG-*b*-PCL-1 and PAA-*g*-MPEG-*b*-PCL-1.5 samples in D_2O at concentrations of 10 mg/ml or 25 mg/ml. ^{1}H and ^{13}C 1D spectra with 64 and 4800 scans respectively, were recorded using a flip angle of 30° with an interscan delay of 3 s in the temperature range of 25 – 60 °C. ^{1}H T_1 measurements were carried out by employing the inversion recovery scheme with 22 recovery delays while T_2 measurements were carried out employing the recently reported PROJECT CPMG scheme [20] with 22 delays. 2D NOESY spectrum was recorded at a mixing time of 64 ms with 512 × 2 K data points. 2D ^{1}H-^{13}C heteronuclear correlation experiment (HSQC) was carried out with 128 × 1 K data points. ^{13}C T_1 and T_2 measurements were performed in a pseudo 3D manner with 10-12 time delays for relaxation forming the third dimension of the HSQC experiment.

4.3.2 Gel Permeation Chromatography

Calibration method

Molecular weights and molecular weight distributions of MPEG and MPEG-*b*-PCL were determined using gel-permeation chromatography (GPC) equipped with spectra series UV-100 and spectra system RI-150 detectors using chloroform (Thermo Separation Products) as an eluent at a flow rate of 1 mL/min at 25 °C. Sample concentration was 2 mg/mL and polystyrenes were used as calibration standards.

4.3.3 Rheology

At lower polymer concentrations, Ubbelohde viscometer and at higher polymer concentrations rheometer were used to calculate the zero shear viscosity (ZSV). Viscosity measurements were performed on Schott Viscometer and rheological measurements were performed using MCR-301 (Anton Paar) stress and strain controlled rheometer. Zero shear viscosity (ZSV) was calculated by steady shear and creep measurements. Newtonian viscosity was taken into account for the calculation of ZSV in case of steady shear measurements. For creep measurements, long time compliance was used to calculate the slope, wherein the inverse of slope gives ZSV. The ZSV (Pa.s) obtained by rheometer was converted into specific viscosity (η_{sp}). The forward and reverse temperature cycle was performed in the range of 25-60 °C at a ramp rate of 1 ^{o}/min. The cup and bob geometry (cup radius 9 mm, bob radius 8.33 mm, gap length 25 mm, and cone angle 120) and a cone and plate geometry (cone 25 mm/2°, plate 50 mm) were used for the measurements. Temperature control on MCR-301 rheometer was achieved using a peltier system. Evaporation of water from the free surface of the sample was minimized by a solvent trap and also by spreading a thin layer of low viscosity silicon oil on the edges of the sample. The storage (G') and loss (G'') moduli were measured at a frequency of 20 rad/s in the temperature range 25-55°C.

4.3.4 Light Scattering

The hydrodynamic radius (R_h) and diffusion coefficient (D_f) of dilute aqueous solutions of PAA-*g*-MPEG-*b*-PCL-1.5 with various polymer concentrations as a function of temperature were determined by dynamic light scattering (DLS) using a Brookhaven Instruments equipped with a He-Ne laser operating at 632.8 nm. The particle size was calculated using 90Plus particle Sizing Software Ver. 3.94. The 3-D dynamic light scattering (LS instruments AG, Switzerland) with a laser wavelength of 632.8 nm was used to study structure and dynamics of PAA-*g*-MPEG-*b*-PCL-1.5. A special beam splitter is used to generate two identical parallel laser beams from the H-Ne laser and cross-correlation geometry is utilized to eliminate the contributions from multiple

scattering. The temperature of the sample was maintained using bath circulator with water circulating channels around a toluene bath where the sample was kept. All the polymer solutions were prepared in distilled water and were filtered using a 0.45 µm Millipore filter in a dust free cylindrical Pyrex cell. Samples were homogenized overnight before carrying out the experiments. In the temperature dependent studies, the samples were kept at a desired temperature for an hour in order to provide sufficient time for the samples to attain equilibrium.

4.4 Results and discussion

4.4.1 Synthesis of MPEG-*b*-PCL block copolymer using Ring Opening Polymerization (ROP)

The ring opening polymerization of ε-caprolactone was performed in a bulk state using the terminal alcohol of MPEG (M_n= 2,000) as an initiator (**Scheme 4.1**) in the presence of $Sn(Oct)_2$ as a catalyst. The polymerization was successfully carried out with almost quantitative yield. The M_n value of PCL in MPEG-*b*-PCL was easily controlled with the feed ratio of ε-caprolactone in the polymerization reaction. **Figure 4.1** shows the ^{1}H NMR spectrum of MPEG-*b*-PCL. The peaks at δ 3.38 and δ 3.65 were attributed to the terminal methyl protons and methylene protons of MPEG respectively. The molecular weight of the PCL segment in the diblock copolymer was determined to be ~2000 from the ratio of intensity of the terminal methoxy proton signal of MPEG at δ 3.38 and the methylene proton signal of PCL at δ 2.31 in ^{1}H NMR spectrum. Also, the M_n values

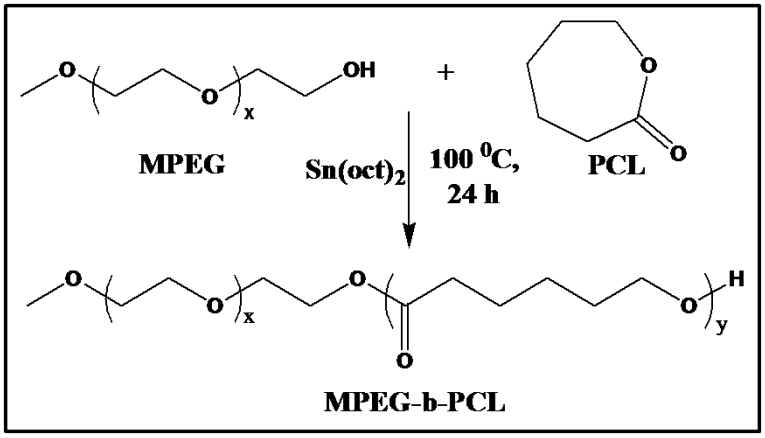

Scheme 4.1: Ring opening polymerization of ε-caprolactone

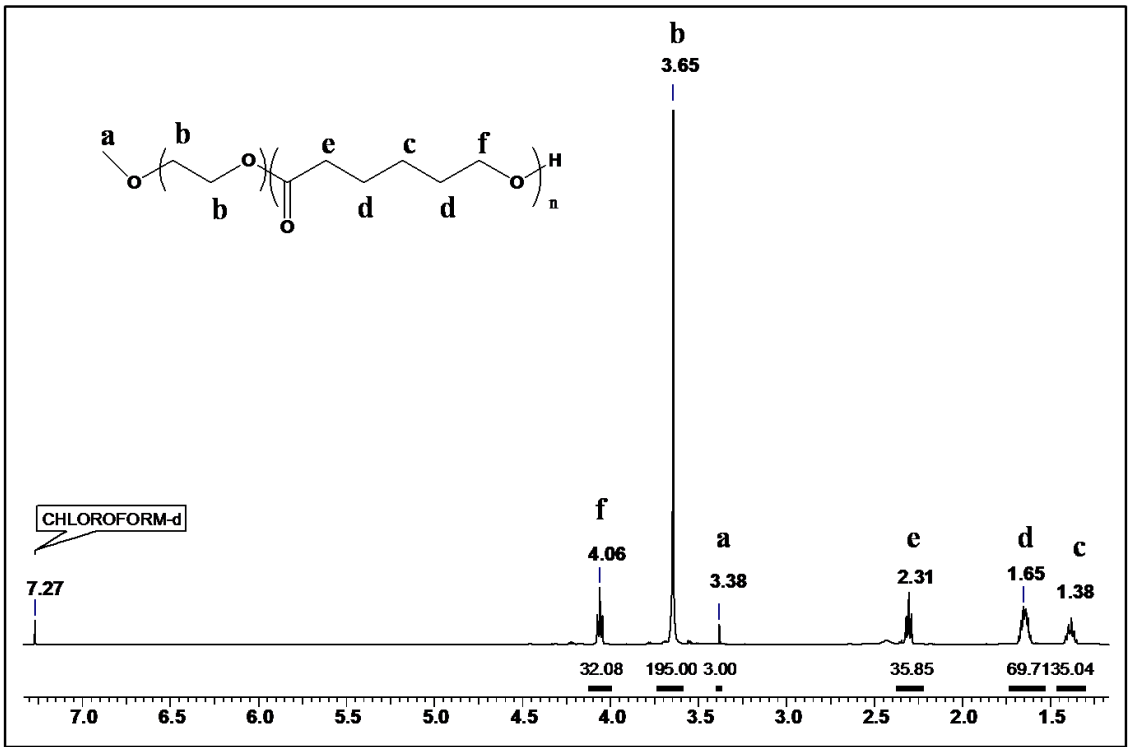

Figure 4.1. ^{1}H NMR spectrum of MPEG-*b*-PCL copolymer in $CDCl_3$

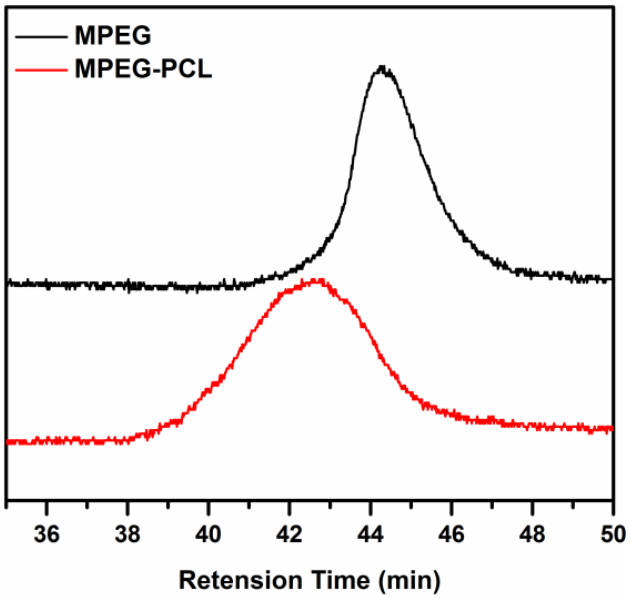

Figure 4.2. GPC data in $CHCl_3$ using polystyrene as standard

calculated from the NMR spectroscopy showed good agreement with the values obtained from GPC. The peaks of MPEG and MPEG-*b*-PCL appear at 44 and 42.5 min in the chromatogram respectively (**Figure 4.2**). The molecular weights (M_n) and polydispersity determined by GPC is given in **Table 4.1**.

Table 4.1. Molecular weight of MPEG and MPEG-*b*-PCL polymers

Sample	$[CL]_0/[MPEG]_0$	^aM_n	^bM_n	^bPDI
MPEG	-	2145	2930	1.2
MPEG-*b*-PCL	20	4140	5630	1.3

[a]Determined from ^1H NMR in $CDCl_3$
[b]Determined from GPC using polystyrene standards

4.4.2 Synthesis of PAA-*g*-MPEG-*b*-PCL polymer

PAA-*g*-MPEG-*b*-PCL polymer was synthesized by coupling reaction between carboxylic group of PAA and the hydroxyl group of MPEG-*b*-PCL using DCCI as a coupling agent and DMAP as a base in DMSO (**Scheme 4.2**). The incorporation of MPEG-*b*-PCL in the polymer was effected with 1.0 and 1.5 mol% on the basis of PAA and the stoichiometry is given in **Table 4.2**. The polymers are abbreviated as PAA-*g*-MPEG-*b*-PCL-1 and PAA-*g*-MPEG-*b*-PCL-1.5 respectively. The water soluble polymer PAA was chosen due to its ease of functionalization with hydrophobic moieties

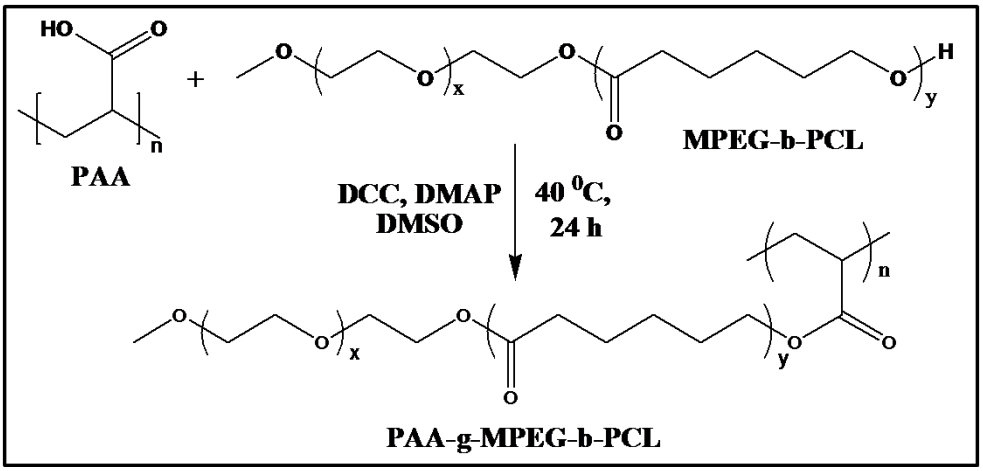

Scheme 4.2: Hydrophobic modification of PAA with MPEG-*b*-PCL copolymer

Table 4.2: Stoichiometry of synthesis of PAA-*g*-MPEG-*b*-PCL polymers

Sample	PAA (mmol)	DCC (mmol)	DMAP (mmol)	MPEG-*b*-PCL (mol%)
PAA-*g*-MPEG-*b*-PCL-1	69.4	6.94	6.94	0.694
PAA-*g*-MPEG-*b*-PCL-1.5	69.4	6.94	6.94	1.041

in both aqueous and organic solvent. In the present work, we have performed the grafting of MPEG-*b*-PCL onto PAA in organic solvents using DCCI coupling chemistry. The side product dicyclohexyl urea (DCU) was easily removed as it is insoluble in the aprotic solvent used for the coupling reaction. The copolymer MPEG-*b*-PCL is expected to be randomly grafted along the PAA backbone chain. We show in **Figure 4.3 (a)**, the ^{1}H spectrum of PAA-*g*-MPEG-*b*-PCL-1.0 recorded in a mixture of D_2O:CD_3OD in the ratio of 70:30. CD_3OD was added to decrease the viscosity of the

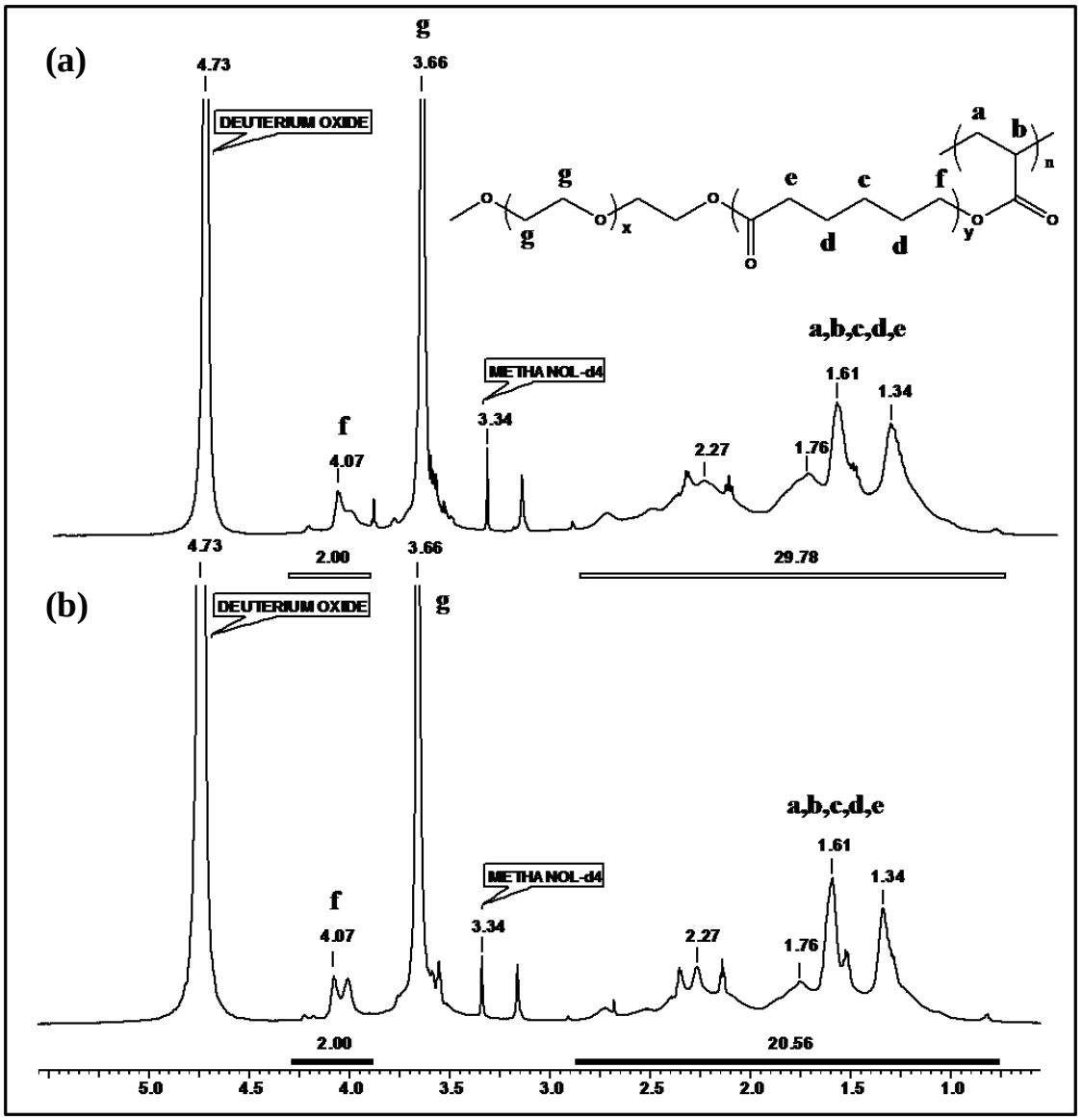

Figure 4.3.: ^{1}H NMR spectrum of (a) PAA-*g*-MPEG-*b*-PCL-1.0 and (b) PAA-*g*-MPEG-*b*-PCL-1.5 in D_2O:CD3OD (70:30)

solution. The peak at δ 4.07 corresponds to the methylene protons of PCL (-O**CH$_2$**CH$_2$CH$_2$CH$_2$CH$_2$CO-). On assigning an integration value of 2 to the peak at δ 4.07, the peaks at δ 0.5-2.8 corresponding to the three protons of PAA and the remaining protons of PCL were calculated to be 29.78. On subtracting an integration value of 8 protons from PCL, a value of 21.78 is obtained which corresponds to the three protons from PAA, thus giving a PCL: PAA ratio of 1:7.26. Now considering 18 repeat units of PCL (~MW=2,000), we obtain 0.80 mol% grafting on PAA. Similar calculations carried out in PAA-*g*-MPEG-*b*-PCL-1.5 gives around 1.31 mol% grafting (**Figure 4.3 (b)**).

4.4.3 Viscosity (η_{sp}) as a function of polymer concentration (C_p)

We show in **Figure 4.4 (a),** the specific viscosities of PAA, PAA-*g*-MPEG-*b*-PCL-1.0 and PAA-*g*-MPEG-*b*-PCL-1.5 as a function of polymer concentration measured at 25 °C. It can be seen that the neat PAA shows a gradual increase in viscosity with increase in concentration. Whereas, the viscosity behaviour of PAA-*g*-MPEG-*b*-PCL-1.0 and PAA-*g*-MPEG-*b*-PCL-1.5 follow some distinct concentration regimes. In dilute regime, where C < C* (C* ~ overlap concentration), the macromolecular chains are isolated and the 'η' is essentially controlled by the intra chain interactions. The viscosity increases gradually and scales 0.5 to the polymer concentration. Here, the viscosities of the grafted polymers are slightly lower compared to the precursor, PAA polymer. This is attributed to the compaction of chain as a result of the intramolecular hydrophobic interactions originating from the PCL chains. In the semi dilute entangled regime, where C > C*, the intermolecular hydrophobic interactions begin to dominate and the viscosity increases moderately. The viscosity scales to 1.5 to polymer concentration and the macromolecular chains are likely to obey Rouse dynamics. In the semi dilute entangled regime, where C >> C*, the viscosity increases rapidly and scales to 4-5 to the polymer concentration. The inter chain hydrophobic associations coupled with molecular entanglements strongly contribute to the dramatic increase in viscosity. The visco- elastic response of these systems can be explained by sticky reptation model. Finally, in concentrated regime, there is an exponential increase in viscosity leading to the formation of a gel.

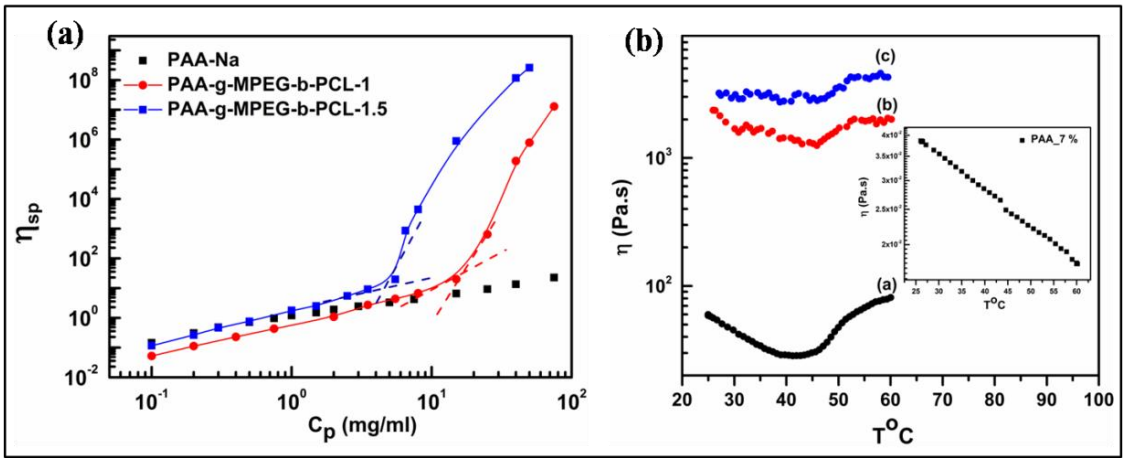

Figure 4.4. (a) Viscosity of PAA and PAA-*g*-MPEG-*b*-PCL as a function of concentration and (**b**) Temperature ramp experiments on (a) PAA-*g*-MPEG-*b*-PCL-1_4 %, (b) PAA-*g*-MPEG-*b*-PCL-1_6 %, (c) PAA-*g*-MPEG-*b*-PCL-1_7 % and inset PAA_7 %

4.4.4 Thermo thickening behaviour: η vs T

We show in **Figure 4.4 (b),** the viscosities of PAA-*g*-MPEG-*b*-PCL-1.0 as a function of temperature for three different polymer concentrations (C_p = 4.0, 6.0 and 7.0 wt %). It can be clearly seen from the figure that the precursor polymer, PAA did not show thermo thickening behaviour and on the contrary, the viscosity decreased slightly with increase in temperature range of 30- 60 °C (inset in **Figure 4.4 (b)**). This is expected largely due to the absence of any associating groups in the polymer which are supposed to form hydrophobic associations. However, the modified PAA polymers exhibited thermo thickening behaviour due to the presence of LCST side chains of MPEG-*b*-PCL. The viscosities of this polymer solution decreased in the range of 30-40 °C indicating the sol state and started to increase above certain critical association temperature and eventually resulted into gel state. The critical association temperature for PAA-*g*-MPEG-*b*-PCL-1.0 with concentrations of 4.0, 6.0 and 7.0 wt% was found to be in the range of 42-45 °C. The magnitude of thermo thickening however decreased with an increase in the polymer concentration. Nevertheless, the phenomenon of thermo thickening was clearly observed in these polymers. In order to see the reversibility of the thermo thickening behaviour of these polymers, we performed η vs T experiments in the forward and reverse cycle of temperature ramping. We show in **Figure 4.5 (a)** η vs T data for PAA-*g*-MPEG-*b*-PCL-1.5 at a

concentration of 1.5 wt%. It can be clearly seen from the figure that the polymer showed thermo thickening behaviour in the forward temperature ramping experiment indicating the sol-gel transition due to the temperature induced hydrophobic associations and the tendency of partial crystallization leading to the ordering of the PCL chains. However, the reversibility of the thermo thickening behaviour was not observed and η vs T data of reverse temperature cycle did not superimpose with the η vs T data of the temperature increase. This can be attributed to the fact that the relaxation of the associated structures could be extremely slow. Further, at high temperature, there can be a strong interaction between the MPEG-*b*-PCL chains

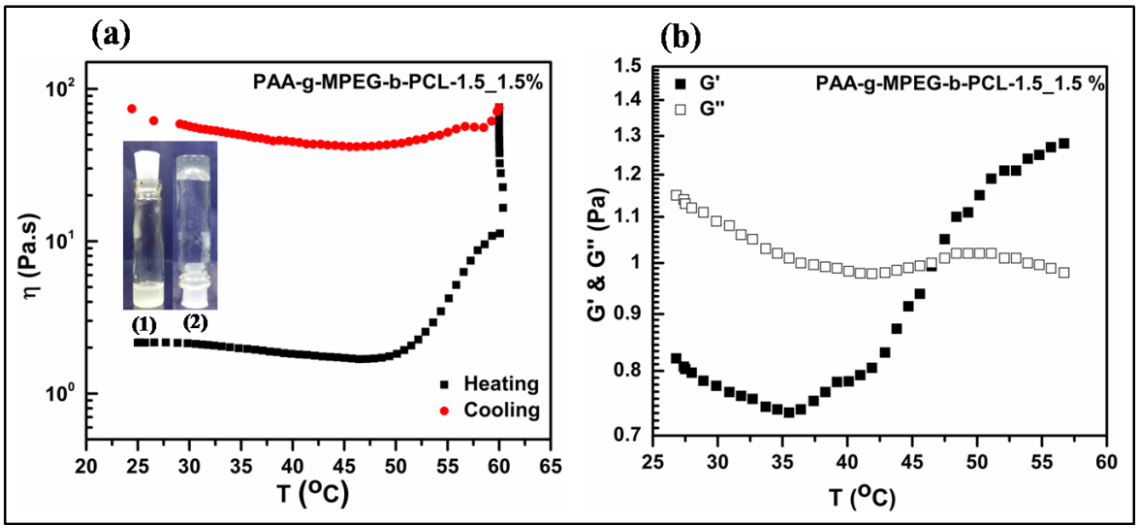

Figure 4.5. (a) Temperature ramp experiments in forward and reverse direction on PAA-*g*-MPEG-*b*-PCL-1.5 at a concentration of 1.5 wt% , Inset is PAA-*g*-MPEG-*b*-PCL-1.5_2.5 wt% solution (1) without heating and (2) after heating at 60 °C and (b) Oscillatory Temperature ramp experiment on PAA-*g*-MPEG-*b*-PCL-1.5 at 1.5 wt% concentration

leading to some permanent compact ordered structures. These ordered structures in the gel prevent the reverse transition from gel to sol state on cooling. The sol-gel transition is clearly visible in inset of **Figure 4.5(a)** wherein, the PAA-*g*-MPEG-*b*-PCL-1.5 (2.5 wt%) solution is easily flow able at RT in sol-state (**Figure 4.5 (a), (1)**) and transforms into gel-state (**Figure 4.5(a), (2)**) upon heating to 60 °C. It is also important to note that the gel-state material becomes increasingly transparent indicating the presence of some ordered structure.

The thermo thickening behaviour of PAA-*g*-MPEG-*b*-PCL-1.5 polymer was also examined by oscillatory rheological experiments as a function of

temperature. The sol-gel transition was monitored from the storage (G') and loss (G") moduli. **Figure 4.5. (b)** shows the change in G' and G" as a function of temperature at a frequency of 20 rad/s. At temperature below ~40 °C, G' is lower than G" (G' < G") indicating that the sample remains in the sol state. However, upon increasing the temperature, at certain temperature (in this case at ~40 °C), there is a cross over between G' and G" which can be considered as the gelation point and the transition from liquid like behaviour to elastic gel like behaviour occurs. Above this temperature, the value of G' becomes higher than G" (G' > G") which implies that the sample is in the gel state. These observations which are macroscopic in nature clearly demonstrate the phenomenon of sol-gel transition in thermo thickening polymers. In order to get further insights into the sol-gel transition, we performed dynamic light scattering and NMR studies on these polymers.

4.4.5 Light Scattering Experiments

4.4.5.1 *Dynamic Light Scattering (DLS)*

In a wide variety of polymer solutions and gels, the light scattered by the fast fluctuations of polymer chains is accompanied by the slow motions of large clusters or quasi-state inhomogenities that are associated with the elastic strain in the network. Due to this difference in the relaxation rates, the fast and slow components can be distinguished in the time correlation function of the scattered intensity. In the DLS of associating polymers, the decay of the correlation function is initially described by a single exponential decay followed at longer times by a stretched exponential decay which is described by,

$$g^{'}(t) = A_f \exp\left(-\frac{t}{\tau_f}\right) + A_s \exp[-(\frac{t}{\tau_s})^{\beta}] \quad (1)$$

where g'(t) is a correlation function, A_f and A_s are the amplitudes for the fast and slow relaxation modes respectively, t is the time and β is the stretched exponent. We performed dynamic light scattering experiments on PAA-*g*-MPEG-*b*-PCL-1.5 (at C_p = 0.125 mg/mL) sample using the Brookhaven 90 plus analyzer at a fixed angle of 90° in the temperature range of 25 °C to 55 °C both in the heating and cooling cycle. We show

in **Figure 4.6** the decay of the correlation function with time at different temperatures. It can be observed from the figure that the correlation function decays faster as the temperature increases. This implies that the size of the polymer particles decrease due to compaction of chains resulting from the temperature induced hydrophobic associations. The decrease in the size of the polymer molecules is clearly reflected in the decrease of hydrodynamic radius of polymer molecules with the increase in temperature (**Table 4.3**). Further, the decrease in particle size resulted in a faster decay of the correlation function with increase in temperature and is also manifested in the increased diffusion coefficients (**Table 4.3**). Eventually, the smaller particles aggregate into bigger particles leading to gelation at higher temperature. However, it is interesting to note that, upon cooling back to 25 °C (the polymer solution was kept for two hours to cool back to room temperature), the decay of the correlation function did not match the decay of the correlation function obtained at initial 25 °C. This indicates that the sol-gel transition is not fully reversible and there could be some permanent structure formation in the heating cycle of the polymer. This finding indeed supports a similar observation in our earlier rheological measurements at heating/ cooling cycles.

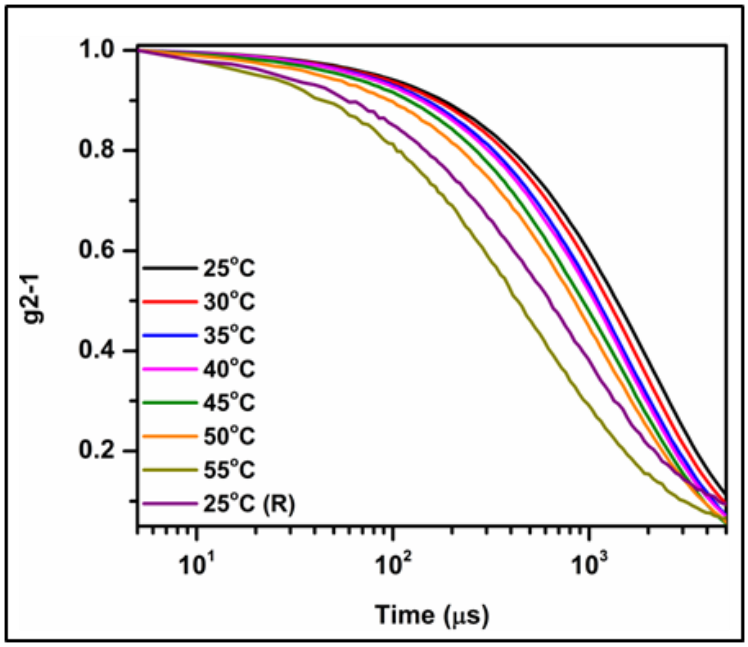

Figure 4.6. Correlation function of PAA-*g*-MPEG-*b*-PCL-1.5 (0.125 mg/ml) on heating from 25 °C to 55 °C (forward direction) and then on cooling back to 25 °C (reverse direction)

Table 4.3: R_h and D_f of PAA-*g*-MPEG-*b*-PCL-1.5 (0.125 mg/ml) with change in temperature

Temperature (°C)	Hydrodynamic Radius, R_h (nm)	Diffusion Coefficient, D_f (m^2/s) x10^{-13}
25	354	6.92
30	320	7.67
35	283	8.67
40	271	9.05
45	242	10.1
50	222	11.0
55	114	21.5
25 (reverse)	171	14.3

4.4.5.2 *Static Light Scattering (SLS)*

We also performed static light scattering experiments at various angles from 15° to 135° on PAA-*g*-MPEG-*b*-PCL-1.5 at four different concentrations (0.4, 0.7, 1.3 and 1.6 mg/mL). As expected, at 25 °C (**Figure 4.7 (a)**), we observed that intensity of the particles increases with an increase in concentration of modified polymer at lower angles. Also, nature of the graph indicates mono disperse particles in the system. On heating the polymer to 55 °C (equilibrated for 1 h), the scattering intensity decreases at

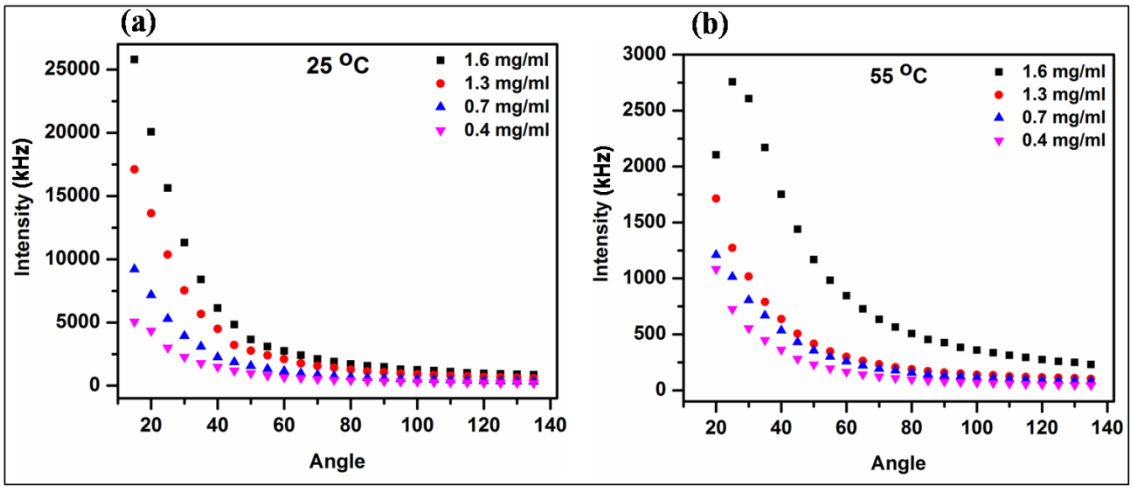

Figure 4.7. Scattering intensity of PAA-*g*-MPEG-*b*-PCL-1.5 as a function of concentration at (a) 25 °C and (b) 55°C

all concentrations as compared to that at 25 °C (**Figure 4.7 (b)**). Also, at 55 °C, the nature of plot at a polymer concentration of 1.6 mg/mL indicates polydispersity of the particles. This implies that PAA-*g*-MPEG-*b*-PCL-1.5 tends to aggregate at higher temperature probably due to inter chain hydrophobic associations which is further in line with the observation made by rheology and NMR studies (see below). Also, this aggregation or assembly of the hydrophobes is concentration dependent which is evident from **Figure 4.7 (b).**

4.4.6 NMR Studies

The changes induced in PAA-*g*-MPEG-*b*-PCL on heating were examined in more detail by various NMR techniques to gain further insights into the mechanism of thermo thickening at the molecular level. Experiments were carried out on 10 mg/mL or 25 mg/mL solutions of PAA-*g*-MPEG-*b*-PCL-1 and PAA-*g*-MPEG-*b*-PCL-1.5 in D_2O. A comparison of the spectrum of PAA-*g*-MPEG-*b*-PCL-1.5 with that of the individual constituents, PAA and MPEG-*b*-PCL at 25°C indicates considerable broadening of signals in PAA-*g*-MPEG-*b*-PCL-1.5 (**Figure 4.8 (a)**). Broad signals corresponding to the protons from the grafts are an indication of some level of assembling in addition to

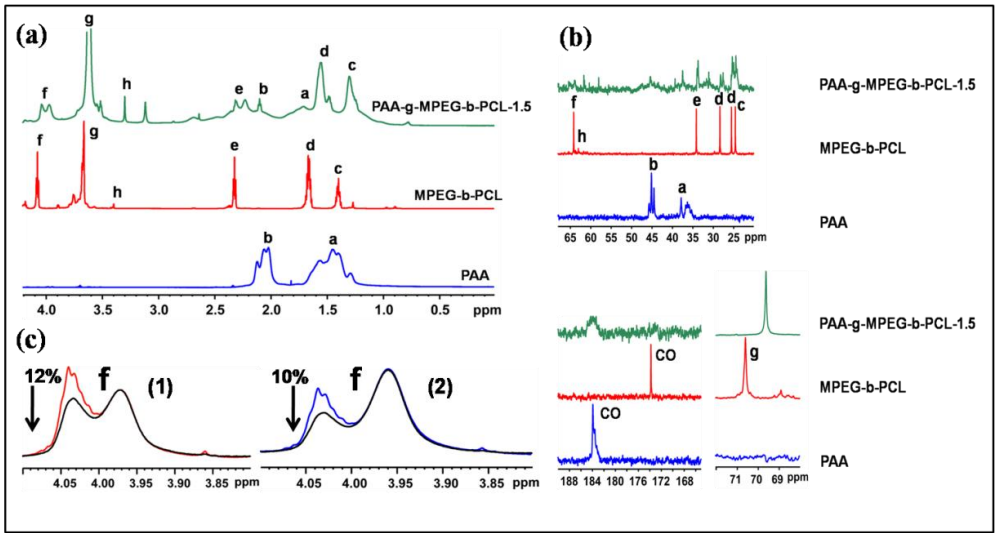

Figure 4.8. (a) Comparison of 700 MHz ^{1}H NMR spectra of PAA, MPEG-*b*-PCL and PAA-*g*-MPEG-*b*-PCL-1.5, (b) Comparison of the ^{13}C NMR spectra of PAA, MPEG-*b*-PCL and PAA-*g*-MPEG-*b*-PCL-1.5 and (c) Overlay of diffusion filtered spectra of PAA-*g*-MPEG-*b*-PCL-1.5 at 25 °C showing the "f" proton of PCL (1) before heating and (2) after heating. Black traces correspond to gradient strength of 2 % and colored traces are at gradient strength of 95 %

the overall increase in molecular weight on grafting. Also, both ^{1}H and ^{13}C spectra indicate that PCL signals have multiple environments in PAA-*g*-MPEG-*b*-PCL when compared to the spectrum of MPEG-*b*-PCL (**Figure 4.8 (a) and (b)**). Even though MPEG-*b*-PCL is insoluble in water, it is known to form micellar structures in aqueous medium by solvent displacement from an organic solvent.[21] The micellar structures have a hydrophobic core comprising of PCL and surrounded by a corona of MPEG which is hydrophilic.[22, 23] In PAA-*g*-MPEG-*b*-PCL, it is reasonable to assume that some of the MPEG-*b*-PCL grafts can associate to form micellar assemblies in which the hydrophobic PCL blocks are loosely associated while MPEG stays hydrated similar to the hydrophilic PAA backbone. Thus, the multiple environments of PCL signals in the spectrum could correspond to PCL blocks in the assembled microdomains and individual graft side chains. This is also supported by the fact that the signal from one of the PCL environments has a faster local diffusion compared to the other (**Figure 4.8 (c)**). A comparison of the spectra of PAA-*g*-MPEG-*b*-PCL

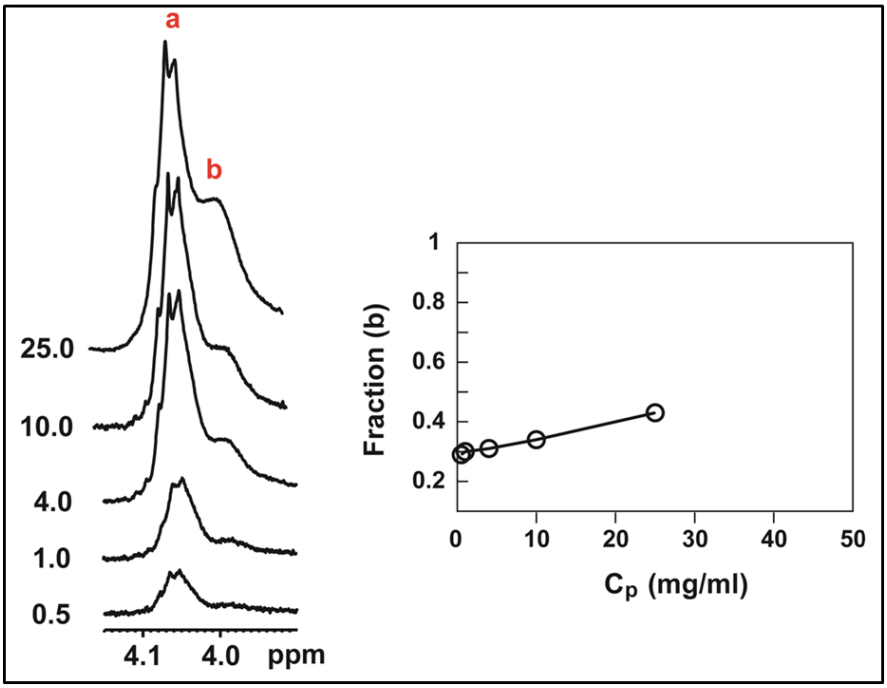

Figure 4.9. Expansion of the 500 MHz ^{1}H spectra of PAA-*g*-MPEG-*b*-PCL-1.0 at different concentrations (0.5-25 mg/ml) recorded at 25 °C showing the "f" proton signal of PCL. The deshielded (a) and shielded (b) components of the "f" proton signal correspond to unassembled and assembled environments. A plot of the fraction of assembled environment, b (estimated from the peak integral) as a function of concentration is shown on the right.

obtained at different concentrations indicates that the signal corresponding to one of the environments increase in area with increase in concentration (**Figure 4.9**). The change in signal area parallels the variation of viscosity with concentration shown in **Figure 4.4 (a)**. An increase in concentration maybe expected to be conducive to more interactions between side chains leading to the formation of assemblies. Thus, the multiple environments of PCL signals in the spectrum could correspond to PCL blocks in the assembled microdomains and individual graft side chains as depicted in **Scheme 4.3**. This is also supported by the fact that the signal from one of the PCL environments has a faster local diffusion compared to the other (**Figure 4.8 (c)**).

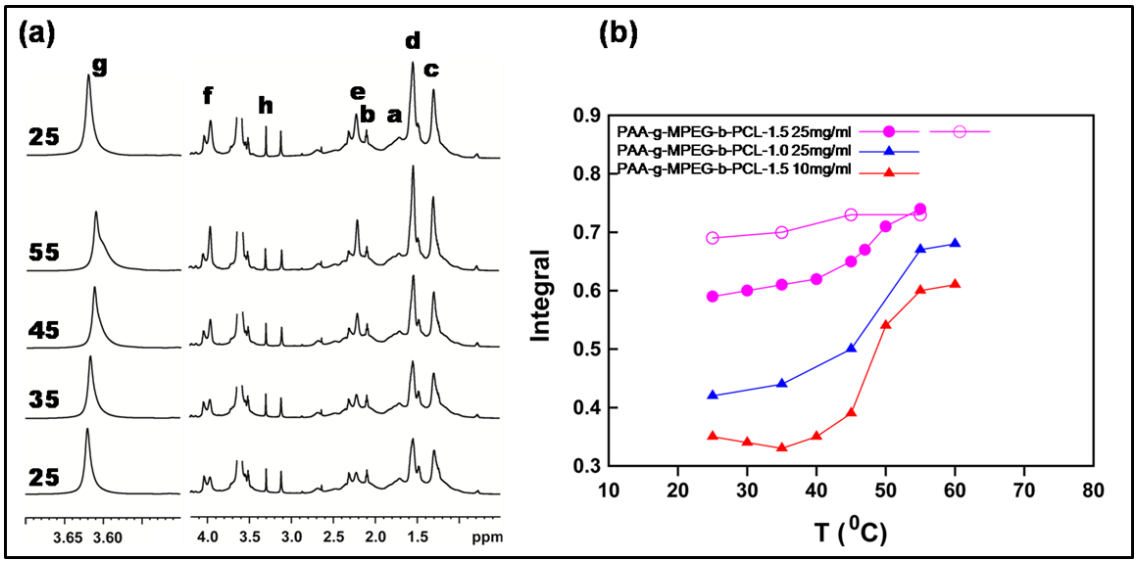

Figure 4.10 (a) Temperature dependent ^{1}H NMR spectra of 25 mg/ml PAA-*g*-MPEG-*b*-PCL-1.5 in D_2O on a 700 MHz spectrometer. The upper trace shows spectrum at 25 °C after cooling down from 60 °C. (b) Variation of the signal area of the PCL proton "f" with temperature. Open symbols show the temperature dependence on reheating the sample (25 – 55 °C) after equilibration at 60 °C

The changes induced in PAA-*g*-MPEG-*b*-PCL-1.5 on heating were monitored by recording NMR spectra in the temperature range 25 – 60 °C (**Figure 4.10 (a)**). PCL signals corresponding to one of the environments become sharper as temperature increases, the most significant effect being observed for protons "f" and "e" from methylene groups located adjacent to -OCH_2 and carbonyl groups. Similar changes are also observed in the ^{13}C spectra (**Figure 4.11 (a)**). Even though PCL blocks of the MPEG-*b*-PCL grafts associate to form hydrophobic microdomains,

initially at room temperature it is likely that water molecules are present in the vicinity of the carboxyl and -OCH_2 groups of PCL. As temperature increases, these water molecules rearrange thereby strengthening the hydrophobic associations in the PCL microdomains. **Figure 4.10 (b)** shows that the variation in the area of one of the "f" proton signals (narrow component) with temperature follows a pattern very similar to the variation of viscosity, with a sharp increase occurring at ~ 42 °C. As hydrophobic interactions begin to dominate on heating, the MPEG-*b*-PCL side chains reorganize, resulting in a greater proportion of microdomains which enhances the area corresponding to the signal from the assembled environment. Also, the increased ordering within the microdomains results in narrowing of the signals. The signal which increases in area and undergoes narrowing with increase in temperature corresponds to the component which diffuses slowly, further indicating that it belongs to the assembled microdomains (**Figure 4.8 (c)**). The temperature induced changes are irreversible as seen by comparing spectra recorded at 25 °C before and after heating to 60 °C (**Figure 4.11 (b)**). **Figure 4.10 (b)** shows a clear difference in the temperature dependence of "f" signal area before and after heating to 60 °C, the pattern being very similar to the trends seen in the viscosity measurements shown in **Figure 4.5 (a)**. The

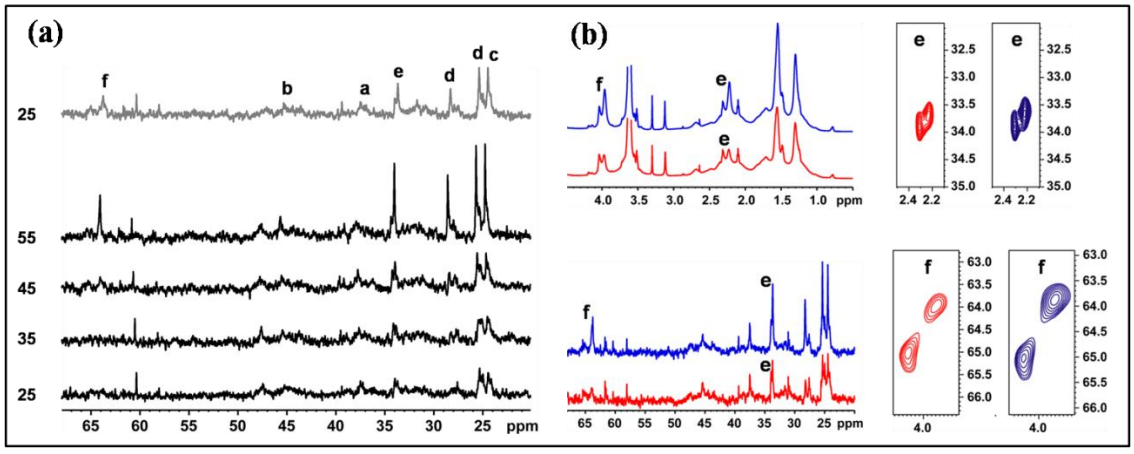

Figure 4.11. (a) Temperature dependent ^{13}C NMR spectra of 25 mg/ml PAA-*g*-MPEG-*b*-PCL-1 in D_2O obtained on a 500 MHz spectrometer. The upper trace shows the spectrum at 25 °C after cooling down from 60 °C and (b) Comparison of the ^{1}H and ^{13}C spectra recorded at 25 °C before (red) and after (blue) heating PAA-*g*-MPEG-*b*-PCL-1.5. Sections from the 2D HSQC spectrum clearly shows the irreversible enhancement of signal intensity of one of the environments corresponding to the PCL methylene protons "e" and "f"

irreversible changes on heating observed in NMR spectra are consistent with the results from rheology and light scattering experiments.

In order to examine the changes occurring in the molecular interactions with temperature, we compared the NOESY spectra of PAA-*g*-MPEG-*b*-PCL-1.5 at 25 °C recorded before and after heating to 60 °C (**Figure 4.12**). The NOESY spectrum recorded before heating shows crosspeaks between the protons of PCL but no strong cross peaks to the MPEG segment. However, the spectrum obtained after heating to 60 °C and then cooling down, shows much stronger cross peaks between the PCL protons as well as crosspeaks between PCL and MPEG protons. This implies that there is a significant reorganization of the side chains in the micro- domains on heating; they probably rearrange to more ordered tightly packed structures which bring the PCL and MPEG segments closer as depicted in **Scheme 4.3**. An increased ordering of the grafted side chains would also lead to restriction in molecular dynamics in the system. We carried out proton relaxation time measurements as a function of

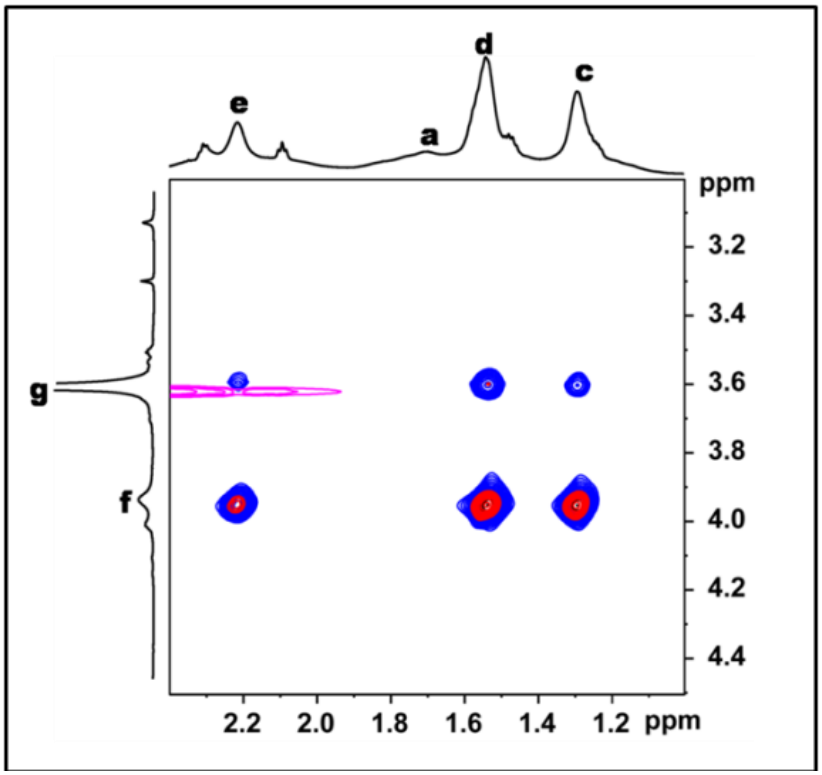

Figure 4.12. 700 MHz NOESY spectrum of a 25 mg/ml solution of PAA-*g*-MPEG-*b*-PCL-1.5 in D_2O at 25 °C obtained with a mixing time of 64 ms before (red) and after heating (blue)

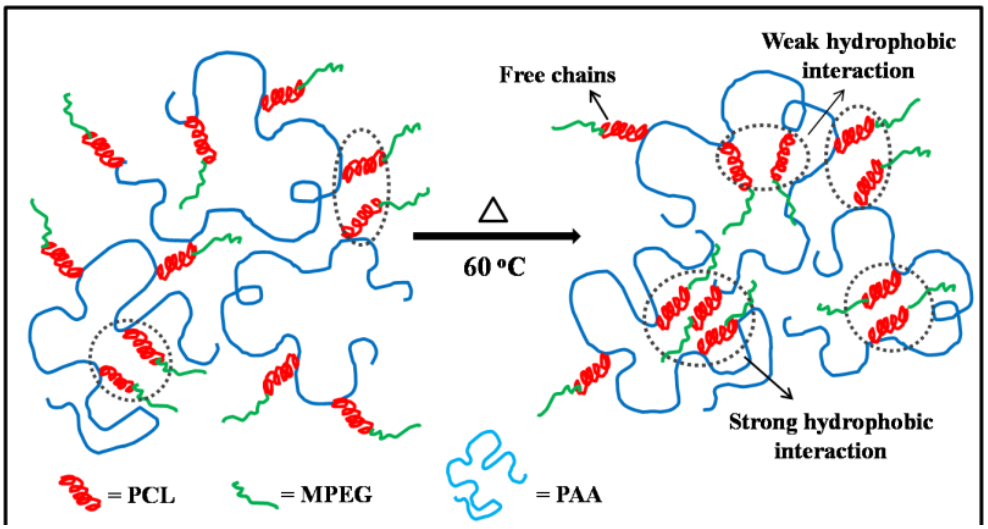

Scheme 4.3: Reorganization of the MPEG-*b*-PCL after heating

temperature on PAA-*g*-MPEG-*b*-PCL-1.5 before heating and after heating to 60 °C and equilibrating at this temperature (**Table 4.4**). **Figure 4.13** shows the dependence of ^{1}H spin-lattice relaxation time (T_1) on temperature, measured before and after heating the sample. Clearly, the protons of the PAA backbone and those of the PCL and MPEG segments fall in different dynamic regimes in a classical T_1 versus correlation time plot.[24] PAA protons show a decrease in T_1 with increasing temperature which is expected for a high molecular weight polymer with very slow motions corresponding to a larger motional correlation time. The protons of PCL shows a slow increase in T_1 with temperature which corresponds to intermediate timescale motions in the vicinity of the minimum in the T_1 vs correlation time curve. On the other hand, the protons of MPEG show a sharp increase in T_1 with temperature, which is expected in the fast motion regime. This behaviour is in accordance with the expected increase in side chain flexibility on moving away from the backbone. Initially, the T_1 values of PCL and MPEG protons vary evenly with temperature however there is a sudden jump in the interval 42 to 55 °C which correlates well with the temperature interval during which a sharp rise is observed in viscosity and rheology experiments. During this interval the dehydration of the side chains is probably significant enough to make hydrophobic interactions the dominating factor in determining the organization of the side chains within the microdomains.

Table 4.4. Temperature dependence of ^{1}H T_1 (700 MHz) of 25 mg/ml PAA-*g*-MPEG-*b*-PCL-1.5

T_1, s (1st heating cycle)						
T, °C	PAA (a)	PCL (c)	PCL (d)	PCL (e)	PCL (f)	MPEG (g)
25	0.824	0.664	0.631	0.655	0.624	0.801
35	0.767	0.701	0.663	0.668	0.675	1.248
45	0.716	0.718	0.681	0.685	0.711	1.537
55	0.667	0.893	0.846	0.856	0.921	2.459
T_1, s (2nd heating cycle)						
25	0.838	0.700	0.679	0.699	0.698	0.829
35	0.766	0.699	0.666	0.689	0.699	1.374
45	0.715	0.730	0.694	0.717	0.730	1.632
55	0.671	0.786	0.745	0.770	0.798	2.041

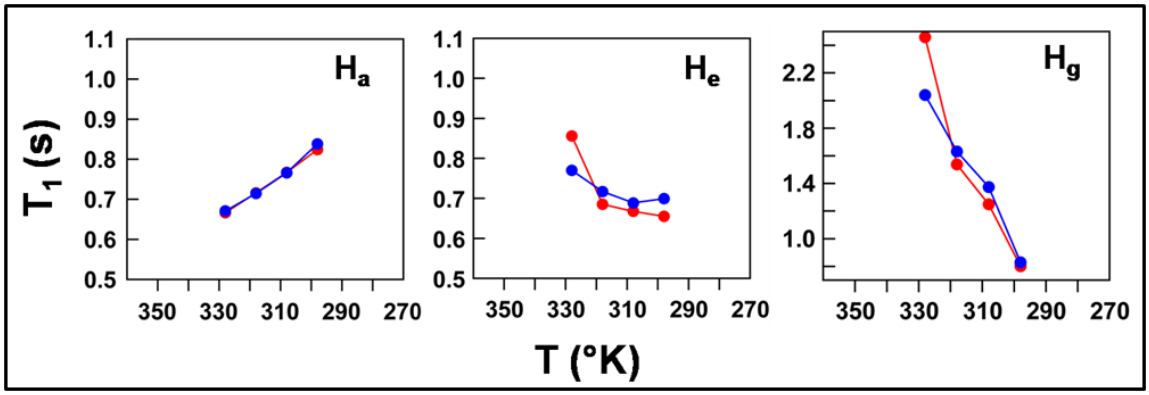

Figure 4.13. Dependence of ^{1}H T_1 on temperature measured for a 25 mg/ml solution of PAA-*g*-MPEG-*b*-PCL-1.5 in D_2O on a 700 MHz spectrometer, showing plots for protons corresponding to PAA, PCL and MPEG. Data obtained before and after heating are shown in red and blue respectively. Temperature increases from right to left opposite to the direction of increasing correlation time for molecular motions

The dependence of T_1 on temperature after heating and equilibrating PAA-*g*-MPEG-*b*-PCL-1.5 at 60 °C shows the same behaviour for the PAA proton. The PCL protons on the other hand show a slight shift in the T_1 versus temperature curve towards the lower mobility direction (**Figure 4.13** and **Table 4.4**).

This is indicated by the fact that we begin to see the minimum of the T_1 versus temperature curve which occurs when $\omega_0\tau_c = 1$, where ω_0 is the Larmor frequency and τ_c is the motional correlation time. MPEG protons continue to be in the fast motion regime but the T_1 at the highest temperature is somewhat lower indicating some degree of slowing down relative to before heating. The ^{13}C T_1 values in the PCL segment are also reduced slightly after heating as expected (**Figure 4.14**, **Table 4.5**).

Spin spin relaxation times (T_2) are also very sensitive to molecular flexibility and is reflected in spectral linewidths. However, in a polymer sample, polydispersity, microstructure variations etc. can also be factors contributing to the linewidths and hence T_2 measurements would be a true indicator of mobility changes. Both ^1H and ^{13}C T_2 relaxation decays are best fit by biexponential decay curves (**Figure 4.15, Table 4.6**). The short and long relaxation times probably correspond to different environments viz. assembled and nonassembled/ loosely assembled side chains which have lower and higher mobilities respectively. Biexponential T_2 decay curves are known to occur in micellar systems due to restricted mobility in the micellar core and faster motions in the periphery.[25, 26] Both PAA and PCL protons show a greater contribution from the fast relaxing component (slow moving) while MPEG proton relaxation is dominated by the slow relaxing component (fast motion), so that the T_2 relaxation data can also fit well by a single exponential decay. This is also evident from

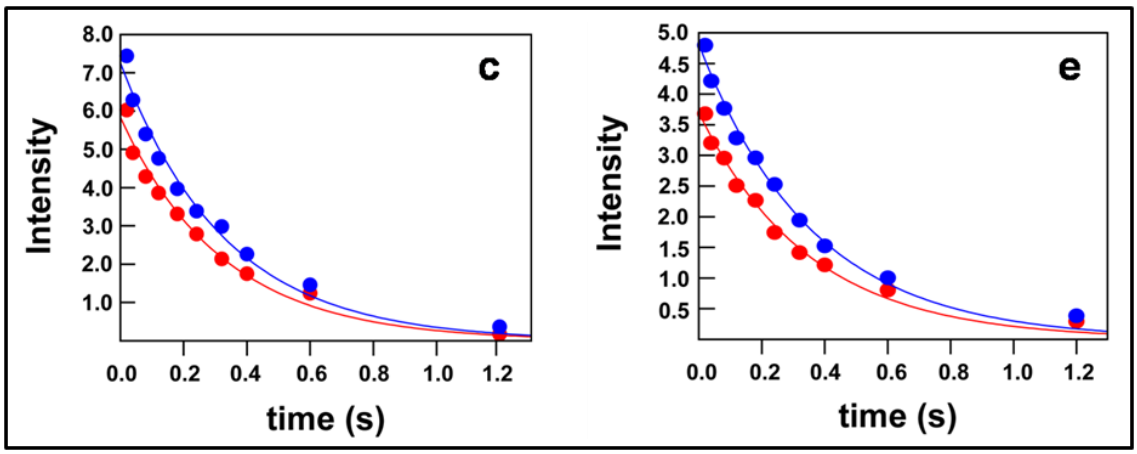

Figure 4.14. Exponential fits to experimental ^{13}C T_1 relaxation data (700 MHz) of PCL carbons c and e of 25 mg/ml PAA-*g*-MPEG-*b*-PCL-1.5 before (red) and after (blue) heating. Intensities (arbitrary units) were determined from contours in the HSQC plane of a pseudo 3D experiment

Table 4.5. ^{13}C T_1 values (700 MHz) of PCL carbons of 25 mg/ml PAA-*g*-MPEG-*b*-PCL-1.5 at 25 °C

"CH_2"	T_1, s	
	Before heating	After heating
c	3.08	3.03
d	3.52	3.43
e	2.86	2.78
f	3.48	3.39

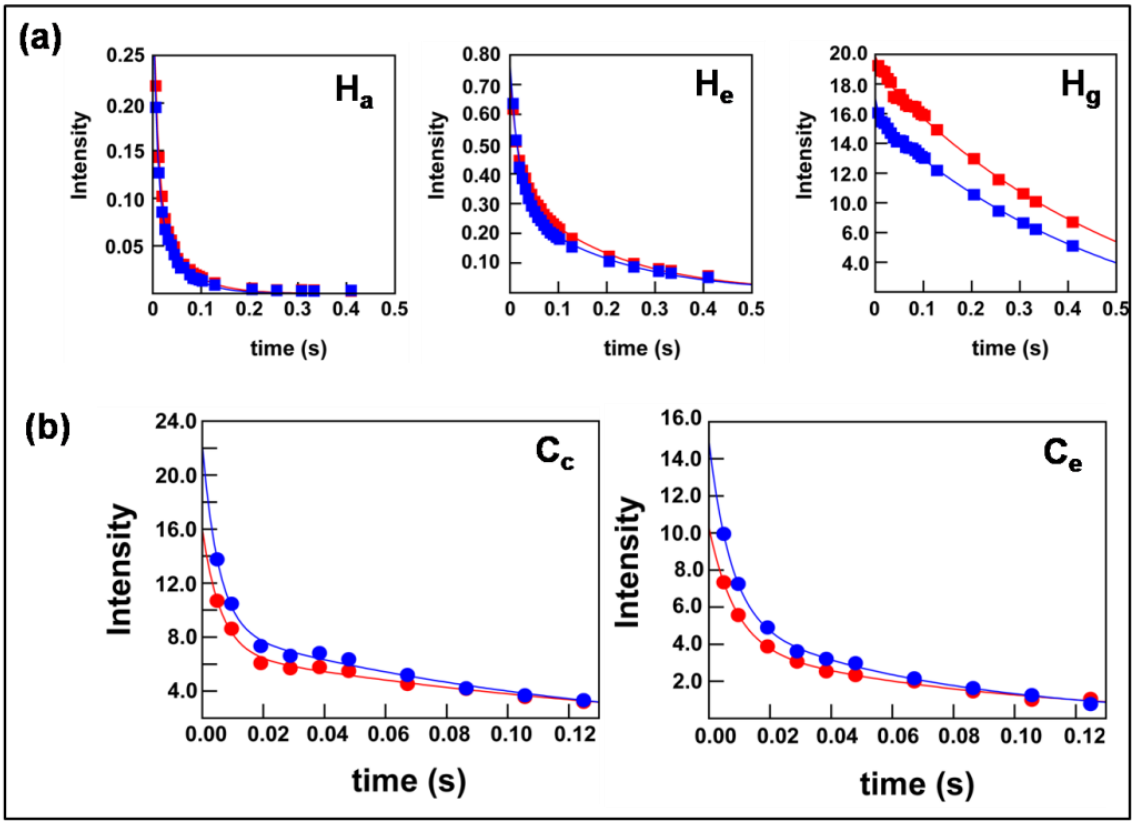

Figure 4.15. (a) Biexponential fits to experimental ^{1}H T_2 relaxation data (500 MHz) of PAA, PCL and MPEG proton in 25 mg/ml PAA-*g*-MPEG-*b*-PCL-1 before (red) and after (blue) heating. (b) Biexponential fits to experimental ^{13}C T_2 relaxation data (700 MHz) of PCL carbons c and e in 25 mg/ml PAA-*g*-MPEG-*b*-PCL-1.5 before (red) and after (blue) heating. In (b), intensities (arbitrary units) were determined from contours in the HSQC plane of a psuedo-3D experiment.

Table 4.6. ^{1}H T_2 (500 MHz) and ^{13}C T_2 (700 MHz) values at 25 °C in PAA-*g*-MPEG-*b*-PCL-1 and PAA-*g*-MPEG-*b*-PCL-1.5

PAA-*g*-MPEG-*b*-PCL-1	^{1}H T_2, ms		PAA-*g*-MPEG-*b*-PCL-1.5	^{13}C T_2, ms	
"CH_2"	**Before heating**	**After heating**	**"CH_2"**	**Before heating**	**After heating**
PAA (a)	Slow component: 57.67 (26%) Fast component: 9.74 (74%)	Slow component: 49.07 (28%) Fast component: 8.11 (72%)	PCL (c)	Slow component: 167.79 (43%) Fast component: 5.98 (57%)	Slow component: 131.41 (38%) Fast component: 5.35 (62%)
PCL (d)	Slow component: 200.0 (50%) Fast component: 19.18 (50%)	Slow component: 207.0 (39%) Fast component: 18.51 (61%)	PCL (e)	Slow component: 87.18 (39%) Fast component: 8.38 (61%)	Slow component: 70.47 (37%) Fast component: 7.07 (63%)
MPEG (g)*	Slow component: 531.9 (95%) Fast component: 14.33 (0.05%)	Slow component: 515.5 (92%) Fast component: 7.0 (0.08%)			

* Biexponential fit is not a significant improvement over single exponential fit (T_2 values 515.5 ms and 505.1 ms before and after heating) in case of proton "g". The results of biexponential fit is shown because spectra at higher temperatures clearly shows that there is a broad, fast relaxing component associated with the MPEG segment which is an indicator of the involvement of MPEG in the increased hydrophobic interactions of sidechains after heating.

the narrow signal observed for MPEG protons before heating, however an underlying broad signal of MPEG becomes visible in the spectrum obtained at 55 °C (**Figure 4.8.(a)**), indicating a low mobility component in the MPEG segment. ^{1}H and ^{13}C T_2 values measured in PAA-*g*-MPEG-*b*- PCL after equilibration at 60 °C are lower with a slight increase in the fraction of the fast relaxing component (**Table 4.6**). These results indicate a slowing down of motions in the assembled microdomains due to increased ordering as temperature is raised; with the compact ordering being retained on cooling back to 25 °C.

The results from relaxation experiments (T_1, T_2) indicate that mobility of the assembled sidechains in the microdomains is reduced after heating. This is consistent with the increased ordering induced when hydrophobic interactions between side chains become more dominant compared to hydrophilic interactions involving sidechains and water. The enhanced hydrophobic interactions are strong enough to induce a stable interchain network cross linked through the ordered microdomains which are not disrupted on cooling down. In contrast to PAA grafted with PEG, which shows reversible thermo thickening [27], the presence of hydrophobic PCL units maybe the reason for the enhanced stability of hydrophobic interactions which leads to irreversible thermo thickening in PAA-*g*-MPEG-*b*-PCL.

4.5 Conclusion

Hydrophobically modified poly(acrylic acid) was prepared using MPEG-*b*-PCL block copolymer using DCC coupling reaction. The incorporation of MPEG-*b*-PCL onto PAA backbone with two different mol% was confirmed using ^{1}H NMR spectroscopy. Rheology experiments on the hydrophobically modified PAA shows that the polymer possesses thermo thickening property which is irreversible in nature. An understanding of the molecular level changes was studied using light scattering and NMR techniques. Light scattering studies indicate that the polymer become smaller in size leading to the increase in diffusion upon heating. Also, temperature dependent NMR studies show decrease in mobility of the MPEG-*b*-PCL side chains on heating. All these observations indicate the formation of enhanced hydrophobic interactions upon heating the modified

polymer which results in the formation of ordered microdomains leading to gelation which is irreversible in nature.

References

[1] A. Durand, D. Hourdet, Synthesis and thermoassociative properties in aqueous solution of graft copolymers containing poly(N-isopropylacrylamide) side chains, Polymer, 40 (1999) 4941-4951.

[2] C.Y. Gong, Y.J. Wang, X.H. Wang, X.W. Wei, Q.J. Wu, B.L. Wang, P.W. Dong, L.J. Chen, F. Luo, Z.Y. Qian, Biodegradable self-assembled PEG-PCL-PEG micelles for hydrophobic drug delivery, part 2: in vitro and in vivo toxicity evaluation, J Nanopart Res, 13 (2011) 721–731.

[3] A.S. Dilgimen, Z. Mustafaeva, M. Demchenko, T. Kaneko, Y. Osada, M. Mustafaev, Water-soluble covalent conjugates of bovine serum albumin with anionic poly (N-isopropyl-acrylamide) and their immunogenicity, Biomaterials, 22 (2001) 2383-2392.

[4] I.Y. Galaev, B. Mattiasson, 'Smart'polymers and what they could do in biotechnology and medicine, Trends in biotechnology, 17 (1999) 335-340.

[5] Y.-Y. Diao, H.-Y. Li, Y.-H. Fu, M. Han, Y.-L. Hu, H.-L. Jiang, Y. Tsutsumi, Q.-C. Wei, D.-W. Chen, J.-Q. Gao, Doxorubicin-loaded PEG-PCL copolymer micelles enhance cytotoxicity and intracellular accumulation of doxorubicin in adriamycin-resistant tumor cells, International journal of nanomedicine, 6 (2011) 1955.

[6] R. Liu, M. Fraylich, B.R. Saunders, Thermoresponsive copolymers: from fundamental studies to applications, Colloid Polym Sci, 287 (2009) 627-643.

[7] S.J. Bae, M.K. Joo, Y. Jeong, S.W. Kim, W.K. Lee, Y.S. Sohn, B. Jeong*, Gelation Behavior of Poly(ethylene glycol) and Polycaprolactone Triblock and Multiblock Copolymer Aqueous Solutions, Macromolecules, 39 (2006) 4873-4879.

[8] S.J. Bae, J.M. Suh, Y.S. Sohn, B.Y. H., S.W. Kim, J. B., Thermogelling Poly(caprolactone-b-ethylene glycol-b-caprolactone) Aqueous Solutions, Macromolecules, 38 (2005) 5260-5265.

[9] M.S. Kim, K.S. Seo, G. Khang, S.H. Cho, H.B. Lee, Preparation of poly(ethylene glycol)-block-poly(caprolactone) copolymers and their applications as thermo-sensitive materials, Wiley Periodicals, Inc., (2004).

[10] C. Lu, S.R. Guo, Y. Zhang, M. Yin, Synthesis and aggregation behavior of four types of different shaped PCL-PEG block copolymers, Polymer International, 55 (2006) 694–700.

[11] H. Takeshita, K. Fukumoto, T. Ohnishi, T. Ohkubo, M. Miya, K. Takenaka, T. Shiomi, Formation of lamellar structure by competition in crystallization of both components for crystalline block copolymers, Polymer, 47 (2006) 8210-8218.

[12] C. He, J. Sun, C. Deng, T. Zhao, M. Deng, X. Chen, X. Jing, Study of the Synthesis, Crystallization, and Morphology of Poly(ethylene glycol)-Poly(E-caprolactone) Diblock Copolymers, Biomacromolecules, 5 (2004) 2042-2047.

[13] S. Jiang, C. He, Y. Men, X. Chen, L. An, S.S. Funari, C.M. Chan, Study of temperature dependence of crystallisation transitions of a symmetric PEO-PCL diblock copolymer using simultaneous SAXS and WAXS measurements with synchrotron radiation, THE EUROPEAN PHYSICAL JOURNAL E, 27 (2008) 357–364.

[14] E.J. Lee, Y.H. Kim, Synthesis and thermo-responsive properties of chitosan-g-poly (N-isopropylacrylamide) and HTCC-g-poly (N-isopropylacrylamide) copolymers, Fibers and Polymers, 11 (2010) 164-169.

[15] S. Ohya, Y. Nakayama, T. Matsuda, Thermoresponsive artificial extracellular matrix for tissue engineering: hyaluronic acid bioconjugated with poly (N-isopropylacrylamide) grafts, Biomacromolecules, 2 (2001) 856-863.

[16] N.R. Gupta, P.P. Wadgaonkar, P. Rajamohanan, G. Ducouret, D. Hourdet, C. Creton, M.V. Badiger, Synthesis and characterization of PEPO grafted carboxymethyl

guar and carboxymethyl tamarind as new thermo-associating polymers, Carbohydrate polymers, 117 (2015) 331-338.

[17] R. Tan, Z. She, M. Wang, Z. Fang, Y. Liu, Q. Feng, Thermo-sensitive alginate-based injectable hydrogel for tissue engineering, Carbohydrate Polymers, 87 (2012) 1515-1521.

[18] K. Akiyoshi, E.-C. Kang, S. Kurumada, J. Sunamoto, T. Principi, F.M. Winnik, Controlled association of amphiphilic polymers in water: thermosensitive nanoparticles formed by self-assembly of hydrophobically modified pullulans and poly (N-isopropylacrylamides), Macromolecules, 33 (2000) 3244-3249.

[19] B. Blanco-Fernandez, A. Concheiro, H. Makwana, F. Fernandez-Trillo, C. Alexander, C. Alvarez-Lorenzo, Dually sensitive dextran-based micelles for methotrexate delivery, RSC Advances, 7 (2017) 14448-14460.

[20] J.A. Aguilar, M. Nilsson, G. Bodenhausen, G.A. Morris, Spin echo NMR spectra without J modulation, Chemical communications, 48 (2012) 811-813.

[21] X. Sui, P. Kujala, G.-J. Janssen, E. de Jong, I.S. Zuhorn, J.C.M. van Hest, Robust formation of biodegradable polymersomes by direct hydration, Polym. Chem., 6 (2015) 691-696.

[22] L. Huynh, C. Neale, R. Pomès, C. Allen, Systematic design of unimolecular star copolymer micelles using molecular dynamics simulations, Soft Matter, 6 (2010) 5491.

[23] K.K. Jette, D. Law, E.A. Schmitt, G.S. Kwon, Preparation and Drug Loading of Poly(Ethylene Glycol)-block-Poly(e-Caprolactone) Micelles Through the Evaporation of a Cosolvent Azeotrope, Pharmaceutical Research, 21 (2004) 1184-1191.

[24] M.H. Levitt, Spin dynamics: basics of nuclear magnetic resonance, (2008).

[25] J. Weiss, H. Wienk, R. Boelens, A. Laschewsky, Block Copolymer Micelles with an Intermediate Star-/Flower-Like Structure Studied by1H NMR Relaxometry, Macromolecular Chemistry and Physics, 215 (2014) 915-919.

[26] A.J. de Graaf, K.W. Boere, J. Kemmink, R.G. Fokkink, C.F. van Nostrum, D.T. Rijkers, J. van der Gucht, H. Wienk, M. Baldus, E. Mastrobattista, T. Vermonden, W.E. Hennink, Looped structure of flowerlike micelles revealed by 1H NMR relaxometry and light scattering, Langmuir : the ACS journal of surfaces and colloids, 27 (2011) 9843-9848.

[27] D. Hourdet, F. L'alloret, A. Durand, F. Lafuma, R. Audebert, J.P. Cotton, Small-Angle Neutron Scattering Study of Microphase Separation in Thermoassociative Copolymers, Macromolecules, 31 (1998) 5323-5335.

Chapter-5

Double Crosslinked Poly(acrylic acid) Hydrogels

5.1 Introduction

Hydrogels contain hydrophilic polymeric chains that are crosslinked either physically[1-3] or chemically[3, 4] thus imparting a 3-dimensional network structure to the hydrogel. Hydrogels have become extremely important materials in tissue engineering and drug delivery application because of their biocompatibility, hydrophilicity and flexible nature which mimics the native extra cellular matrix.[5-8] The controlled release of active ingredients such as drugs, proteins and other micronutrients at the required site on demand is a biggest challenge in medical and pharmaceutical areas. In this context, smart responsive polymeric hydrogels have become promising materials for drug delivery [9, 10] and tissue engineering applications [11-13] due to their controlled swelling-deswelling kinetics and tuneable properties. Major efforts are being continuously made in designing and synthesizing smart hydrogels that are sensitive to external stimuli such as temperature [14, 15] pH [9, 15-19] magnetic [20] and electric field [21] etc. Recently, redox stimuli have attracted much attention in hydrogels [22-24]. In redox stimuli, the volume transition is effected by breaking and reformation of crosslinks triggered by reduction and oxidation. Further, the redox stimuli provide a rapid and reversible switching between the oxidized and reduced states.

Zrinyi et al. [25] have reported on the redox-responsive, biocompatible hydrogel based on Poly (aspartic acid) [PASP]. They have synthesized Poly (aspartic acid) hydrogels simultaneously using two different crosslinking agents namely cystamine and diaminobutane. The advantages of Poly (aspartic acid) hydrogels in terms of their biodegradability, biocompatibility, and non-toxicity have been highlighted. The cystamine crosslinking agent, which contains disulphide (S-S) bonds could be cleaved using reducing agents such as glutathione and dithiothreitol (DTT). Consequently, the degree of crosslinking of the hydrogel was reduced which resulted in increasing the swelling ratio of the hydrogel. However, the hydrogels based on Poly (aspartic acid) exhibited weak mechanical strength and were prepared in toxic solvents such as DMSO, DMF etc. and the gelation times were long and in the order of 2-3 days. Gyarmati et al. [26] have reported on the reversible response of the poly (aspartic acid)

hydrogel to the external redox and the pH stimuli. The hydrogels were prepared with the pendant thiol linkages and covalent bonds were formed by in-situ crosslinking with diaminobutane. The formation of dual crosslinking was later demonstrated by oxidation resulting into di-sulphide linkages. However, the implication of this on the swelling controlled drug delivery has not been reported. Ming Zhong et al. [27] have reported on the dual crosslinked poly (acrylic acid) hydrogels which showed superior mechanical properties with high water absorbency. The dual crosslinking was affected by covalent linking with bis-acrylamide and reversible dynamic linking by Fe^{3+} ions. However, the dynamics of breaking and reformation of the ionically linked network under deformation is not clear. Further, the selective breaking of one network and its influence on swelling and controlled drug delivery in these networks has not been reported. This concept of making double crosslinked hydrogels and breaking of one crosslinking independently is quite interesting and can have important technological implications which are not explored.

In this chapter, we have synthesized double crosslinked Poly (acrylic acid) based hydrogels using two different crosslinking agents namely Jeffamine (jeff) (Huntsman, amine terminated copolymer of PEO-PPO) and Cystamine (cys). The jeffamine provides a good mechanical strength due to presence of additional H-bonding while the cystamine with disulphide bonds incorporates the redox sensitivity to the hydrogels. The hydrogels were easily prepared in aqueous medium at room temperature and the gelation could be completed within a few minutes. Poly (acrylic acid) (PAA) based hydrogels have been extensively studied for controlled drug delivery applications.[15, 18, 28, 29] Large number of pharmaceutical formulations of creams, ointments etc. contain PAA (Carbopols) with FDA approval and acts as a rheological control agent. The double crosslinked hydrogels based on PAA showed remarkable increase in the mechanical strength as compared to the double crosslinked PASP hydrogels. With one step ahead, we also demonstrated the selective cleavage of one crosslinking by DTT and its implications on the controlled release of an anticancer drug, Doxorubicin (Dox) and an antimicrobial Ag nanoparticle.

5.2 Experimental

5.2.1 Materials

Poly (acrylic acid) (MW= 2,50,000) (PAA), Cystamine di-hydrochloride, 1-Ethyl-3-(3 dimethylaminopropyl)carbodiimide hydrochloride (EDC.HCl), dithiothreitol (DTT) were obtained from Sigma Aldrich, USA. Jeffamine (MW=2,000) was obtained from Texaco Chemical Company, USA. Doxorubicin HCl was obtained from Prolab Marketing Pvt. Ltd., New Delhi. Silver nitrate ($AgNO_3$) was procured from S.D. Fine chemicals Ltd (India) and sodium borohydride ($NaBH_4$) was purchased from Merck (India). All the chemicals were of analytical grade and used as received.

5.2.2 Synthesis of cross linked PAA hydrogels

300 mg of Poly(acrylic acid) was dissolved in distilled water and stirred until the solution became homogeneous. To this solution was added varied compositions of cystamine dihydrochloride and jeffamine dissolved prior in small amounts of distilled water. The solution was kept stirring for about 10 min or till it became homogeneous. The pH of the solution was adjusted to 7.5-8.0 by adding 1M NaOH solution followed by the addition of EDC.HCl to it. The total volume of the reaction was kept constant at 10 ml for all the experiments. After stirring for approx 10 sec, the solution was poured immediately into cylindrical teflon moulds of different sizes. The gelation took place in 10-15 min. Then the gels were removed from moulds and used for further studies. The gels were then kept in distilled water for 4 days with periodic replenishment with fresh water for the removal of any unreacted reagents and polymer. PAA hydrogels containing both the crosslinking agents in different molar ratios were prepared. The stoichiometry for the synthesis is given in **Table 5.1**. The obtained PAA hydrogels are denoted by PAA-xcys or PA-xjeff where x denotes the mol % of the cys/ jeff added.

5.2.3 Preparation of Porous cross linked PAA hydrogels

Porous PAA hydrogels were prepared by cryogenic treatment of fully swollen hydrogels followed by removal of ice crystals by lyophilization. The fully swollen PAA hydrogels (12 mm x12 mm) were placed in liquid nitrogen till complete freezing and then freeze dried in lyophilizer for 24 h to obtain porous hydrogels.

5.3 Characterization

5.3.1 FT-IR

The structural characterization of PEG-PU hydrogels was performed by FT-IR. FT-IR spectra of the hydrogels were recorded on Perkin Elmer (USA) in a diffuse reflectance spectroscopy mode (DRS). The pellets of the dried hydrogels were made using KBr powder.

5.3.2 Swelling Measurements

The swelling behaviour of PAA hydrogels was studied using gravimetric method. The as-prepared hydrogels were immersed in distilled water at room temperature for several days to remove any unreacted reactants. The hydrogels were then dried completely in an oven till the constant weight. These xerogels were then immersed in four different solvents namely distilled water, PBS (pH 7.4, 0.01 M), sodium citrate- citric acid buffer (pH 3, 0.01 M) and NaCl (0.1 M) kept at 37 °C. The gels were removed and gently pressed between two filter papers to remove any excess solvent on the surface and weighed in an analytical balance. The equilibrium swelling ratio (Q_e) was determined using the formula:

$$Q_e = \frac{W_s - W_d}{W_d} x100 \qquad (1)$$

Where W_s and W_d are the weights of the swollen and dried samples respectively.

For the kinetics studies, the swelling ratio was measured as a function of time and the time dependent water uptake was determined using,

$$F(t) = kt^n \qquad (2)$$

Where k is the swelling rate constant, n is the swelling exponent.

5.3.3 Mechanical Properties

The stress-strain measurements in the unidirection were carried out using Instron 5943 mechanical tester at room temperature. The compressive tests were performed on both

as-prepared hydrogels and equilibrium swollen hydrogels in PBS (pH 7.4, 0.01 M). The cylindrical test specimens were having dimension of 15 mm diameter x 15 mm height. The compression speed was 2 mm/min with a pre tension load of 1 kN. For each test, 3-representative samples were taken and the average value of the result is taken.

5.3.4 In-situ Gelation

The in-situ gelation of PAA with two crosslinking agents in aqueous medium was studied using Anton Paar MCR-301 controlled stress rheometer with cup and bob geometry (CC17). PAA aqueous solutions with different molar ratio of crosslinking agents (Cystamine: Jeffamine) and EDC coupling agents were taken in a cup and bob. The parameters, storage modulus (G') and loss modulus (G") were measured as a function of time at 25 °C. The percentage strain was 0.15 % and the frequency was 10 Hz throughout the experiment. The time at which the crossover between G' and G" occurs is taken as the time of gelation.

5.3.5 Scanning electron microscopy (SEM)

Scanning electron Microscopy (SEM) was used to investigate the morphology of the hydrogels using Quanta 200 3D dual beam having electron source of tungsten (W) filament with emission at resolution of 20 kV in high vacuum. The hydrogels were lyophilized and sputter coated with a thin layer of gold. EDAX measurements were carried out to confirm the presence of AgNPs in the hydrogels. Transmission Electron Microscopy (TEM) was performed on JEOL (JEM 2000) operating at 200 kV. The sample was prepared by sonicating the AgNPs obtained in the supernatant and dispersing it over a copper grid. The copper grid was dried for a day before analysis.

5.3.6 In-vitro Release Studies

5.3.6.1 *Doxorubicin loading and release from the hydrogels*

For the drug loading into the hydrogel, fully dried double crosslinked PAA gel (xerogel) was immersed in 10 ml of PBS (pH 7.4, 0.01 M) solution containing 0.5 mg of drug, doxorubicin hydrochloride. The container was kept in a shaking water bath at 37 °C for

36 h. After the gel reached the equilibrium swelling, the swollen gel was removed and dried in oven at 30 °C till the constant weight. The supernatant liquid was collected and assayed by UV-Vis spectroscopy at 478 nm. The percentage loading of dox in PAA hydrogel was estimated by the following formula:

$$\%Loading\ of\ dox = \frac{W_x - W_y}{W_x} x100 \qquad (3)$$

Where W_x is the amount of dox added in PBS solution, W_y is the amount of dox in supernatant solution after the swelling of the hydrogel.

The release of dox from the PAA xerogels was studied using the following procedure: The dox loaded PAA xerogels were immersed in 10 ml of PBS solution containing 1 mM DTT in a sample tube kept in a water bath at 37 °C with a gentle shaking. The control xerogels were immersed in 10 ml PBS solution without DTT. At predetermined time intervals, 1 ml aliquot was withdrawn from the tubes and replenished with same amount of fresh PBS. The amount of dox present in the collected PBS was determined by UV-Vis spectrometry. The % dox release was calculated using the equation:

$$\%Cumulative\ \ dox\,released = \frac{W_t}{W_e} x100 \qquad (4)$$

Where W_t is the weight of the dox released at time 't' and W_e is total amount of dox loaded.

5.3.6.2 *Silver Nanoparticles loading and release from the hydrogels*

Preparation of Ag nanoparticles in the hydrogels was carried out using the following method [30]: The completely dried PAA-5cys-5jeff hydrogels were immersed in 5 mM solution of silver nitrate for overnight to reach equilibrium. The gels were then washed thoroughly to remove any silver nitrate from the surface. The swollen gels were then immersed in 10 mM sodium borohydride solution for about 2 h to obtain AgNPs in the gels. The formation of the AgNPs was observed by the change in the colour of the gels to dark brown. The percentage loading of AgNPs in PAA hydrogel was estimated by completely degrading the hydrogels embedded with AgNPs using probe sonicator and measuring the UV absorbance of the outside solution. The formation of AgNPs in the

hydrogels was confirmed by UV-Vis spectroscopy.

The release of AgNPs from the PAA hydrogels was studied using the following procedure: The AgNPs loaded PAA hydrogels were immersed in 10 ml of distilled water containing 1 mM DTT in a sample tube kept in a water bath at 37 °C with a gentle shaking. The control hydrogels were immersed in 10 ml PBS solution without DTT. At the predetermined time intervals, 1 ml aliquot was withdrawn from the tube and replenished with same amount of fresh distilled water. The amount of AgNPs present in the collected distilled water was determined by UV-Vis spectroscopy at 400 nm. The % AgNPs release was calculated using equation 4, where W_t is the weight of the AgNPs released at time 't' and W_e is total amount of AgNPs loaded.

5.4 Results and discussion

5.4.1 Synthesis of cross linked PAA hydrogels

The double crosslinked PAA hydrogels were prepared using two different crosslinking agents namely cystamine and jeffamine simultaneously. The coupling reaction between the –COOH groups of PAA and the $–NH_2$ groups of crosslinking agents was performed using water soluble EDC coupling agent. Unlike the previous report on the synthesis of double crosslinked Poly(aspartic acid) hydrogels in DMSO solvent, which is toxic and undesirable [25], we have prepared double crosslinked PAA hydrogels in an aqueous

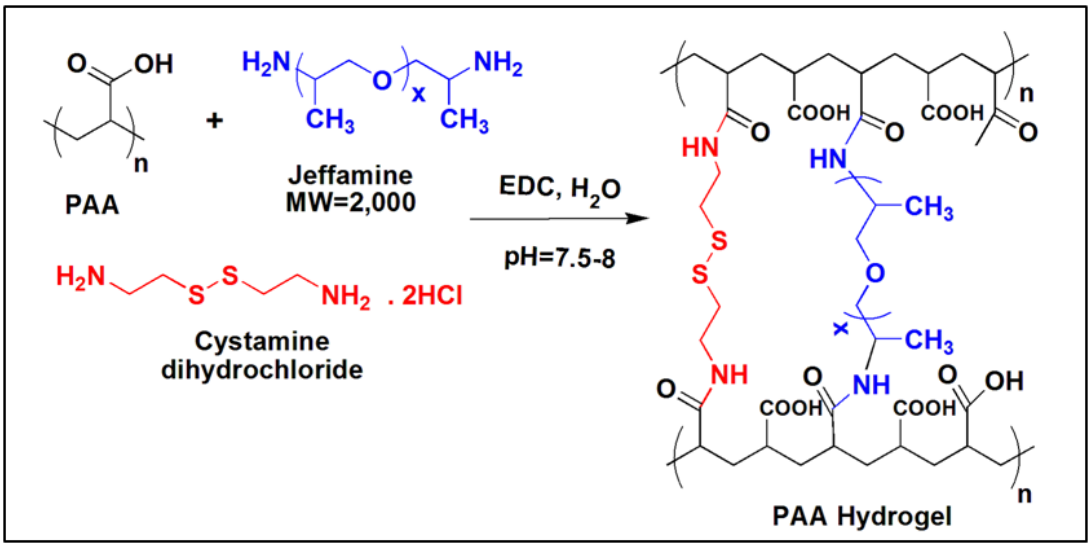

Scheme 5.1: Reaction scheme for synthesis of PAA-cys-jeff double crosslinked hydrogels

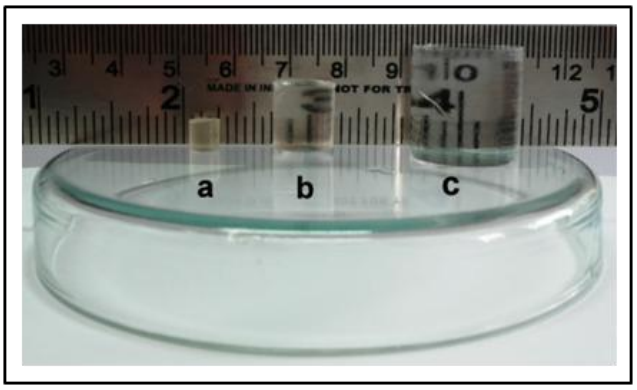

Figure 5.1. Cross linked PAA-5jeff hydrogel (a) dried in oven (b) as-prepared and (c) fully swollen in distilled water

medium under mild basic conditions (pH= 8). The coupling reaction was found to be faster at this pH. Further, the hydrogels could be synthesized within 3-5 min depending on the amount of crosslinking agents used for the reaction. Hydrogels containing both the crosslinking agents in different mole ratios were prepared and the stoichiometry for the synthesis is shown in **Table 5.1**. The reaction pathway for the crosslinking between PAA and the two crosslinking agents is shown in **Scheme 5.1**. The advantages of both

Table 5.1. Stoichiometry for the synthesis of PAA hydrogels

Sample	**PAA** ($molx10^{-3}$)	**Cystamine** ($molx10^{-3}$)	**Jeffamine** ($molx10^{-3}$)	**EDC.HCl** ($molx10^{-3}$)
PAA-5cys	4.17	0.208	0	1.04
PAA-7.5cys	4.17	0.312	0	1.56
PAA-10cys	4.17	0.417	0	2.085
PAA-5jeff	4.17	0	0.208	1.04
PAA-7.5jeff	4.17	0	0.312	1.56
PAA-10jeff	4.17	0	0.417	2.085
PAA-2.5cys+7.5jeff	4.17	0.104	0.312	2.085
PAA-5cys+5jeff	4.17	0.208	0.208	2.085
PAA-7.5cys+2.5jeff	4.17	0.312	0.104	2.085

jeffamine and cystamine are that, they are soluble in water and can provide a homogeneous aqueous reaction medium for the crosslinking reaction. The obtained hydrogels were completely transparent in the dry and swollen state and exhibited good mechanical strength in the swollen condition. We show in **Figure 5.1**, the images of dry, as-prepared and fully swollen hydrogels in water.

5.4.2 Porous PAA hydrogels

Scanning Electron Microscopy was performed on lyophilized mono and double cross linked equilibrium swollen PAA hydrogels in order to observe the change in the

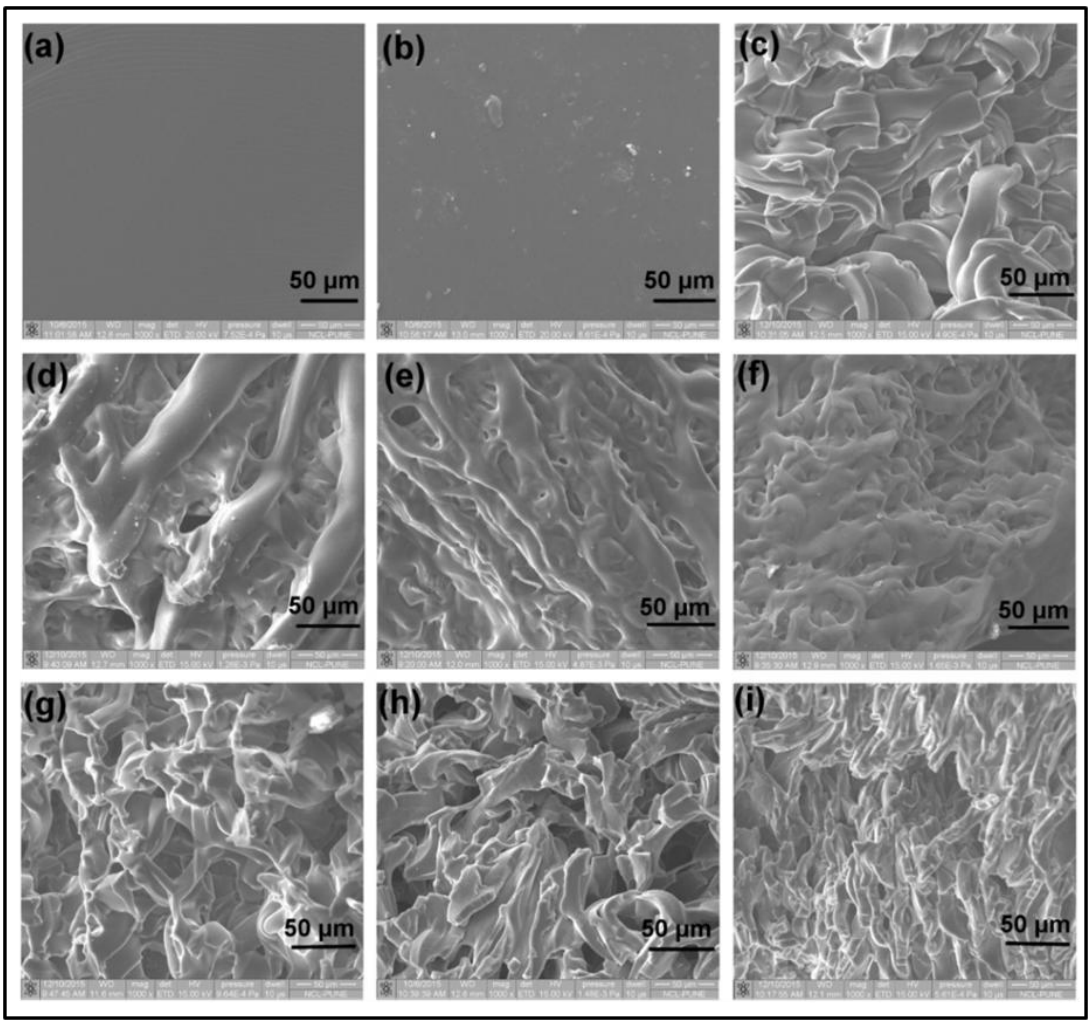

Figure 5.2. SEM micrographs of dried (in oven) and lyophilized PAA hydrogels with different cross linking ratios: (a)PAA-5jeff (dried in oven), (b) PAA-5cys+5jeff(dried in oven), (c)PAA-5cys+5jeff, (d)PAA-5cys, (e)PAA-7.5cys, (f)PAA-10cys, (g)PAA-5jeff, (h)PAA-7.5jeff, (i)PAA-10jeff

morphology with variation in cross linking density (**Figure 5.2**). The SEM images clearly indicate the porous structure in crosslinked PAA hydrogels upon lyophilization of the equilibrium swollen gels. Also, the porosity clearly decreases as the cross linking density of the cross linking agents increases. The porosity was absent in the dried hydrogels (in oven) (**Figure 5.2 (a) & (b)**) due to the collapse of the hydrogel structure.

5.4.3 Structural Characterization

5.4.3.1 *FTIR Spectroscopy*

The structural elucidation of PAA-cys-jeff gel was performed using FT-IR spectroscopy. The stacked plots of FT-IR spectra of PAA-cys-jeff gel before and after the addition of DTT reagent are shown in **Figure 5.3.** In the FTIR spectra, the characteristic peaks at 1560 cm^{-1} and 1654 cm^{-1} appear due to stretching mode of –NH groups and –C=O groups respectively. These two peaks in the hydrogels indicate the formation of amide linkages between PAA and Cystamine/Jeffamine by EDC coupling reaction. Further, we observed that on addition of DTT, in PAA-5cys+5jeff hydrogel, a sharp peak appears at 2874 cm^{-1}. This peak is attributed to the formation of –SH groups by successful breaking of S-S groups selectively in PAA hydrogel in the presence of DTT as shown in **Figure 5.3.**

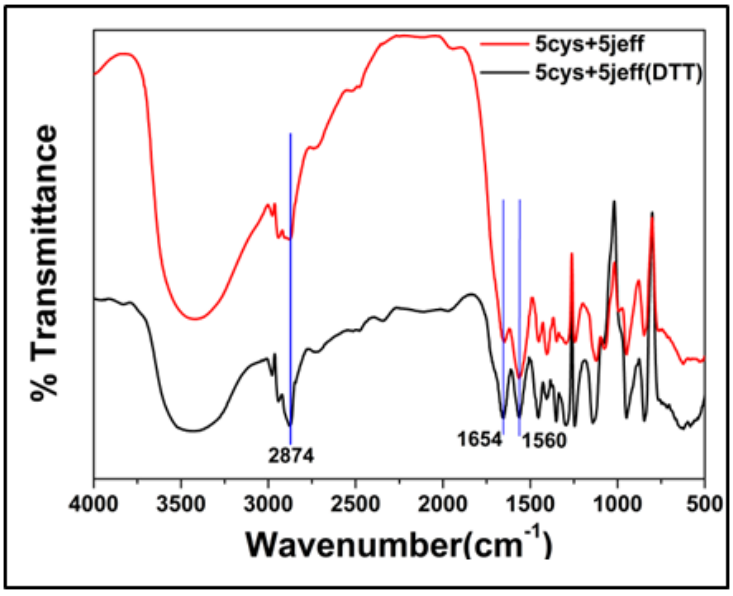

Figure 5.3. FTIR spectra of PAA-5jeff in presence and absence of DTT

5.4.4 Swelling Measurements

5.4.4.1 *Swelling Behaviour of mono cross linked PAA hydrogels*

We show in **Figure 5.4**, the comparative study of equilibrium swelling ratios of mono crosslinked PAA hydrogels using jeffamine and cystamine independently. The mole % of crosslinking agent was 5.0, 7.5 and 10.0. The equilibrium swelling ratios were measured in water, 0.1 M NaCl and the two buffer solutions, PBS (pH 7.4, 0.01 M), sodium citrate-citric acid buffer (pH 3, 0.01 M). It can be readily seen that all the hydrogels showed very high swelling in water but exhibited low swelling in NaCl and buffer solutions. This is indeed expected. The hydrogels being polyelectrolyte in nature, the polymer chain dimensions are strongly affected by the presence of salt and reduce the electrostatic repulsion in the expanded polymer chain resulting into contraction of the chains. This in turn reduces the equilibrium swelling of hydrogel. Similarly, in the case of buffer solutions, the cations effectively screen the charge repulsion and reduce the degree of swelling. It is well known that the swelling in hydrogels strongly depends on the degree of crosslinking. The swelling decreases as the degree of crosslinking increases. This is clearly observed in equilibrium swelling ratios of all the hydrogels in

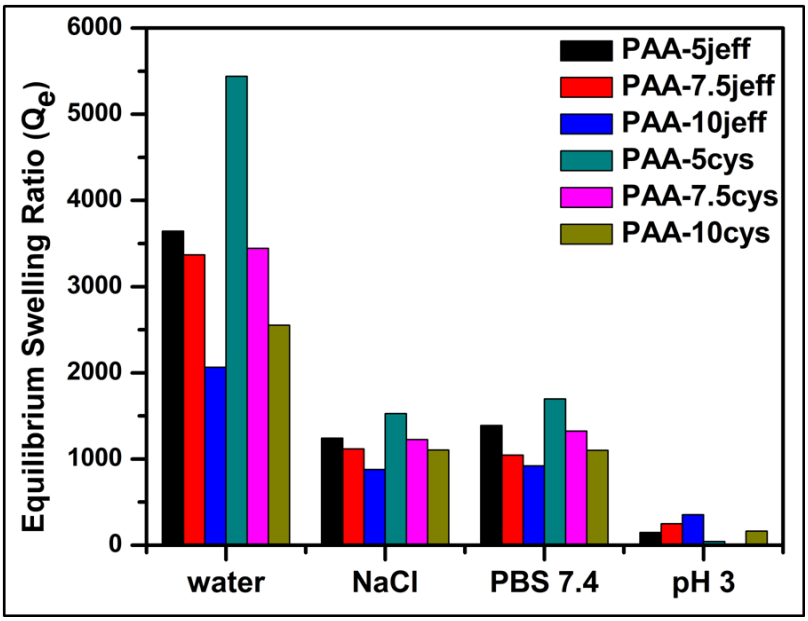

Figure 5.4. Equilibrium swelling ratios of mono crosslinked PAA hydrogels in water, NaCl (0.1M), PBS (pH 7.4, 0.01M), sodium citrate-citric acid buffer (pH 3, 0.01M)

water, NaCl and buffer solutions. However, it is important to note here that the equilibrium swelling ratios of cystamine crosslinked hydrogels were found to be higher than the equilibrium swelling ratios of jeffamine crosslinked hydrogels at the same mol % of the cross linkers. This is contrary to the fact that, cystamine is a small molecule and can undergo more crosslinking with tight network structure and expected to show lower equilibrium swelling ratios. The higher swelling ratios in this case can be explained on the basis that disulphide bonds in cystamine are susceptible to basic environment and can be cleaved at the reaction pH of 8.0. Therefore, the incorporation of cystamine molecules which form the effective crosslinks in the network structure could be less and as a result show higher equilibrium swelling ratios.

5.4.4.2 *Swelling Behaviour of double cross linked PAA hydrogels*

We show in **Figure 5.5 (a)**, the equilibrium swelling ratios of double crosslinked hydrogels in different solvents. The kinetics of swelling of double crosslinked hydrogels in three different solvents- water, PBS (pH 7.4, 0.01M), NaCl (0.1M) was also studied using xerogels of known weight with precise dimensions (cylinders of 12 mm height x 12 mm diameter). The swelling ratios of hydrogels were measured with respect to time till they reached the equilibrium swelling which took about ~25 h. The plots of swelling ratios vs time were constructed (**Figure 5.5 (b)**). The swelling exponent 'n' was

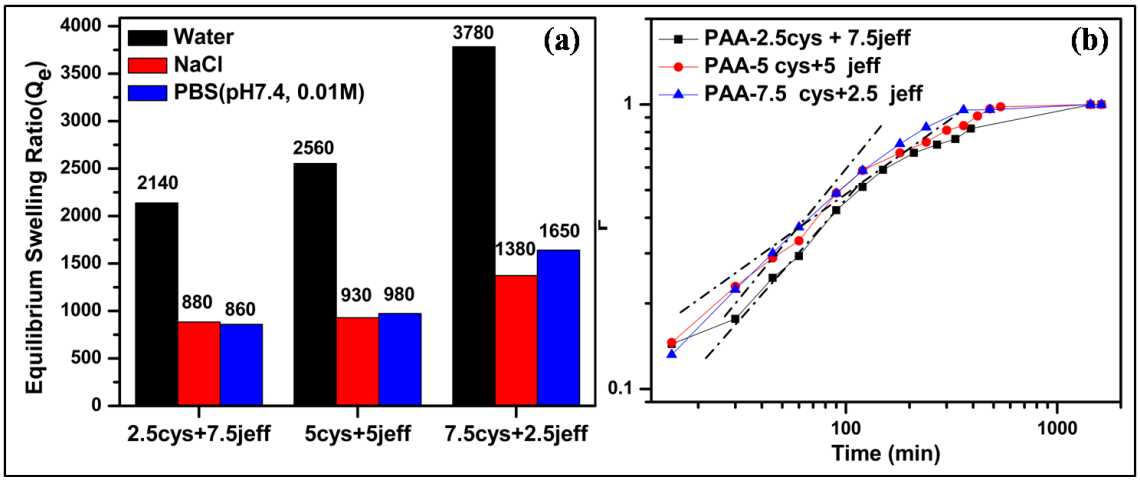

Figure 5.5. (a) Equilibrium swelling ratios of double crosslinked PAA hydrogels in water, NaCl (0.1M), PBS (pH 7.4, 0.01M) and (b) Fickian curve with respect to time of dual cross linked PAA with different mol% of cystamine and jeffamine in water

calculated from the slope of the linear region in the initial swelling profile. The value of swelling exponent 'n' was found to be between 0.5-1.0 indicating the non Fickian behaviour of the swelling.

5.4.4.3 *Selective breaking of one crosslinking in a double crosslinked hydrogel and its influence on swelling*

The double crosslinked PAA hydrogels that we have synthesized contain both Cystamine and jeffamine crosslinking agents. The disulphide linkage (S-S) in cystamine can be cleaved by redox reagents such as dithiothreitol (DTT) due to significant difference in their redox potentials.

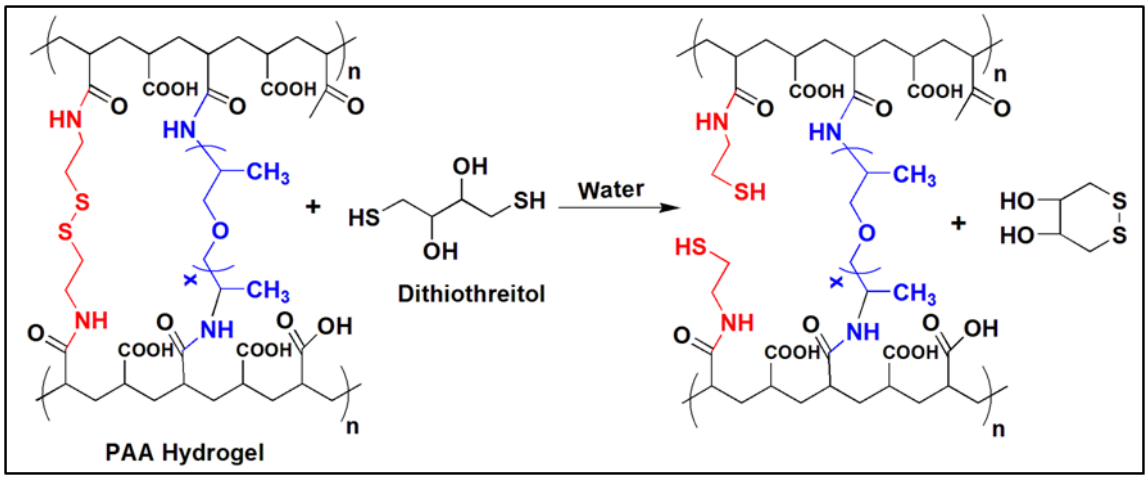

Scheme 5.2: Selective cleavage of cystamine in the presence of DTT in double cross linked PAA hydrogels

Accordingly, the equilibrium swollen double crosslinked PAA hydrogels were immersed in water, NaCl and PBS solutions containing DTT. The schematics of selective breaking of S-S bonds in cystamine without affecting the jeffamine crosslinks is shown in **Scheme 5.2**. The selective breaking of S-S bonds in cystamine resulting into decrease in the degree of crosslinking was manifested in the increase in equilibrium swelling ratios of hydrogels. We show in **Figure 5.6**, the equilibrium swelling ratios of PAA hydrogels in water, NaCl and PBS (pH 7.4, 0.01 M) solution after the cleavage of cystamine crosslinking. It can be seen that there is a significant increase in the swelling ratio due to decrease in the degree of crosslinking as a result of the breaking of S-S

bonds in cystamine. By varying concentration of DTT judiciously, one can think of controlling the degree of swelling in hydrogels which can have large implications in the controlled drug delivery applications. These aspects will be discussed in the later sections.

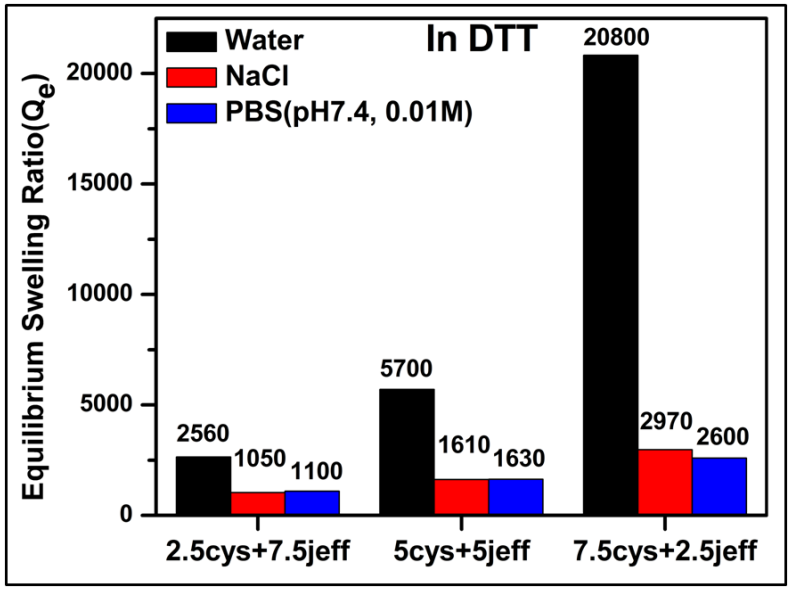

Figure 5.6. Equilibrium swelling ratios of double crosslinked PAA hydrogels in water, NaCl (0.1M), PBS (pH 7.4, 0.01M) in presence of DTT

5.4.5 Mechanical Properties

The mechanical strength of mono and double crosslinked hydrogels in terms of elastic modulus (E') in the as-prepared and equilibrium swollen (in PBS) state were determined using Instron 5943 in the compression mode (**Figure 5.7**). Typical stress-strain curves (in compression) for mono crosslinked PAA hydrogels (as-prepared) with cystamine and jeffamine are shown in **Figure 5.7**. The elastic modulus (E') was determined from the slope of the initial linear region of the stress-strain curves. The results are shown in **Table 5.2**. It can be seen from the results that as expected the elastic modulus increased with increase in degree of crosslinking in all the hydrogels. The equilibrium swollen hydrogels in PBS showed lower elastic moduli compared to the as-prepared hydrogels. Interestingly, in the case of mono crosslinked hydrogels, the jeffamine crosslinked

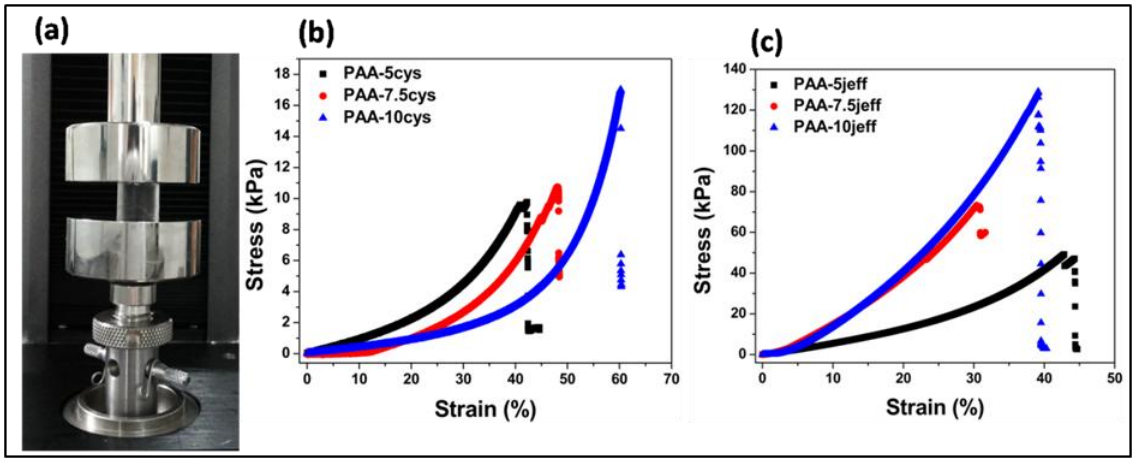

Figure 5.7. (a) The image of an Instron 5943 during compression study of as-prepared PAA-5jeff hydrogel; Compressive strength studies of mono crosslinked PAA hydrogels with (b) Cystamine, (c) Jeffamine

Table 5.2: Elastic moduli of mono cross linked PAA hydrogels with different degree of crosslinking

Hydrogel samples	**Elastic Modulus (E') (kPa)**	
	As Prepared	**Equilibrium swollen in PBS**
PAA-5cys	9.0	3.0
PAA-7.5cys	9.5	8.0
PAA-10cys	10.0	4.0
PAA-5jeff	55.0	50.0
PAA-7.5 jeff	110.0	90.0
PAA-10 jeff	160.0	100.0
PAA-7.5cys+2.5jeff	25.0	20.0
PAA-5cys+5jeff	100.0	65.0
PAA-2.5cys+7.5jeff	130.0	100.0

hydrogels showed higher elastic moduli as compared to cystamine crosslinked PAA hydrogels. This is also reflected in double crosslinked PAA hydrogels where the jeffamine content increased systematically. This clearly indicates that jeffamine undergoes more efficient crosslinking in the hydrogels formation. Further, the values of E' obtained for both mono and double crosslinked PAA hydrogels in the as-prepared and fully swollen state are quite high as compared to the earlier PASP hydrogels. Also, the equilibrium swollen hydrogels shows lower mechanical strength as compared to the as-prepared hydrogels. This could be attributed to the fact that equilibrium swollen hydrogels contain large amount of fluid which makes them soft resulting in to lower mechanical strengths. Further, the values of E' obtained for both mono and double crosslinked PAA hydrogels in the as-prepared and fully swollen state are quite high as shown in **Table 5.2**. With this range of mechanical strengths they are easy to handle and show great potential in controlled drug delivery applications.

5.4.6 In-situ Gelation

In the in-situ gelation study, PAA, jeffamine, cystamine, NaOH was homogeneously mixed and charged to the cup. Immediately, after the addition of EDC coupling agent, G' and G" were measured as a function of time. The crossover point of G' and G" was

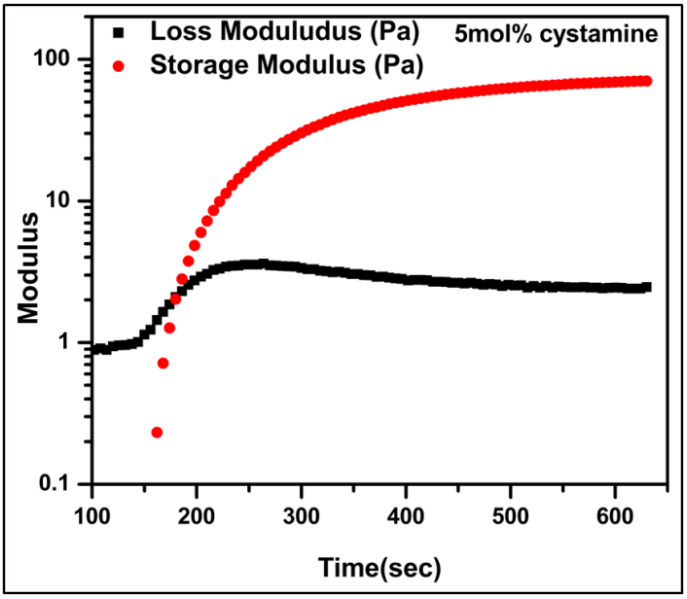

Figure 5.8. Gelation time for PAA hydrogels with different crosslinking

taken as the gelation time (**Figure 5.8**). We show in **Table 5.3**, the time of gelation (averaged with repetition of 3 samples) for hydrogels with different molar ratios of jeffamine and cystamine. It can be readily seen from the results that in all the samples, the gelation could take place in 1 min. Particularly, the crosslinking agent, jeffamine seems to be more reactive than cystamine wherein, the sample with more jeffamine showed faster gelation in 30 sec. A similar gelation times were also observed outside the rheometer in moulds where one can visualize the gelation with naked eye. These remarkable fast gelation times were comparable to gelation times observed in photo crosslinking methods.

Table 5.3. Gelation time for PAA hydrogels with different crosslinking

Sample	Time of Gelation (seconds)
PAA-2.5cys+7.5jeff	30
PAA-5cys+5jeff	45
PAA-7.5cys+2.5jeff	60

5.4.7 Morphological Analysis

Scanning Electron Microscopy was performed on dried AgNPs incubated gels in order to observe the change in morphology of the gels (**Figure 5.9 (a)**). The SEM image clearly indicates the porous structure in PAA-5cys+5jeff hydrogels with AgNPs present on the surface. To further confirm the formation of AgNPs, Transmission Electron Microscopy (TEM) was performed by collecting the supernatant from the gel. From **Figure 5.9 (b)**, it is clear that the AgNPs were successfully formed inside the hydrogel matrix with an average size of 10 nm. The AgNPs were spherical in shape with a face centered cubic (fcc) structure, clearly observed as diffraction rings. Further confirmation of the presence of AgNPs in the hydrogel was obtained using Energy dispersive X-ray analysis (EDAX). Optical absorption peak at approximately 3 keV due to surface Plasmon resonance confirms the presence of Ag in hydrogel (**Figure.5.10**)

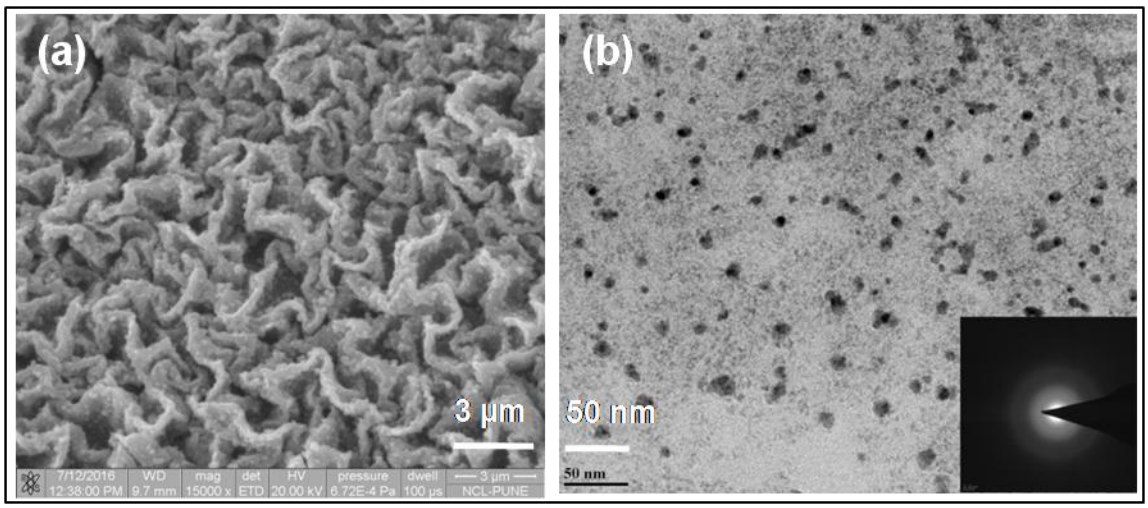

Figure 5.9. (a) SEM and (b) TEM image of AgNPs in PAA-5cys+5jeff

We show in **Table 5.4**, the % of each element present in the hydrogel as obtained from EDAX.

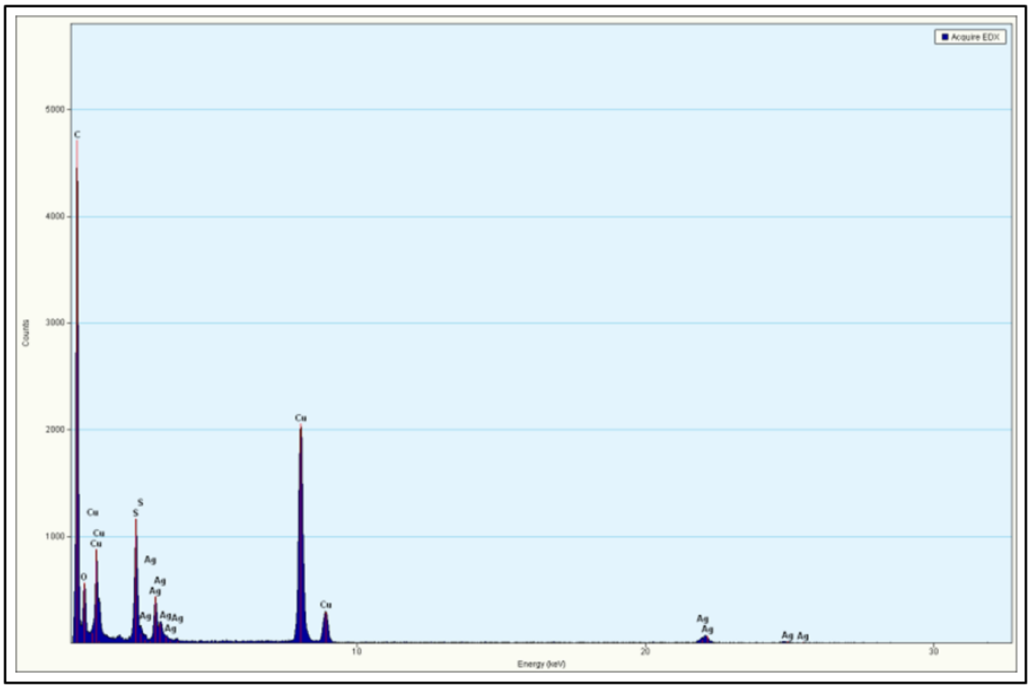

Figure 5.10. EDAX image of Ag embedded in PAA-5cys+5jeff hydrogel

Table 5.4: Weight % of each element by EDAX

Element	Ag embedded in PAA-5cys+5jeff hydrogel
C (K)	63.44
O (K)	3.83
S (K)	4.54
Cu (K)	22.30
Ag (K)	5.86

5.4.8 Doxorubicin loading and release from the hydrogels

In order to see the implication of selective breaking of one crosslinking in the drug delivery applications, we incorporated an anticancer drug, doxorubicin hydrochloride into double crosslinked PAA hydrogel (PAA-5cys+5jeff) and studied the release of dox in PBS (pH 7.4, 0.01 M) upon selective breaking of disulphide (S-S) bonds in cystamine using DTT. The loading of dox into the hydrogel was performed by immersing the dry PAA-5cys+5jeff xerogel into PBS containing dox hydrochloride. The swelling of the hydrogel induced the diffusion of dox into the hydrogel. We show

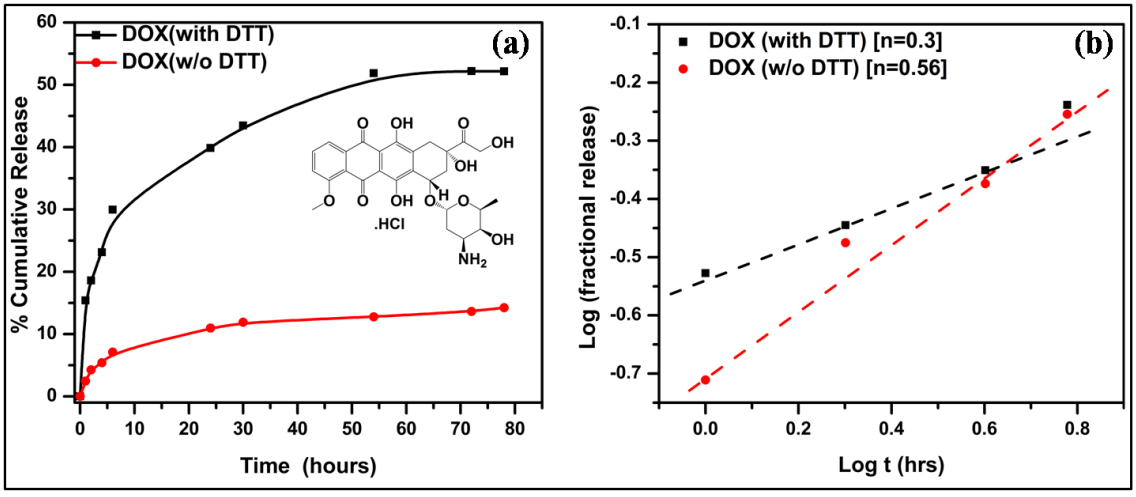

Figure 5.11. (a) Cumulative release of DOX with time from PAA-5cys+5jeff in the presence and absence of DTT and inset shows Structure of Doxorubicin. HCl and (b) Fractional release of dox form PAA-5cys+5jeff in the presence and absence of DTT

in **Figure 5.11 (a)**, the cumulative release of dox from PAA-5cys+5jeff as a function of time with and without the treatment of DTT. It is seen from the figure that, the hydrogel without the treatment of DTT showed ~15.0 % dox release in 40-80 h whereas, the DTT treated hydrogel cleaved the di-sulphide linkage and reduced the degree of crosslinking and in turn increased the swelling of hydrogel. The increase in swelling of the hydrogel influenced the faster and higher amount (~ 60 %) of dox release from the hydrogel over a period of 40-80 h. The release of dox from the DTT treated hydrogel was clearly visible upon the colour change of the hydrogel from deep red to almost transparent which is shown in **Figure 5.12**. The release of dox from the xerogel involves the simultaneous absorption of water/buffer and desorption of dox via a swelling controlled diffusion mechanism. The mechanism of dox release from the PAA-5cys+5jeff was determined by fitting the data to Ritger-Peppas equation mentioned below[31]:

$$M_t / M_\infty = kt^n \qquad (5)$$

Where M_t/M_∞ denotes the fractional release of the drug from the hydrogel, 'k' denotes the proportionality constant, 'n' is the release exponent and 't' is the time. The release exponent was calculated from the slope of natural logarithmic plot of fractional release (initial linear region of the 60 % release) vs. time. We show in **Figure 5.11 (b)**, the fractional release of dox from PAA-5cys+5jeff hydrogel with respect to time in the absence and presence of DTT. It is observed that, the dox release from the hydrogel with DTT follows Fickian behaviour (n<0.5) and without DTT shows a non-Fickian behaviour (n>0.5).

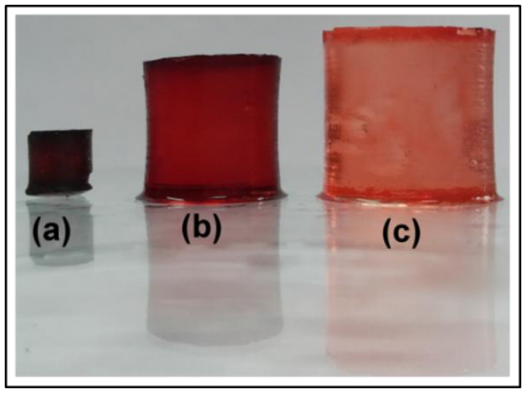

Figure 5.12. PAA-5cys+5jeff loaded with DOX (a) dried in oven, (b) swollen in PBS (pH7.4, 0.01M) without DTT and (c) swollen in PBS (pH7.4, 0.01M) with DTT

5.4.9. Silver Nanoparticles loading and release from the hydrogels

We also studied the release of AgNPs from the double cross crosslinked PAA hydrogels by selectively cleaving the cystamine bonds using DTT. The release of AgNPs in the DTT treated gels is clearly visible in **Figure 5.13** where the hydrogel which has released AgNPs becomes transparent. **Figure 5.14 (a)** shows the cumulative release of AgNPs from the gel as a function of time in the presence of DTT. It is observed that the hydrogel in the absence of DTT shows 5% AgNPs release in 7 days whereas in presence of DTT, a faster release has been observed (48 %). This slow release of nanoparticles from hydrogels could be explained by strong coordination bond between

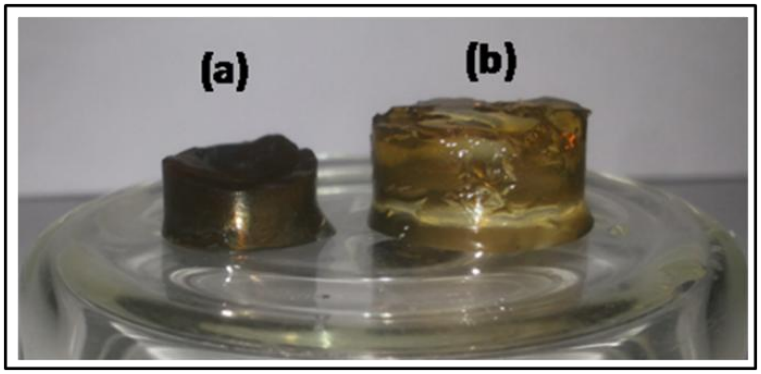

Figure 5.13. PAA-5cys+5jeff loaded with (a) AgNPs (without DTT treated) and (b) AgNPs (with DTT treated)

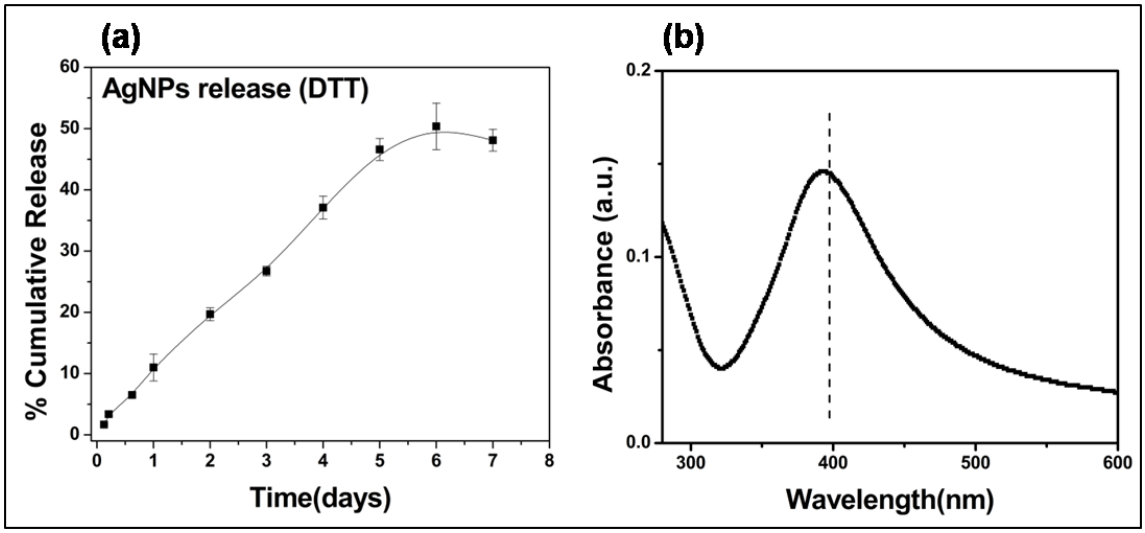

Figure 5.14. (a) Cumulative release of AgNPs with time from PAA-5cys+5jeff in the presence of DTT and (b) UV spectra of AgNPs embedded in PAA-5cys+5jeff hydrogel

Ag and –COONa groups of the gels. On addition of DTT, there is an increase in the swelling of gels that helps in the release of nanoparticles. The total AgNPs present inside the gel was calculated by probe sonicating the gel for 10 min and calculating the UV absorbance at 400 nm (**Figure 5.14 (b))**.

5.5 Conclusion

In conclusion, we have successfully synthesized double crosslinked PAA hydrogels simultaneously using two crosslinking agents namely, cystamine and jeffamine. The two diamines were coupled to PAA using EDC coupling agent. All the hydrogels were characterized in terms of structure, morphology, swelling and mechanical strength. The hydrogels obtained showed good mechanical strength in terms of compressive strength and exhibited strong dependence on the degree of crosslinking and extent of swelling. Jeffamine showed more efficient crosslinking compared to cystamine. The selective breaking of disulfide linkage in the cystamine was affected using DTT which resulted in decrease in the degree of crosslinking and increase in the swelling of the hydrogels. This phenomenon of in-situ breaking of one crosslinking and increasing the swelling ratio could be used in the swelling-controlled drug delivery systems. The implication of selective breaking of crosslinks on the swelling-controlled release of an anti-cancer drug, doxorubicin was demonstrated. Further, in order to incorporate antimicrobial properties to the hydrogels, we successfully prepared AgNPs inside the gels. The gels could be used for controlled release of AgNPs over a period of time by selectively cleavage of Cystamine bonds. These double cross linked hydrogels show great promise in drug delivery and tissue engineering applications.

References

[1] S.S. Halacheva, T.J. Freemont, B.R. Saunders, pH-responsive physical gels from poly(meth)acrylic acid-containing crosslinked particles: the relationship between structure and mechanical properties, Journal of Materials Chemistry B, 1 (2013) 4065.

[2] Y. Hu, Z. Du, X. Deng, T. Wang, Z. Yang, W. Zhou, C. Wang, Dual physically cross-linked hydrogels with high stretchability, toughness, and good self-recoverability, Macromolecules, 49 (2016) 5660-5668.

[3] M.F. Akhtar, M. Hanif, N.M. Ranjha, Methods of synthesis of hydrogels… a review, Saudi Pharmaceutical Journal, 24 (2016) 554-559.

[4] M.D. Konieczynska, M.W. Grinstaff, On-Demand Dissolution of Chemically Cross-Linked Hydrogels, Accounts of Chemical Research, 50 (2017) 151-160.

[5] L.S. Nair, C.T. Laurencin, Polymers as Biomaterials for Tissue Engineering and Controlled Drug Delivery, in: K. Lee, D. Kaplan (Eds.) Tissue Engineering I, Springer Berlin Heidelberg, Berlin, Heidelberg, (2006) 47-90.

[6] T.R. Hoare, D.S. Kohane, Hydrogels in drug delivery: Progress and challenges, Polymer, 49 (2008) 1993-2007.

[7] S. Van Vlierberghe, P. Dubruel, E. Schacht, Biopolymer-based hydrogels as scaffolds for tissue engineering applications: a review, Biomacromolecules, 12 (2011) 1387-1408.

[8] J.A. Hunt, R. Chen, T. van Veen, N. Bryan, Hydrogels for tissue engineering and regenerative medicine, Journal of Materials Chemistry B, 2 (2014) 5319-5338.

[9] S.M.H. Bukhari, S. Khan, M. Rehanullah, N.M. Ranjha, Synthesis and Characterization of Chemically Cross-Linked Acrylic Acid/Gelatin Hydrogels: Effect of pH and Composition on Swelling and Drug Release, International Journal of Polymer Science, 2015 (2015) 1-15.

[10] A. Chang, pH-sensitive starch-g-poly(acrylic acid)/sodium alginate hydrogels for controlled release of diclofenac sodium, Iranian Polymer Journal, 24 (2015) 161-169.

[11] Z.A. Hamid, A. Blencowe, B. Ozcelik, J.A. Palmer, G.W. Stevens, K.M. Abberton, W.A. Morrison, A.J. Penington, G.G. Qiao, Epoxy-amine synthesised hydrogel scaffolds for soft-tissue engineering, Biomaterials, 31 (2010) 6454-6467.

[12] S.Y. Choh, D. Cross, C. Wang, Facile synthesis and characterization of disulfide-cross-linked hyaluronic acid hydrogels for protein delivery and cell encapsulation, Biomacromolecules, 12 (2011) 1126-1136.

[13] J. Choi, H.J. Kung, C.E. Macias, O.K. Muratoglu, Highly lubricious poly(vinyl alcohol)-poly(acrylic acid) hydrogels, Journal of biomedical materials research. Part B, Applied biomaterials, 100 (2012) 524-532.

[14] Z.M. Rzaev, S. Dincer, E. Pişkin, Functional copolymers of N-isopropylacrylamide for bioengineering applications, Progress in Polymer Science, 32 (2007) 534-595.

[15] D. Das, P. Ghosh, S. Dhara, A.B. Panda, S. Pal, Dextrin and Poly (acrylic acid)-Based Biodegradable, Non-Cytotoxic, Chemically Cross-Linked Hydrogel for Sustained Release of Ornidazole and Ciprofloxacin, ACS applied materials & interfaces, 7 (2015) 4791-4803.

[16] X. Gao, C. He, C. Xiao, X. Zhuang, X. Chen, Biodegradable pH-responsive polyacrylic acid derivative hydrogels with tunable swelling behavior for oral delivery of insulin, Polymer, 54 (2013) 1786-1793.

[17] X. Zhang, S. Malhotra, M. Molina, R. Haag, Micro- and nanogels with labile crosslinks – from synthesis to biomedical applications, Chem. Soc. Rev., 44 (2015) 1948-1973.

[18] H. Hosseinzadeh, Controlled release of diclofenac sodium from pH-responsive carrageenan-g-poly (acrylic acid) superabsorbent hydrogel, Journal of chemical sciences, 122 (2010) 651-659.

[19] I. Manavi-Tehrani, M. Rabiee, M. Parviz, M.R. Tahriri, Z. Fahimi, Preparation, Characterization and Controlled Release Investigation of Biocompatible pH-Sensitive PVA/PAA Hydrogels, in: Macromolecular symposia, Wiley Online Library, (2010), 457-465.

[20] J. Dobson, Magnetic nanoparticles for drug delivery, Drug development research, 67 (2006) 55-60.

[21] T. Shiga, Y. Hirose, A. Okada, T. Kurauchi, Bending of poly (vinyl alcohol)–poly (sodium acrylate) composite hydrogel in electric fields, Journal of applied polymer science, 44 (1992) 249-253.

[22] J. Zhang, F. Yang, H. Shen, D. Wu, Controlled Formation of Microgels/Nanogels from a Disulfide-Linked Core/Shell Hyperbranched Polymer, ACS Macro Letters, 1 (2012) 1295-1299.

[23] X.Z. Shu, Y. Liu, Y. Luo, M.C. Roberts, G.D. Prestwich, Disulfide cross-linked hyaluronan hydrogels, Biomacromolecules, 3 (2002) 1304-1311.

[24] A.N. Zelikin, Q. Li, F. Caruso, Disulfide-stabilized poly (methacrylic acid) capsules: formation, cross-linking, and degradation behavior, Chemistry of materials, 20 (2008) 2655-2661.

[25] M. Zrinyi, T. Gyenes, D. Juriga, J.-H. Kim, Volume change of double cross-linked poly (aspartic acid) hydrogels induced by cleavage of one of the crosslinks, Acta biomaterialia, 9 (2013) 5122-5131.

[26] B. Gyarmati, Á. Némethy, A. Szilágyi, Reversible response of poly(aspartic acid) hydrogels to external redox and pH stimuli, RSC Advances, 4 (2014) 8764-8771.

[27] M. Zhong, Y.T. Liu, X.Y. Liu, F.K. Shi, L.Q. Zhang, M.F. Zhu, X.M. Xie, Dually cross-linked single network poly(acrylic acid) hydrogels with superior mechanical properties and water absorbency, Soft matter, 12 (2016) 5420-5428.

[28] M.J. Kutyła, M.W. Boehm, J.R. Stokes, P.N. Shaw, N.M. Davies, R.P. McGeary, J. Tuke, B.P. Ross, Cyclodextrin-crosslinked poly (acrylic acid): adhesion and controlled release of diflunisal and fluconazole from solid dosage forms, Aaps Pharmscitech, 14 (2013) 301-311.

[29] T. Hussain, M. Ansari, N.M. Ranjha, I.U. Khan, Y. Shahzad, Chemically cross-linked poly (acrylic-co-vinylsulfonic) acid hydrogel for the delivery of isosorbide mononitrate, The Scientific World Journal, 2013 (2013).

[30] M.V. Patwadkar, C.S. Gopinath, M.V. Badiger, An efficient Ag-nanoparticle embedded semi-IPN hydrogel for catalytic applications, RSC Adv., 5 (2015) 7567-7574.

[31] P.N.A. Ritger Philip L. , A simple equation for description of solute release II. Fickian and anomalous release from swellable devices, Journal of Controlled Release,, 5 (1987) 37-42.

Chapter-6

Poly(acrylic acid) Hydrogels Crosslinked with PEG Cross Linkers using Furan-Maleimide Click Chemistry

6.1 Introduction

In view of the importance of Hydrogels in drug delivery and bio-medical fields, Green Chemistry approaches to synthesize hydrogels are gaining lot of interest these days. Various chemical methods have been explored for the synthesis of hydrogels in the absence of toxic organic solvents and other catalysts/ initiators in order to minimize the side effects in physiological/ biological environment.[1] Over the past few decades, research has been focused on reactions that fulfill important criteria such as, selectivity, efficiency and versatility.[2] Accordingly, "click" reactions have become very prominent.[3-5] Diels-Alder (DA) reaction which is an important type of click reaction (commonly called as Huisgen 1,3-dipolar cyclo addition reaction), has gained much attention as it provides efficient and clean method for making new bonds by intra or intermolecular coupling reactions.[6-8] DA reaction is a [4+2] cycloaddtion reaction that involves reaction between diene and dienophile and the reaction is highly chemo selective in nature which generally takes place without the use of any protecting groups.[6, 9-12] In addition to experimental convenience of DA reactions, they are associated with negligible side reactions and thermal degradation which gives DA reactions an edge over other click reactions like thiol-ene coupling. In addition to this, the furan reagents used in furan-maleimide click chemistry are derived from renewable resources, thus such reactions could be safely categorized under green chemistry.[13] Extensive work has been reported in the literature on DA reactions utilized for crosslinking of polymers in organic solvents. However, there are very few reports in which water has been used as a reaction medium and suggests that water induces an accelerating effect on the rate of DA reactions thus making water a highly suitable solvent for the reaction.[14, 15] Since water could be used as a solvent, DA reactions show great promise in preparing smart hydrogels as injectables.[16] The gelation time in DA reactions strongly depends on temperature and it decreases as the temperature increases.[16] DA reactions are thermally reversible in nature and the furan-maleimide bonds can be cleaved at higher temperatures in presence of DMSO as a solvent. However, in the present work, our focus is mainly on the furan-maleimide bond formation in aqueous media to prepare hydrogels for biological applications.

Wei and co-workers first reported the thermo responsive hydrogels based on the aqueous DA reactions using various polymer chains bearing pendant furfuryl groups and PEO bismaleimide as a cross linking agent.[17-19] Hydrogels synthesized using DA reactions have been explored in areas such as drug delivery, tissue engineering and sensor technology.[20, 21] Although a large number of reports have been published on polymer preparation via DA reaction, [22-25] a limited study has been carried out for the preparation of hydrogels in aqueous medium. In order to further increase the mechanical strength of the hydrogels synthesized using DA reaction, inorganic nanoparticle could be incubated inside the polymer matrix like clays, Ag or Au nanoparticles, carbon nanotubes, graphene, fullerenes etc.[26-28] Along with enhancing mechanical properties, nanoparticles of Au and Ag incubate antimicrobial properties to the hydrogels.[29, 30] Mesoporous silica nanoparticles composites with chitosan hydrogels have been studied recently in order to enhance the mechanical properties of the hydrogels.[31] MSNs along with enhancing the mechanical properties, act as a sustained drug delivery carrier due to the presence of extensive mesoporosity in the particles.[32-34]

In the present work, we have synthesised poly(acrylic acid) based hydrogels via click chemistry approach. Poly(acrylic acid) was modified by the reaction of free carboxylic groups of the main backbone with furfuryl amine using DCC coupling reaction. Polyethylene glycol with different molecular weights was modified to obtain their respective bismaleimides. The hydrogel formation could be achieved in aqueous medium by simply mixing the two reagents (both FDA approved) in the absence of any catalyst. The effect of temperature was studied on gelation time. The main focus of the work is to study the effect of chain length of PEG cross linkers on the gelation time and the mechanical strengths of the hydrogels formed. The hydrogels formed shows decreasing gelation time and increasing mechanical strength with increase in the molecular weight of the PEG cross linkers which could be possibly due to the additional strength provided by the hydrogen bonding between carboxylic groups in PAA and oxygen molecules in PEG. Further, in order to enhance the mechanical properties of the hydrogels, we incorporated Mesoporous Silica Nanoparticles inside the

hydrogels.[35, 36] Another advantage associated with MSNs is the presence of uniform pores in nanometres range which could be utilized for the encapsulation hydrophobic drug inside the pores which is otherwise difficult in highly hydrophilic hydrogel system. The hydrogels obtained using furan maleimide click chemistry approach has potential application for in-situ encapsulation of cells/ biomolecules for drug delivery and as scaffolds for tissue engineering.

6.2 Experimental

6.2.1 Materials

Poly(acrylic acid) (MW=125000 g/mol), poly (ethylene glycol) (MW=2000 g/mol, 6000 g/mol and 8000 g/mol) dicyclohexyl-carbodiimide hydrochloride (DCC), dimethyl amino pyridine (DMAP), furfurylamine, triethylamine, hydroquinone, maleic anhydride, p-amino benzoic acid, tetraethylorthosilicate (TEOS) (99%), (3-aminopropyl) triethoxysilane (APTES), and cetyltrimethylammonium bromide (CTAB) (99%) were obtained from Sigma Aldrich, St. Louis, MO, USA. All chemicals were used as received.

6.2.2 Synthesis of furan grafted poly(acrylic acid) (PAA-furan)

Ten grams (0.14 mol) of poly(acrylic acid) was dissolved in 150 ml N-methyl pyrrolidone by stirring at room temperature. After complete dissolution (for 6 h), furfuryl amine (1.35 g, 0.014 mol) and dicyclohexyl carbodiimide predissolved in 50 ml NMP was added to the solution and the reaction was carried out at 60 ºC for 24 h. After 24 h, the reaction mixture was cooled down to room temperature followed by the addition of 1 M NaOH solution (to convert remaining carboxylic groups to sodium salt). The precipitate obtained was filtered under vacuum and washed with excess NMP to remove unreacted molecules. The precipitate was then dissolved in water, dialyzed against distilled water for 48 h (with frequent change of water) and finally lyophilized to obtain pure product in the solid form. (Yield= 90 %)

^{1}H NMR (400 MHz, D_2O) of PAA-*g*-furan copolymer: δ 1.48 (-C**H**$_2$ of PAA), δ 2.08 (-

C**H** of PAA), δ 4.31 (2H, -NH-C**H**$_2$-C=C of furan side chain), δ 6.35 (2 H, -NH-CH$_2$-C=C**H**- of furan side chain), δ 7.42 (1H, -OC**H**=CH-).

6.2.3 Synthesis of N- (4-Carboxyphenyl) maleamic acid (p-CPMA)

Maleic anhydride (10 g, 46 mol) and p-amino benzoic acid (14 g, 46 mol) were dissolved in N,N-dimethyl formamide (DMF) and the reaction mixture was stirred at room temperature for 6 h under inert atmosphere. After completion of the reaction, the product was precipitated in large amount of water to obtain crude p-CPMA. The crude product was then filtered, dried and recrystallized three times with water to obtain pure p-CPMA. (Yield= 75 %)

^{1}H NMR (200 MHz, DMSO) of p-CPMA: δ 10.61 (H, COOH), δ 7.89 and 7.75 (4 H in phenyl), δ 6.46 (1 H, CO-CH=C**H**-COOH), δ 6.35 (1 H CO-C**H**=CH-COOH).

6.2.4 Synthesis of N- (4-Carboxyphenyl) maleimide (p-CPMI)

In a round bottomed flask, added p-CPMA (5 g, 0.022 mol), sodium acetate (0.3 g) and acetic anhydride (12 ml) and the reaction mixture was stirred at 55 ºC for 2 h. The reaction mixture was then cooled down to room temperature and the product was precipitated in large amount of water to obtain crude p-CPMI. The product was then filtered, dried and recrystallized three times in methanol: water mixture (6:1) to obtain pure p-CPMI. (Yield= 80 %)

^{1}H NMR (200 MHz, DMSO) of p-CPMI: δ 13.07 (H, COOH), δ 8.03 and 7.53 (4 H in phenyl), δ 7.22 (2 H, CO-C**H**=C**H**-CO).

6.2.5 Synthesis of N- [4- (Chlorocarbonyl)phenyl] maleimide (p-CPMIC)

A mixture of p-CPMI (2 g, 9.2 mmol), thionyl chloride (10 ml, 134 mmol) with a catalytic amount of hydroquinone (3 mg, 0.03 mmol) was taken in 100 ml round bottomed flask and the reaction mixture was refluxed for 3 h. After completion of reaction, thionyl chloride was evaporated out and the residual product was recrystallized from diethyl ether to obtain pure solid product. (Yield= 75 %)

^{1}H NMR (200 MHz, DMSO) of p-CPMIC: δ 8.07 and 7.48 (4 H in phenyl), δ 7.21 (2 H,

CO-C**H**=C**H**-CO).

6.2.6 Synthesis of bismaleimide of poly(ethylene glycol) (PEG-bismaleimide)

PEG-2000 (2g, 1 mmol) was dissolved in 50 ml to toluene in a round bottomed flask and 30 ml of toluene was distilled off under vacuum in order to remove any traces of water in PEG. To the solution was the added triethyl amine and p-CPMIC (3 eq) drop wise and the reaction was allowed to take place at room temperature for 24 h under inert atmosphere. The solution was then precipitated in diethylether twice. The precipitate was filtered under vacuum and dried to obtain pure product in the solid form. (Yield= 90 %)

The same procedure was used to synthesize PEG-bismaleimide of 6,000 and 8,000 molecular weights.

^{1}H NMR (200 MHz, D_2O) of PEG-bismaleimide (2,000): δ 8.15 (4 H in phenyl), δ 7.49 (4 H in phenyl), δ 7.01 (4 H CO-C**H**=C**H**-CO) and δ 3.65 (209.75 H, OC**H**$_2$C**H**$_2$O).

^{1}H NMR (200 MHz, D_2O) of PEG-bismaleimide (6,000): δ 8.15 (4 H in phenyl), δ 7.49 (4 H in phenyl), δ 7.01 (4 H CO-C**H**=C**H**-CO) and δ 3.65 (609.81 H, OC**H**$_2$C**H**$_2$O).

^{1}H NMR (200 MHz, D_2O) of PEG-bismaleimide (8,000): δ 8.15 (4 H in phenyl), δ 7.49 (4 H in phenyl), δ 7.01 (4 H CO-C**H**=C**H**-CO) and δ 3.65 (870.63 H, OC**H**$_2$C**H**$_2$O).

6.2.7 Gelation between PAA-furan and PEG-bismaleimide using Furan-Maleimide Click Chemistry

30 mg of PAA was dissolved in 300 μl of distilled water. In a separate vial, PEG bismaleimide (MW 2000 g/mol, 6000 g/mol and 8000 g/mol) were taken in the same mol % with respect of furan groups on PAA and dissolved in 300 μl of distilled water. After complete dissolution, the two solutions were mixed together, votexed for 5 min and kept at room temperature for 4 h for gelation to take place completely. The gels formed were then used for various studies mentioned in the later sections. The gelation was confirmed by vial inversion method.

6.2.8 Synthesis of Mesoporous Silica Nanoparticles

One gram of Cetyltrimethylammonium bromide (CTAB) was dissolved in 480 mL of deionized water using an overhead stirrer at room temperature followed by the addition of 2 M NaOH solution (3.5 mL). The solution was allowed to stir for 30 min at 80 °C. 5 mL of tetraethyl orthosilicate (TEOS) was added drop wise to the above mixture. The mixture was stirred at 6000 rpm for another 2 h at 80 °C. The resultant white precipitate was collected by vacuum filtration and washed with copious amount of water. The precipitate was dried in vacuum oven overnight to obtain mesoporous silica in powder form.

6.2.9 Outer Surface Functionalization of MSNs with amino groups

For the outer surface functionalization of MSNs, 1 g of MSNs (containing CTAB) were dispersed in 100 mL anhydrous toluene followed by addition of 200 µL of 3-aminopropyltriethoxysilane (APTES) in presence of catalytic amount of triethylamine (Et_3N). The reaction mixture was refluxed for 18 h under argon atmosphere. The product was obtained using vacuum filtration, washed with toluene (to remove any unreacted APTES) and finally with ethanol. The template (CTAB) was removed by refluxing the material with acidic methanol solution for 6 h. The amine grafted and template removed MSNs were finally washed with methanol and vacuum dried. The obtained material was denoted as MSN-NH_2.

6.2.10 Gelation between PAA-furan and PEG-bismaleimide incubated with MSNs

30 mg of PAA was dissolved in 300 µl of distilled water and added to it amine grafted MSNs in different ratios. The solution was sonicated for 30 min for complete dispersion of the MSNs in the polymer solution. In a separate vial PEG-bismaleimide (MW 8000) was taken in the same mol % with respect of furan and dissolved in 300 µl of distilled water. After complete dissolution, the two solutions were mixed together, votexed for 5 min and kept at room temperature for 4 h for gelation to take place completely. The gels formed were then used for various studies mentioned in the later sections.

6.3 Characterizations

6.3.1 Scanning electron microscopy (SEM)

Scanning electron Microscopy (SEM) was used to investigate the morphology of the hydrogels using Quanta 200 3D dual beam having electron source of tungsten (W) filament with emission at resolution of 20 kV in high vacuum. The hydrogels were lyophilized and sputter coated with a thin layer of gold. EDAX measurements were carried out to confirm the presence of porosity in the hydrogels. EDAX measurements performed on the MSNs loaded hydrogels further confirmed the presence of MSNs in the hydrogels by the presence of a characteristic peak of silicon.

6.3.2. Tomography

Three-dimensional non-destructive imaging of as-prepared hydrogels loaded with MSNs was performed using high-resolution X-ray μ-CT (Versa XRM-500, Xradia Inc., USA) and compared with hydrogel without MSNs. The hydrogels were placed on a sample stage and scanned using X-rays of 40 kV energy and 0.7 μm voxel size.

6.3.3 In-situ Gelation

The in-situ gelation of PAA with two crosslinking agents in aqueous medium was studied using Anton Paar MCR-301 controlled stress rheometer with cone and plate geometry (CC17). PAA aqueous solutions with 10 mol% of furan grafting and PEG-bismaleimides with different molecular weights as crosslinking agents were taken in a plate and the gelation was monitored. The parameters, storage modulus (G') and loss modulus (G") were measured as a function of time at different temperatures. The percentage strain was 0.15 % and the frequency was 10 Hz throughout the experiment. The time at which the crossover between G' and G" occurs is taken as the time of gelation.

6.3.4 Mechanical Properties

The stress-strain measurements in the unidirection were carried out using Instron 5943 mechanical tester at room temperature. The compressive tests were performed on as-prepared hydrogels in distilled water. The cylindrical test specimens were having

dimension of 15 mm diameter x 15 mm height. The compression speed was 2 mm/min with a pre tension load of 1 kN. For each test, 3-representative samples were taken and the average value of the result is taken.

6.4 Results and discussion

6.4.1 Synthesis of furan grafted poly(acrylic acid) (PAA-furan)

The grafting of furfuryl amine onto poly(acrylic acid) backbone was carried out using DCC coupling reaction between amine groups of furfurylamine and carboxylic groups on PAA using NMP as a solvent at 60 ºC. The reaction scheme is given in **Scheme 6.1**. Different mole% of furfurylamine (5, 10 and 15 mol%) was grafted onto PAA. However, we observed that when the grafting exceeds 10 mol%, the product becomes

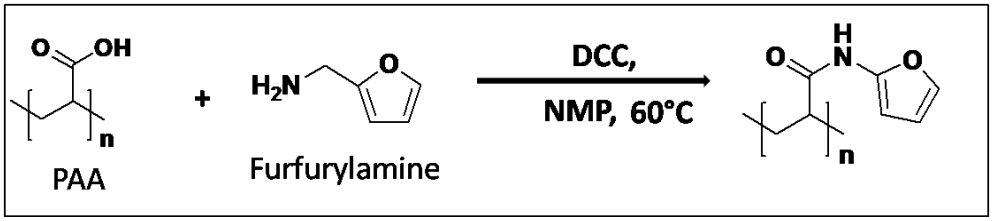

Scheme 6.1: Reaction scheme for synthesis of PAA-furan

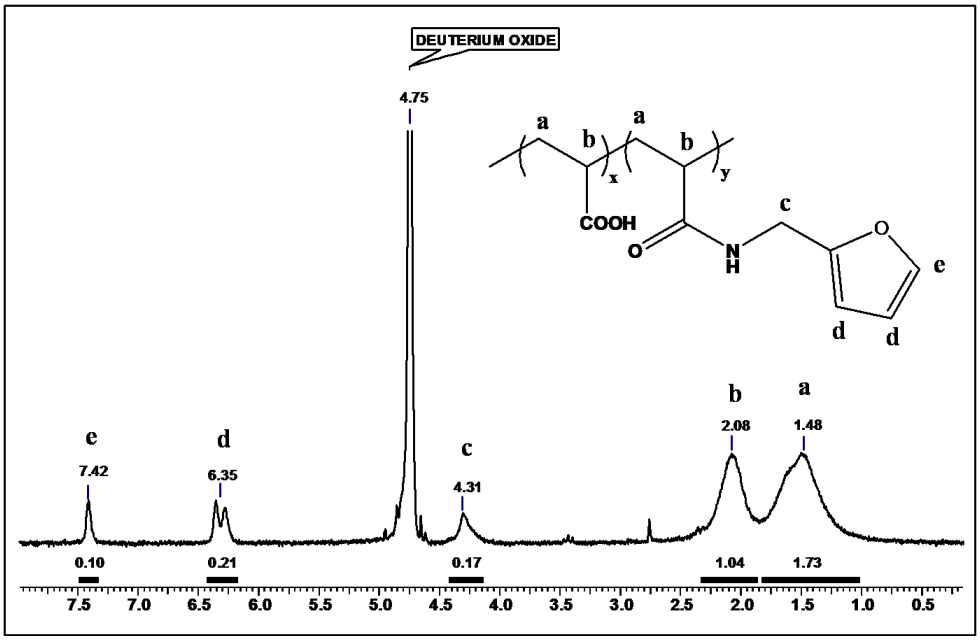

Figure 6.1. ^{1}H NMR spectrum of PAA-*g*-furan (10 mol%) copolymer in D_2O

insoluble in water (due to increase in hydrophobicity of the PAA). Thus, in all the experiments, 10 mol% grafting was kept constant. The successful formation of PAA-10 mol% furan was confirmed by comparing the ratios of area under the peaks at δ 2.08 (one proton of PAA) and the peaks at δ 7.42 and δ 6.35 (one and two protons respectively of furan groups) as shown in **Figure 6.1**.

6.4.2 Synthesis of bismaleimides incorporated poly(ethylene glycol) (PEG-bismaleimide)

The synthesis of PEG-bismaleimide with three different molecular weights of PEG (2000 g/mol, 6000 g/mol and 8000 g/mol) was carried out in four steps as depicted in **Scheme 6.2**. All the products in four steps and the end product, PEG-bismaleimides were characterized by the ^{1}H NMR spectroscopy as shown in **Figure 6.2,6.3,6.4 and 6.5**. The formation of PEG-bismaleimides was confirmed by comparing the ratios of area under the peaks at δ 3.65 (due to methylene protons of PEG) and the peaks at δ 3.65 (due to phenyl groups). The integration values were well corroborated with the formation of bismaleimide at the telechelic position of PEGs as shown in **Figure 6.5**.

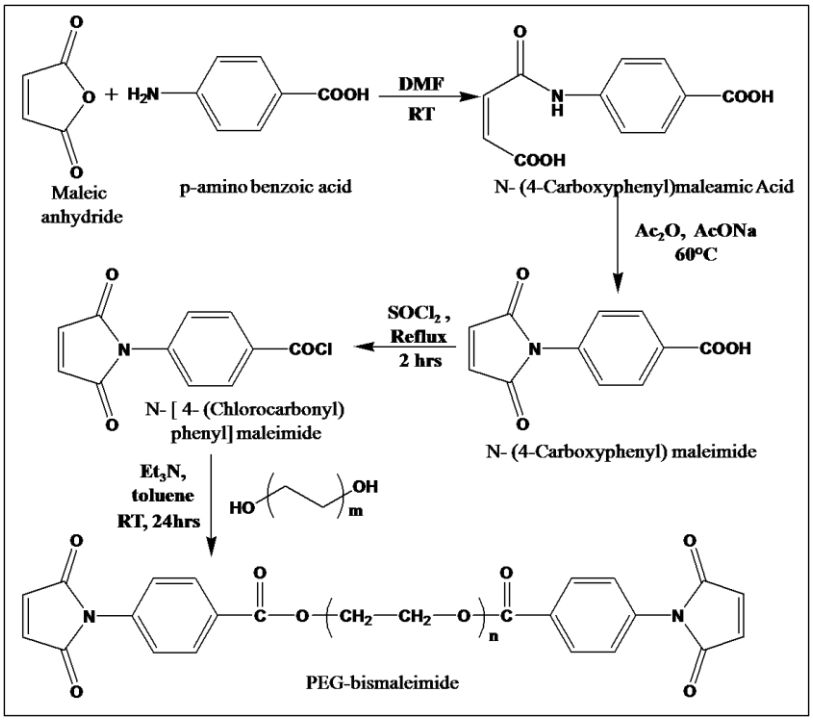

Scheme 6.2: Reaction scheme for synthesis of PEG-bismaleimide

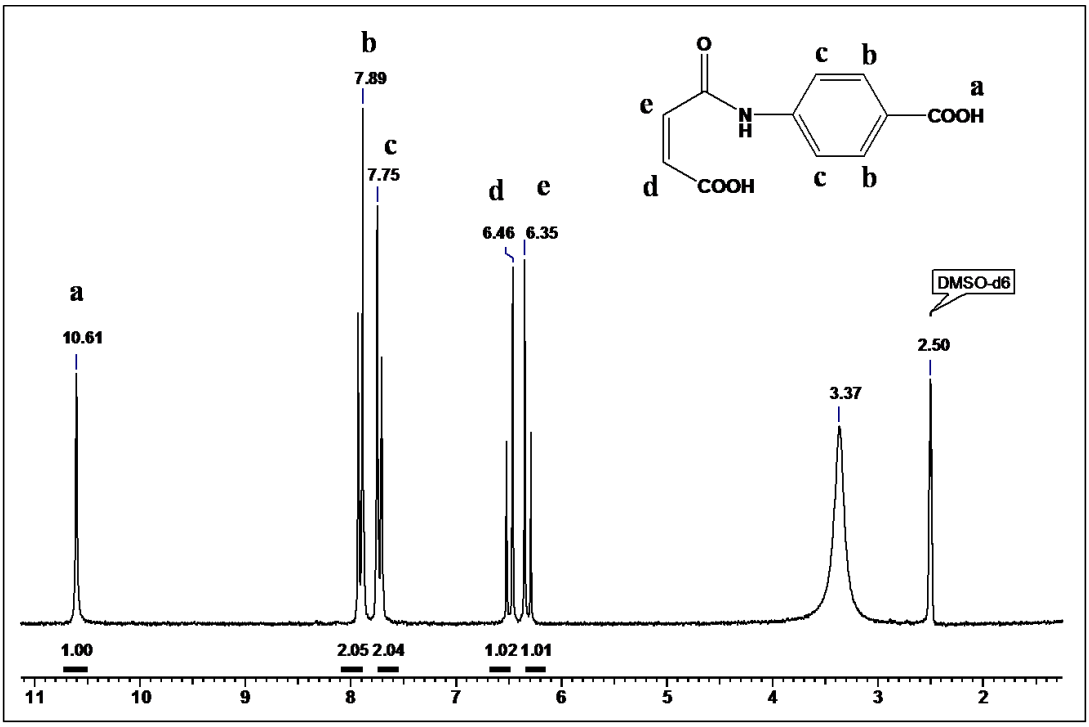

Figure 6.2. ^{1}H NMR spectrum of N-(4-carboxyphenyl) maleamic acid in DMSO-d_6

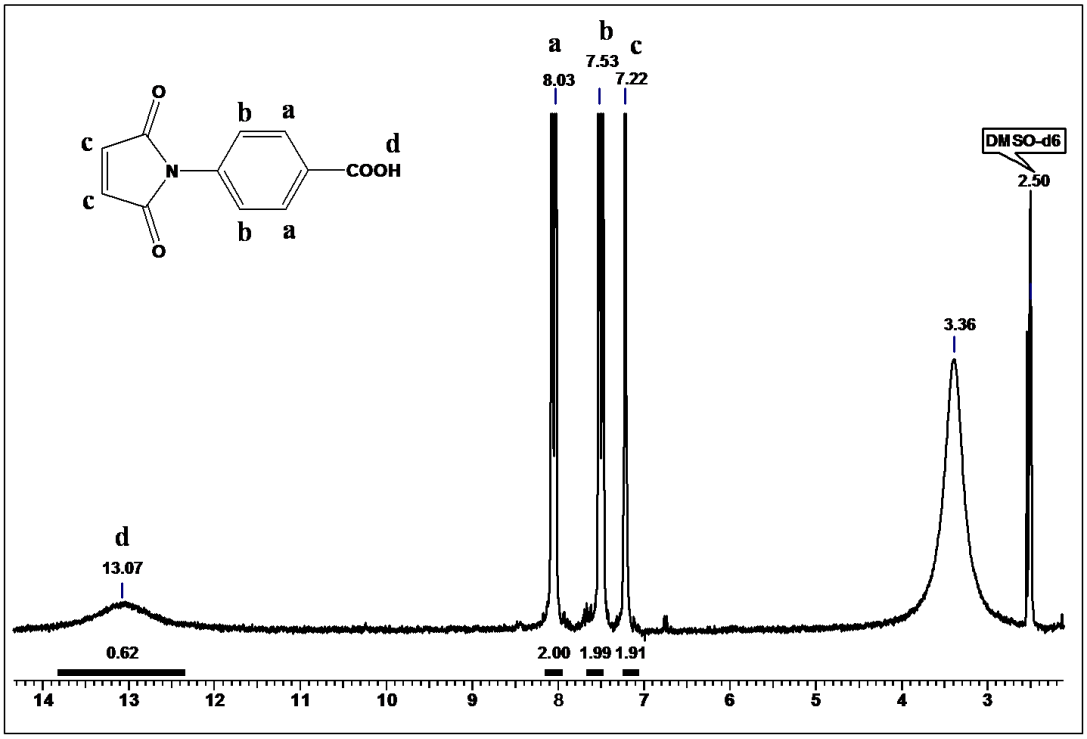

Figure 6.3. ^{1}H NMR spectrum of N-(4-carboxyphenyl) maleimide in DMSO-d_6

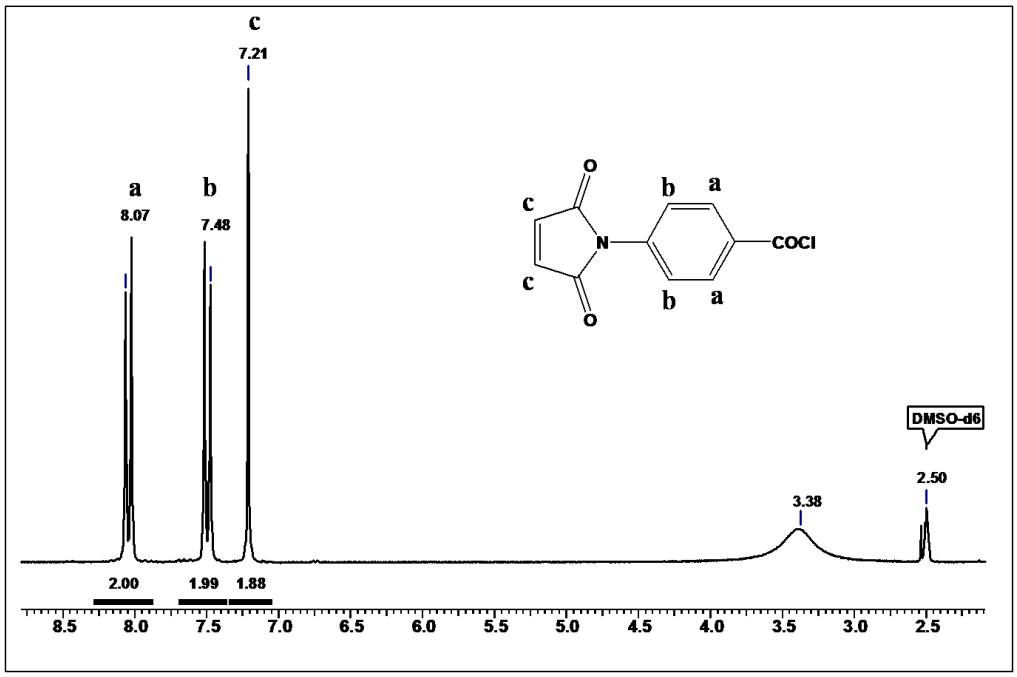

Figure 6.4. ^{1}H NMR spectrum of N-[4-(Chlorocarbonyl) phenyl] maleimide in DMSO-d_6

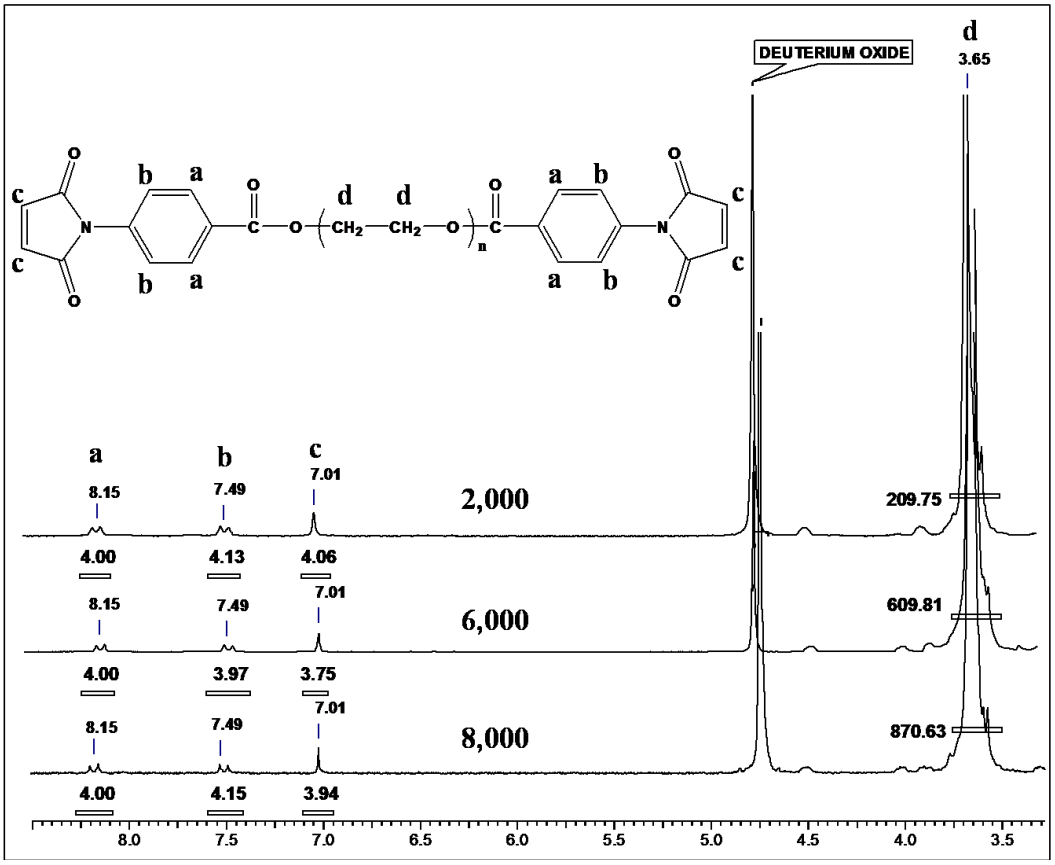

Figure 6.5. ^{1}H NMR spectrum of PEG-bismaleimide (2000, 6000 and 8000) in D_2O

6.4.3 Gelation between PAA-furan and PEG-bismaleimide using Furan-Maleimide Click Chemistry

PAA hydrogels were synthesized using furan-maleimide click chemistry using PEG with different molecular weights (2000 g/mol, 6000 g/mol and 8000 g/mol) as cross linking agents. The schematics of the click reaction between PAA-furan and PEG-bismaleimides are given in **Scheme 6.3**. The furan maleimide click reaction takes place in the absence of any catalyst in aqueous medium at room temperature within few hours. In the present work, we studied the effect of molecular weight of PEG on the gelation time and mechanical properties of the hydrogels formed which will be discussed in details in the following sections. **Figure 6.6** shows the samples of as-prepared and fully swollen PAA hydrogels prepared using PEG-bismaleimide-8000 as a cross linker.

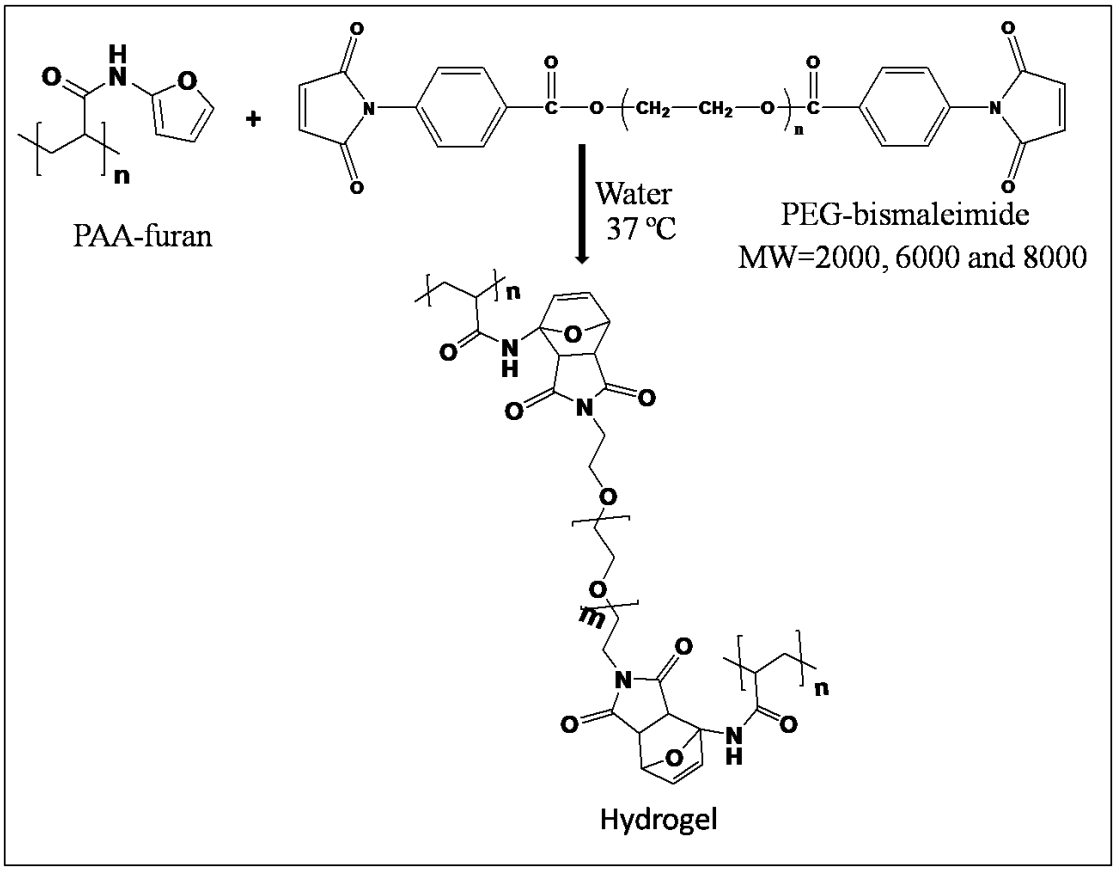

Scheme 6.3: Furan-Maleimide click reaction between PAA-furan and PEG-bismaleimide (MW= 2000, 6000 and 8000)

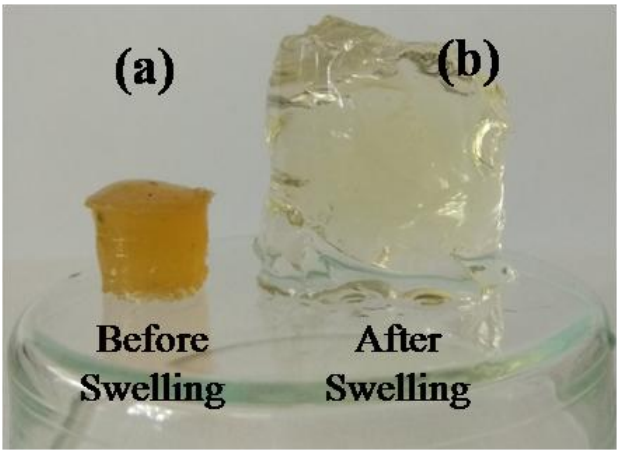

Figure 6.6. Cross linked PAA hydrogel (a) as-prepared and (b) fully swollen in distilled water

6.4.4 In-situ gelation studies

The gelation studies were performed at different temperatures to study the effect of temperature on the gelation time. In the in-situ gelation study, PAA-furan and PEG-bismaleimide (MW= 2000, 6000 and 8000), were homogeneously mixed and charged in the parallel plate geometry of the rheometer. Immediately after charging, the G' and G" were measured as a function of time. The crossover point of G' and G" was taken as the gelation time (**Figure 6.7**). We show in **Figure 6.8**, the time of gelation (averaged with

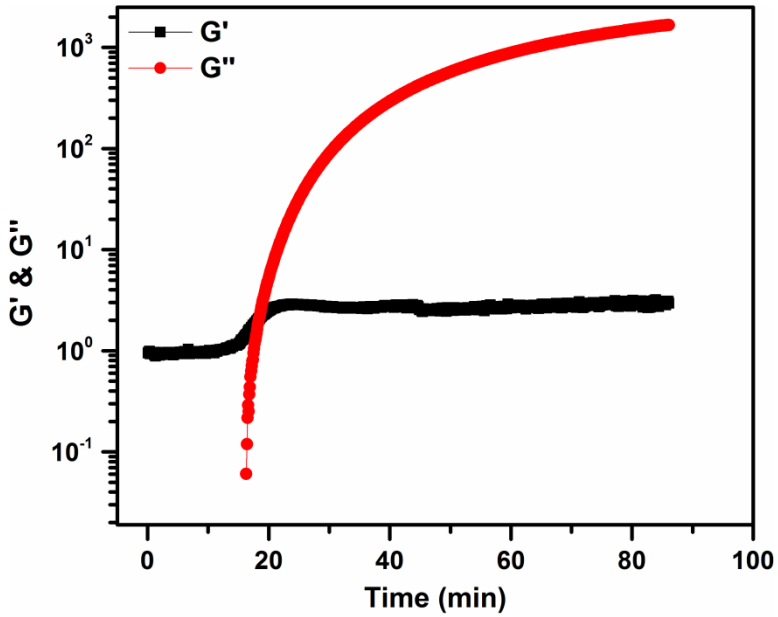

Figure 6.7. Gelation time for PAA hydrogels as indicated by the crossover point of G' and G"

repetition of 3 samples) for hydrogels with different PEG-bismaleimide and at five different temperatures. It can be readily seen from the results that in all the samples, the gelation time decreases with increase in temperature. It is intriguing to note that the gelation time decreases with increase in the molecular weight of the PEG-bismaleimide cross linker. This could be attributed to the fact that with increase in the molecular weight of PEG-bismaleimide, the hydrogen bonding between the oxygen atoms of the PEG and the free carboxyl groups of the PAA increases significantly. Longer the chain of PEG (i.e. higher MW), higher is the H-bonding interaction between the two complimentary clicking moieties which dramatically accelerates the Diels Alder reaction resulting into shorter gelation time. This observation is in-line with the previous report where it is demonstrated that the presence of H-bonding interaction between the complimentary clicking moieties rapidly increases the Diels-Alder cycloaddtion between a furan and a bismaleimide. [37]

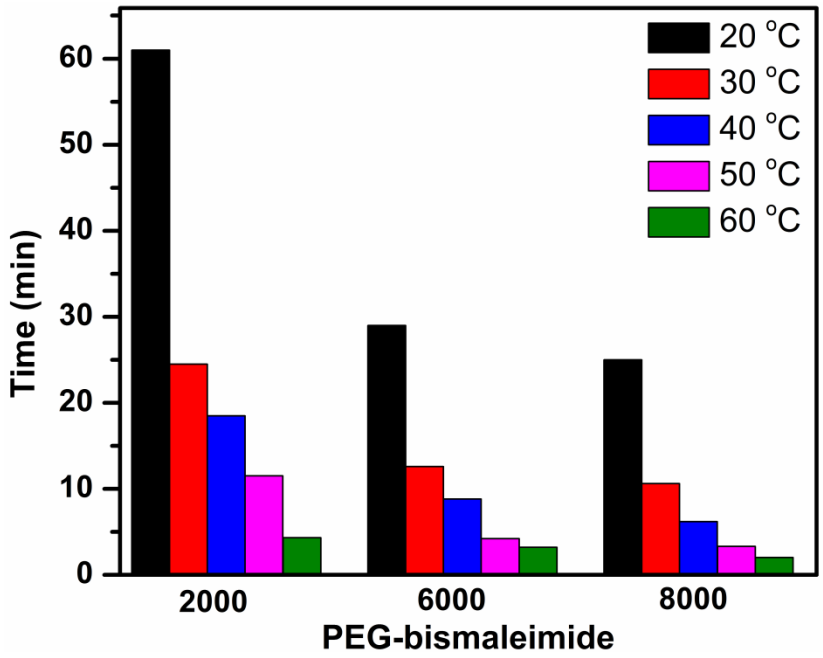

Figure 6.8. Gelation time for PAA hydrogels on crosslinking with different molecular weights of PEG-bismaleimide (MW= 2000, 6000 and 8000) at different temperatures

In order to observe any change in the morphology of hydrogels upon click reaction, we performed Scanning Electron Microscopy on the lyophilized fully swollen PAA hydrogels (**Figure 6.9**).

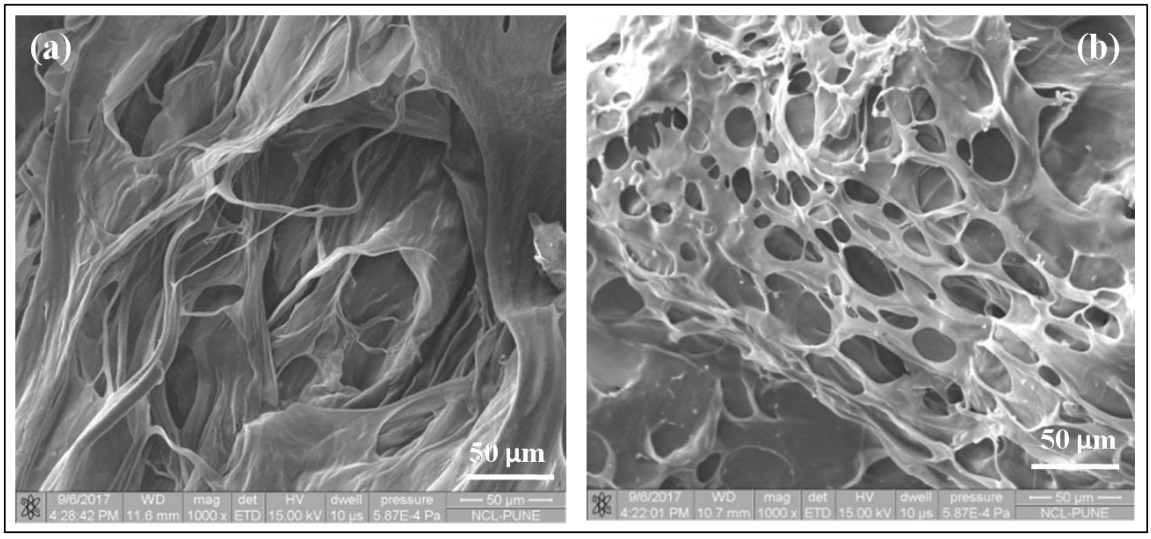

Figure 6.9. SEM images of lyophilized PAA hydrogels crosslinked with (a) PEG-bismaleimide (MW= 6000) (b) PEG-bismaleimide (MW= 8000)

The SEM images clearly indicate the porous structure in the crosslinked PAA hydrogels upon lyophilization of the swollen gels. Also, the porosity clearly decreases as the molecular weight of PEG cross linker increases. This could be again due to the efficient crosslinking of PEG-bismaleimide-8000 which has more number of oxygen atoms giving rise to greater H-bonding interactions in the click reaction and more compactness in the hydrogels.

6.4.5 Mechanical Properties

6.4.5.1 *PAA hydrogels cross linked with PEG-bismaleimides*

The mechanical strength of the crosslinked PAA hydrogels in the as prepared state with different molecular weights of PEG-bismaleimide (MW= 2000, 6000 and 8000) were determined using Instron 5943 in the compression mode. Typical stress-strain curves (in compression) are shown in **Figure 6.10** from which the percentage compressibility and compressive strengths were determined. The results are shown in **Table 6.1**. It can be readily seen from the results that although the percentage compressibility remains in the range of 65-70% for all the samples, the compressive strength of the PAA hydrogels progressively increase with increase in the molecular weights of the PEG cross linkers. This indicates the efficient crosslinking of PEG-bismaleimides of higher MWs as

mentioned in the previous sections.

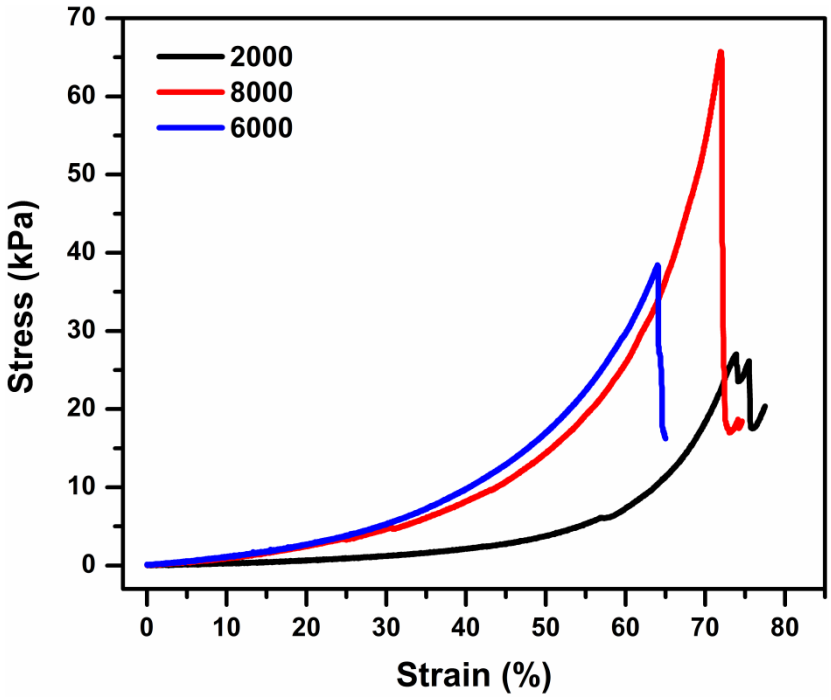

Figure 6.10. Compressive strength studies of PAA hydrogels with different molecular weights of PEG-bismaleimides (MW= 2000, 6000 and 8000)

Table 6.1: Mechanical Strengths of PAA hydrogels cross linked with different molecular weights of PEG-bismaleimide

Sample	% Compressibility	Compressive Strength (kPa)
PAA-PEG-2000	73.774	27.227
PAA-PEG-6000	63.964	38.739
PAA-PEG-8000	71.972	65.966

Thus, increase in the mechanical strength of the hydrogels with increase in the molecular weight of PEG can be attributed to the efficient crosslinking of PEG-bismaleimides of high MWs facilitated by the H-bonding interactions. In order to further enhance the mechanical strength of the hydrogels, we thought of incorporating functionalized mesoporous silica nanoparticles (MSNs) in to the hydrogels during the click reaction. Accordingly, we first prepared amine-functionalized MSNs and homogeneously mixed with PAA-furan before the click reaction.

6.4.6 Synthesis and functionalization of Mesoporous Silica Nanoparticles (MSNs)

The synthesis of MSNs was carried out by sol-gel method using cetyltrialkyl ammonium bromide (CTAB) as a structure-directing agent and tetraethyl orthosilicate (TEOS) as a silica precursor in presence of base as a catalyst. Functionalization of the

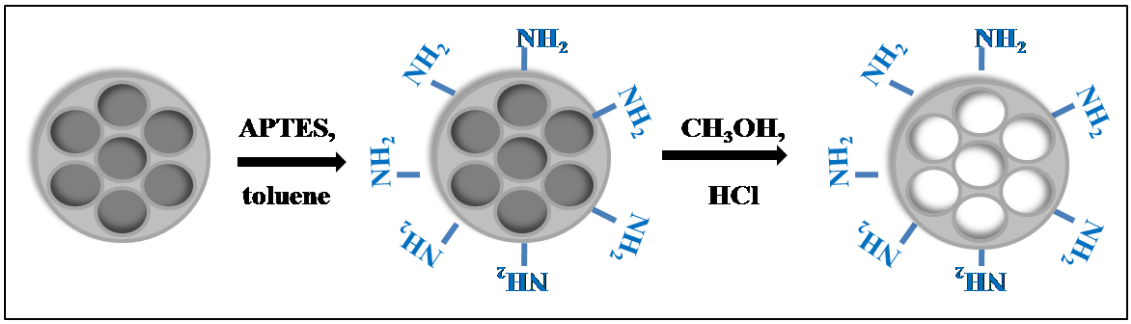

Scheme 6.4. Synthesis of amine grafted MSNs

outer surface of MSNs with amine moieties was performed using aminopropyl triethoxysilane (APTES) in presence of catalytic amount of triethylamine (**Scheme 6.4**). SEM images of amine grafted MSNs show uniform discrete spherical nanoparticles with particle sizes in the diameter range of MSN-NH_2 (120±10 nm) as shown in **Figure 6.11**.

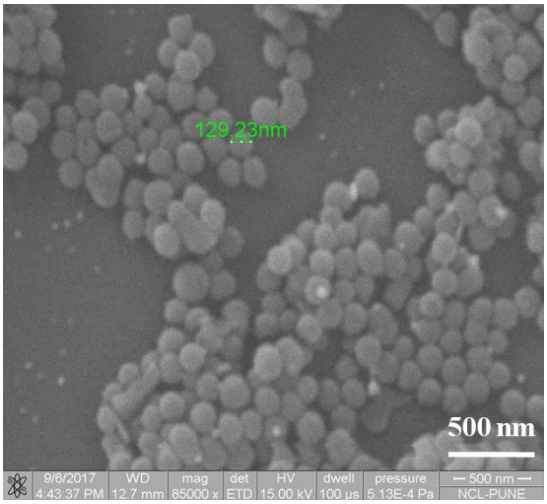

Figure 6.11. SEM image of as amine grafted MSNs

6.4.7 Gelation between PAA-furan and PEG-bismaleimide incubated with MSNs

PAA hydrogels incubated with amine grafted MSNs were synthesized using furan-maleimide click chemistry using PEG-bismaleimide (MW= 8000) as cross linking

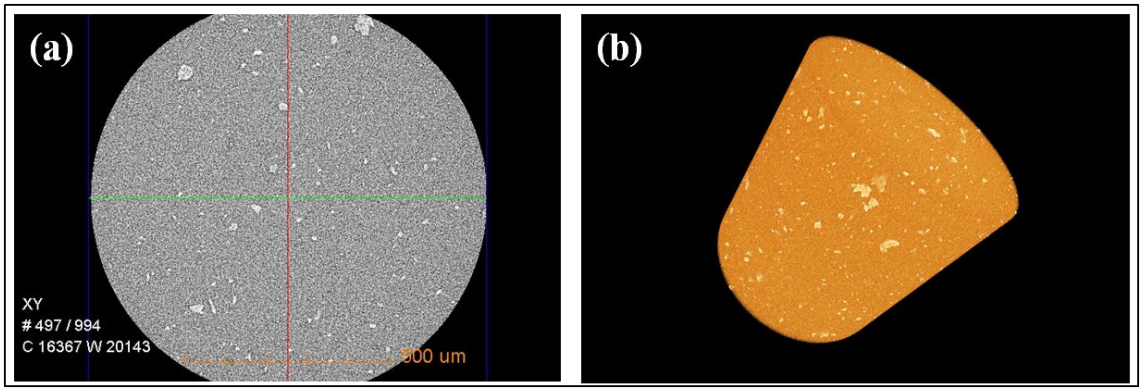

Figure 6.12. (a) 2-dimensional and (b) 3-dimensional μ-CT images of MSNs incubated PAA hydrogels crosslinked with PEG-bismaleimide (MW= 8000)

agent. The idea of amine functionalization of MSNs was mainly to felicitate the reaction between the $–NH_2$ groups of MSNs and the free –COOH groups of PAA which will form ionic bonding between the MSNs and the hydrogel and prevent the leaching of MSNs from the hydrogel. The incorporation of MSNs (5 mg) in PAA hydrogels cross linked with PEG-bismaleimide (MW= 8000) was confirmed by X-ray μ-CT, SEM and EDAX techniques as shown in **Figure 6.12 and 6.13**.

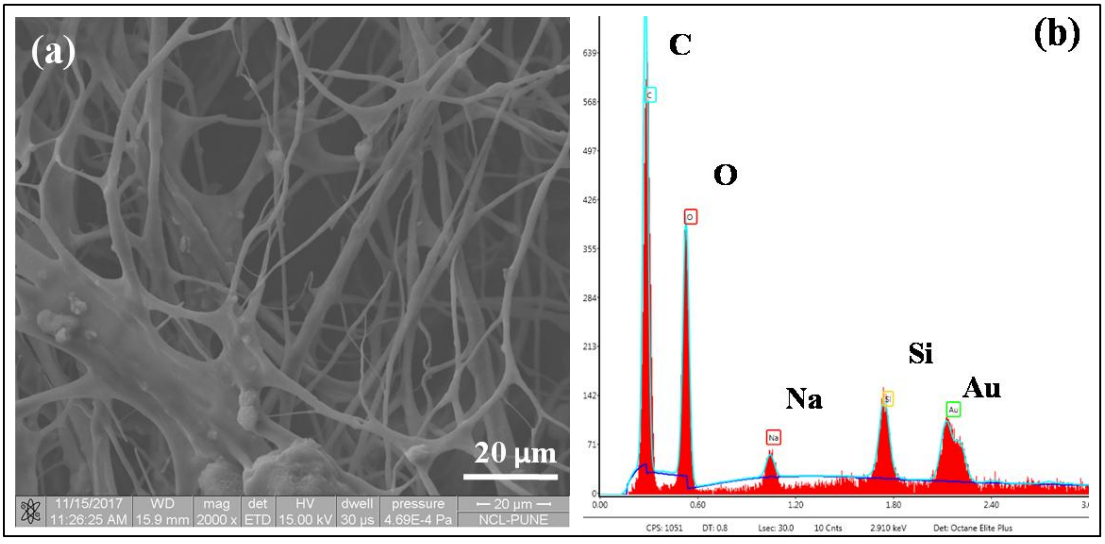

Figure 6.13. (a) SEM and (b) EDAX of MSNs loaded PAA hydrogel crosslinked with PEG-bismaleimide (MW= 8000)

6.4.8 Mechanical strengths PAA hydrogels incorporated with MSNs

The mechanical strengths of PAA hydrogels with increasing amounts of MSNs were determined using Instron 5943 in the compression mode and were compared with the

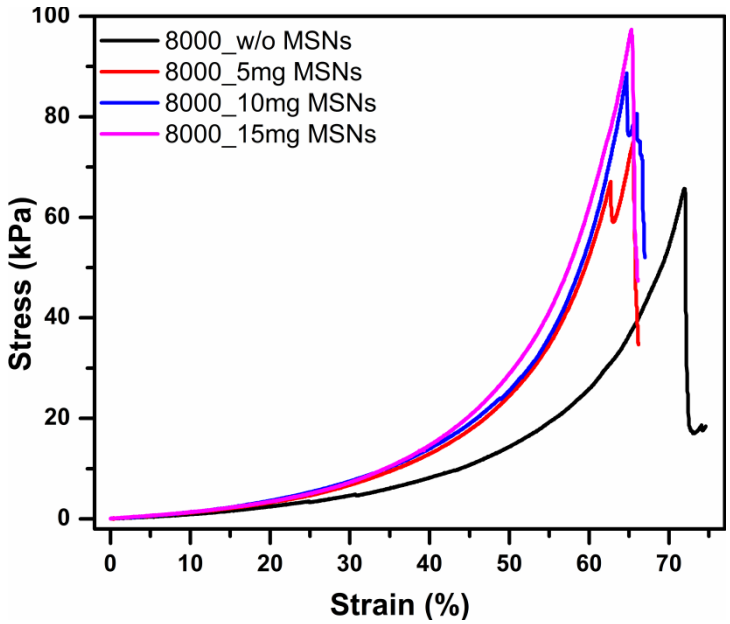

Figure 6.14. Compressive strength studies of PAA hydrogels with different amounts of MSNs cross linked with PEG-bismaleimide (MW= 8000)

Table 6.2: Mechanical Strengths of PAA hydrogels cross linked with PEG-bismaleimide (MW= 8000) by varying amounts of MSNs

Sample	% Compressibility	Compressive Strength (kPa)
PAA-PEG_w/o MSNs	72	66
PAA-PEG-5mg MSNs	65	74
PAA-PEG-10mg MSNs	65	90
PAA-PEG-15mg MSNs	65	97

hydrogel without MSNs. The results of the stress-strain curves and the compressibility and compression strengths are given in **Figure 6.14** and **Table 6.2** respectively. The results clearly indicate that, incorporation of MSNs in the PAA hydrogels significantly increase the compression strength of the hydrogels. However, the percentage compression decreased compared to the sample without MSNs which is expected due to

the formation of rigid structure in the hydrogel. Further, with the improved mechanical strength, the porous structure created in the hydrogel by MSNs will be an added advantage to incorporate drugs in the pores for controlled release applications.

6.5 Conclusions

We synthesized PAA hydrogels using PEG-bismaleimide as cross linking agents by Furan-Maleimide "Click-Chemistry" approach. PEGs with different MWs were modified with maleimide groups at telechelic positions and furan groups were introduced onto PAA to facilitate the Diels-Alder cycloaddtion between a furan and a bismaleimide. The in-situ gelation times due to click reaction were determined using rheometer with parallel plate geometry. The studies reveal that the gelation time is inversely proportional to the temperature and decreases with increase in the molecular weight of PEG-bismaleimide cross linker. This was attributed due to the presence of H-bonding interaction between the complimentary clicking moieties which rapidly increases the Diels-Alder cycloaddtion between a furan and a bismaleimide. The mechanical strength of the hydrogels showed an increasing trend with increase in the MW of PEG-bismaleimide. The high MW of PEG-bismaleimide provided greater intermolecular H-bonding and efficient crosslinking in the click reaction. This was manifested in the increasing trend of the compressive strengths. Further, amine functionalized MSNs were incorporated in to PAA hydrogels with the aim of generating pore structure and improved compressive strengths. This could be achieved successfully. The presence of pores gives an advantage of incubating drug molecules within and show great promise as injectables in controlled drug delivery.

References

[1] C. García-Astrain, A. Gandini, C. Peña, I. Algar, A. Eceiza, M. Corcuera, N. Gabilondo, Diels–Alder "click" chemistry for the cross-linking of furfuryl-gelatin-polyetheramine hydrogels, RSC Advances, 4 (2014) 35578-35587.

[2] M.A. Tasdelen, Diels–Alder "click" reactions: recent applications in polymer and material science, Polymer Chemistry, 2 (2011) 2133-2145.

[3] H.C. Kolb, K.B. Sharpless, The growing impact of click chemistry on drug discovery, Drug discovery today, 8 (2003) 1128-1137.

[4] V. Crescenzi, L. Cornelio, C. Di Meo, S. Nardecchia, R. Lamanna, Novel hydrogels via click chemistry: synthesis and potential biomedical applications, Biomacromolecules, 8 (2007) 1844-1850.

[5] C.D. Hein, X.-M. Liu, D. Wang, Click chemistry, a powerful tool for pharmaceutical sciences, Pharmaceutical research, 25 (2008) 2216-2230.

[6] H.C. Kolb, M. Finn, K.B. Sharpless, Click chemistry: diverse chemical function from a few good reactions, Angewandte Chemie International Edition, 40 (2001) 2004-2021.

[7] V.V. Rostovtsev, L.G. Green, V.V. Fokin, K.B. Sharpless, A stepwise huisgen cycloaddition process: copper (I)-catalyzed regioselective "ligation" of azides and terminal alkynes, Angewandte Chemie, 114 (2002) 2708-2711.

[8] C.W. Tornøe, C. Christensen, M. Meldal, Peptidotriazoles on solid phase:[1, 2, 3]-triazoles by regiospecific copper (I)-catalyzed 1, 3-dipolar cycloadditions of terminal alkynes to azides, The Journal of organic chemistry, 67 (2002) 3057-3064.

[9] C. Barner-Kowollik, F.E. Du Prez, P. Espeel, C.J. Hawker, T. Junkers, H. Schlaad, W. Van Camp, "Clicking" polymers or just efficient linking: what is the difference?, Angewandte Chemie International Edition, 50 (2011) 60-62.

[10] I. Kosif, E.-J. Park, R. Sanyal, A. Sanyal, Fabrication of maleimide containing thiol reactive hydrogels via Diels− Alder/retro-Diels− Alder strategy, Macromolecules, 43 (2010) 4140-4148.

[11] E. Goiti, M.B. Huglin, J.M. Rego, Some properties of networks produced by the Diels–Alder reaction between poly (styrene-co-furfuryl methacrylate) and bismaleimide, European Polymer Journal, 40 (2004) 219-226.

[12] S. Yigit, R. Sanyal, A. Sanyal, Fabrication and functionalization of hydrogels through "click" chemistry, Chemistry–An Asian Journal, 6 (2011) 2648-2659.

[13] A. Gandini, The furan/maleimide Diels–Alder reaction: a versatile click–unclick tool in macromolecular synthesis, Progress in Polymer Science, 38 (2013) 1-29.

[14] G. Graziano, Rate enhancement of Diels–Alder reactions in aqueous solutions, Journal of physical organic chemistry, 17 (2004) 100-101.

[15] X.-L. Sun, L. Yang, E.L. Chaikof, Chemoselective immobilization of biomolecules through aqueous Diels–Alder and PEG chemistry, Tetrahedron letters, 49 (2008) 2510-2513.

[16] H.L. Wei, J. Yang, H.J. Chu, Z. Yang, C.C. Ma, K. Yao, Diels–Alder reaction in water for the straightforward preparation of thermoresponsive hydrogels, Journal of Applied Polymer Science, 120 (2011) 974-980.

[17] H.-L. Wei, Z. Yang, Y. Chen, H.-J. Chu, J. Zhu, Z.-C. Li, Characterisation of N-vinyl-2-pyrrolidone-based hydrogels prepared by a Diels–Alder click reaction in water, European Polymer Journal, 46 (2010) 1032-1039.

[18] H.-L. Wei, Z. Yang, L.-M. Zheng, Y.-M. Shen, Thermosensitive hydrogels synthesized by fast Diels–Alder reaction in water, Polymer, 50 (2009) 2836-2840.

[19] H.-L. Wei, Z. Yang, H.-J. Chu, J. Zhu, Z.-C. Li, J.-S. Cui, Facile preparation of poly (N-isopropylacrylamide)-based hydrogels via aqueous Diels–Alder click reaction, Polymer, 51 (2010) 1694-1702.

[20] H. Tan, J.P. Rubin, K.G. Marra, Direct Synthesis of Biodegradable Polysaccharide Derivative Hydrogels Through Aqueous Diels-Alder Chemistry, Macromolecular rapid communications, 32 (2011) 905-911.

[21] K.C. Koehler, K.S. Anseth, C.N. Bowman, Diels–Alder mediated controlled release from a poly (ethylene glycol) based hydrogel, Biomacromolecules, 14 (2013) 538-547.

[22] A. Dag, H. Durmaz, G. Hizal, U. Tunca, Preparation of 3-arm star polymers (A3) via Diels–Alder click reaction, Journal of Polymer Science Part A: Polymer Chemistry, 46 (2008) 302-313.

[23] Y. Chujo, K. Sada, T. Saegusa, Reversible gelation of polyoxazoline by means of Diels-Alder reaction, Macromolecules, 23 (1990) 2636-2641.

[24] Y.-L. Liu, C.-Y. Hsieh, Y.-W. Chen, Thermally reversible cross-linked polyamides and thermo-responsive gels by means of Diels–Alder reaction, Polymer, 47 (2006) 2581-2586.

[25] N. Teramoto, Y. Arai, M. Shibata, Thermo-reversible Diels–Alder polymerization of difurfurylidene trehalose and bismaleimides, Carbohydrate polymers, 64 (2006) 78-84.

[26] Y. Kojima, A. Usuki, M. Kawasumi, A. Okada, Y. Fukushima, T. Kurauchi, O. Kamigaito, Mechanical properties of nylon 6-clay hybrid, Journal of Materials Research, 8 (1993) 1185-1189.

[27] K. Yano, A. Usuki, A. Okada, T. Kurauchi, O. Kamigaito, Synthesis and properties of polyimide–clay hybrid, Journal of Polymer Science Part A: Polymer Chemistry, 31 (1993) 2493-2498.

[28] F. Zhao, D. Yao, R. Guo, L. Deng, A. Dong, J. Zhang, Composites of polymer hydrogels and nanoparticulate systems for biomedical and pharmaceutical applications, Nanomaterials, 5 (2015) 2054-2130.

[29] Y.M. Mohan, K. Lee, T. Premkumar, K.E. Geckeler, Hydrogel networks as nanoreactors: A novel approach to silver nanoparticles for antibacterial applications, Polymer, 48 (2007) 158-164.

[30] E.I. Suvorova, V.V. Klechkovskaya, V.V. Kopeikin, P.A. Buffat, Stability of Ag nanoparticles dispersed in amphiphilic organic matrix, Journal of Crystal Growth, 275 (2005) 2351-2356.

[31] M. Zhu, Y. Zhu, L. Zhang, J. Shi, Preparation of chitosan/mesoporous silica nanoparticle composite hydrogels for sustained co-delivery of biomacromolecules and small chemical drugs, Science and technology of advanced materials, 14 (2013) 045005.

[32] Y. Zhu, J. Shi, W. Shen, H. Chen, X. Dong, M. Ruan, Preparation of novel hollow mesoporous silica spheres and their sustained-release property, Nanotechnology, 16 (2005) 2633.

[33] A. Ahmed, J. Hearn, W. Abdelmagid, H. Zhang, Dual-tuned drug release by nanofibrous scaffolds of chitosan and mesoporous silica microspheres, Journal of Materials Chemistry, 22 (2012) 25027-25035.

[34] B. Song, C. Wu, J. Chang, Dual drug release from electrospun poly (lactic-co-glycolic acid)/mesoporous silica nanoparticles composite mats with distinct release profiles, Acta biomaterialia, 8 (2012) 1901-1907.

[35] Y. Liu, H. Meng, S. Konst, R. Sarmiento, R. Rajachar, B.P. Lee, Injectable dopamine-modified poly (ethylene glycol) nanocomposite hydrogel with enhanced adhesive property and bioactivity, ACS applied materials & interfaces, 6 (2014) 16982-16992.

[36] R. Guo, X. Du, R. Zhang, L. Deng, A. Dong, J. Zhang, Bioadhesive film formed from a novel organic–inorganic hybrid gel for transdermal drug delivery system, European Journal of Pharmaceutics and Biopharmaceutics, 79 (2011) 574-583.

[37] R.J. Pearson, E. Kassianidis, D. Philp, A completely selective and strongly accelerated Diels–Alder reaction mediated by hydrogen bonding, Tetrahedron letters, 45 (2004) 4777-4780.

Chapter-7

Summary and Conclusions

The objective of the thesis was to design and synthesize new associating polymers (APs) and hydrogels/ nanogels based on synthetic polymer poly(acrylic acid) (PAA) and natural polymer carboxymethyl cellulose (CMC) for drug delivery and tissue engineering applications. Although extensive work is carried out and reported on APs and hydrogels in terms of synthesis, stimuli responsive properties and their wide applications in various areas including biomedical, still there is an enormous scope in designing and developing new APs and hydrogels with improved mechanical properties for controlled drug delivery and tissue engineering applications. Exploring new methodologies and green chemistry approach to synthesize APs and hydrogels has attracted major attention of the researchers. Amongst APs, thermo-associating polymers have become important as injectables in controlled release technology. In this thesis work, we have synthesized new thermo-associating polymers based PAA-*g*-PCL-*b*-PEG copolymers and studied their thermo-thickening behavior in aqueous medium using rheology, light scattering and 2-D NMR techniques. We also prepared Mesoporous Silica Nanoparticles (MSNs) and functionalized with polysaccharide for the controlled release of anticancer drug. Further, a double crosslinked hydrogel based on PAA was synthesized and characterized for controlled drug delivery application using a strategy of selective breaking of one crosslinking molecule in the hydrogel. Finally, a "click-chemistry approach was used in preparing PAA based hydrogels through Diels-Alder cycloaddtion reaction between furan modified PAA and telechelically bismaleimide modified PEG. The details of these studies are discussed in the foregoing sections.

In the first chapter, an elaborate literature survey is reported on APs, thermo-associating polymers, hydrogels and nanogels with respect to their synthesis, properties and applications specifically for drug delivery and tissue engineering. Characterization techniques like rheology, light scattering, 2-D NMR spectroscopy for studying the various properties of associating polymers and hydrogels were briefly explained. The second chapter explains the scope and objectives of the thesis work.

In the third chapter, we report on the synthesis of Mesoporous Silica Nanoparticles (MSNs) and functionalization with amine groups. Further, the amine functionalized

MSNs were reacted with a polysaccharide, namely, carboxy methyl cellulose (CMC) using an EDC coupling reaction. The presence of porosity and grafting of CMC on to the surface of MSNs was confirmed by XRD, N_2 adsorption, TGA, SEM, TEM, ζ Potential and DLS techniques. The pores of MSNs were incubated with hydrophobic drug, curcumin, which has both anticancer and antibacterial activity. It was observed that CMC modified MSNs helped in the enhanced permeation of MSNs inside the tumor cells. The MTT assay of breast cancer cell line, MDA-MB-231 revealed that curcumin loaded and CMC grafted MSNs (MSN-cur-CMC) showed better cell inhibition compared to the curcumin loaded MSN-cur-NH_2 or free curcumin and cells undergo apoptotic pathway. The nanogels containing carboxymethyl cellulose grafted MSNs show great potential in targeted drug delivery applications.

In the fourth chapter, we investigated on the thermo thickening behavior of PAA grafted LCST block copolymer MPEG-*b*-PCL (PAA-*g*-MPEG-*b*-PCL) in aqueous medium using rheology, light scattering and NMR techniques. The controlled synthesis of block copolymer PEG-*b*-PCL with equal molecular weights was carried out by ring opening polymerization (ROP) taking a known molecular weight of MPEG as an initiator. Subsequently, the grafting reaction of MPEG-*b*-PCL onto PAA was carried out between the carboxylic groups of PAA and terminal hydroxyl groups of PCL in MPEG-*b*-PCL. The structural characterization of PAA-*g*-MPEG-*b*-PCL was performed using NMR spectroscopy and gel permeation chromatography. The results from multiple experimental techniques gave insights into the molecular mechanism of the thermo thickening process. The modified polymer shows great potential as injectables in controlled drug release systems and rheology control agents for cosmetics creams/ ointments.

In the fifth chapter, we report on the synthesis of double crosslinked Poly(acrylic acid) hydrogels using two different crosslinking agents namely, Jeffamine (jeff) and Cystamine (cys). Jeffamine provides a good mechanical strength while cystamine with disulphide bonds incorporates redox sensitivity to the hydrogels. The hydrogels were easily prepared in aqueous medium at room temperature and the gelation could be

completed within a few minutes. We demonstrated the selective cleavage of one crosslinking (cystamine) by DTT and its implications on the controlled release of an anticancer drug, Doxorubicin (Dox) and antimicrobial Ag nanoparticles.

In the sixth chapter, we report on the synthesis of PAA based hydrogels using Furan-Maleimide "Click-Chemistry" approach. PEGs with different MWs were modified with maleimide groups at telechelic positions and PAA was modified with furan groups to induce click reaction with the maleimide groups of the PEGs. The gelation process and gelation times were studied using a rheometer. The studies reveal that the gelation time is inversely proportional to the temperature and decrease as the molecular weight of PEG-bismaleimide cross linker increases. The correlation between the length of the PEG-bismaleimide and the mechanical strength of the hydrogels was investigated. It was observed that the mechanical strength of the hydrogels increased with the MW of the PEG-bismaleimide. This was attributed due to the presence of greater H-bonding interaction originating from high MW PEG between the complimentary clicking moieties which rapidly increases the Diels-Alder cycloaddtion between a furan and a bismaleimide resulting into higher crosslinking with more strength. The mechanical strengths of hydrogels were further increased by incorporating MSNs inside the hydrogels. The porous structures of the hydrogels could be utilized for incubation of drug molecules for the controlled release applications. These hydrogels show great promise in biomedical applications both as injectables and as scaffolds in tissue engineering.

Publications

1) Sadiya Anjum, Pramod Gurawe, Manohar V. Badiger, Arun Torris, **Neha Tiwari**, Bhuvanesh Gupta; Design and development of trivalent aluminum ions induced self-healing polyacrylic acid novel hydrogels, *Polymer*, **2017**, 126, 196-205

2) **Neha Tiwari,** Laxman Nawale, Dhiman Sarkar and Manohar V. Badiger; Carboxymethyl Cellulose grafted Mesoporous Silica, Hybrid Nanogels for Enhanced Cellular Uptake and Release of Curcumin, *Gels*, **2017**, 3, 8; doi:10.3390/gels3010008

3) **Neha Tiwari** and Manohar V. Badiger; Enhanced Drug Release by Selective Cleavage of Cross links in a Double Cross-linked Hydrogel, *RSC Advances*, **2016**, 6, 102453-102461

4) Mrityujoy Kar, **Neha Tiwari**, Mitali Tiwari, Mayurika Lahiri and Sayam Sen Gupta; Poly-L-Arginine Grafted Silica Mesoporous Nanoparticles for Enhanced Cellular Uptake and their Application in DNA Delivery and Controlled Drug Release, *Particle & Particle Systems Characterization*, **2013**, 30, 166-179

5) Soumen Das, Debasis Pati, **Neha Tiwari**, Anuya Nisal and Sayam Sen Gupta; Synthesis of Silk Fibroin–Glycopolypeptide Conjugates and Their Recognition with Lectin, *Biomacromolecules*, **2012**, 13 (11), 3695-3702

6) **Neha Tiwari,** and Manohar V. Badiger; Thermothickening behavior of MPEG-b-PCL grafted poly (acrylic acid): A molecular insight, **Manuscript submitted to ACS Applied Materials and Interfaces**

7) **Neha Tiwari** and Manohar V. Badiger; Effect of chain length of PEG cross linkers on poly (acrylic acid) hydrogels synthesized by furan-maleimide click chemistry, **Manuscript under preparation**

Book Chapter

1) Manohar V. Badiger and **Neha Tiwari**; Polymer Grafted Smart Mesoporous Silica Nanoparticles: Challenges and Advances in Controlled Drug Delivery Applications, Submitted to Nova Science Publishers (under review)